IDENTIFICATION, KINETIC AND STRUCTURAL CHARACTERIZATION OF SMALL MOLECULE INHIBITORS OF ALDEHYDE DEHYDROGENASE 3A1 (ALDH3A1) AS AN ADJUVANT THERAPY FOR REVERSING CANCER CHEMO-RESISTANCE

Bibek Parajuli

Submitted to the faculty of the University Graduate School
in partial fulfillment of the requirements
for the degree
Doctor of Philosophy
in the Department of Biochemistry and Molecular Biology
Indiana University

October 2013

Accepted by the Graduate Faculty of Indiana University, in partial fulfillment of the requirements for the degree of Doctor of Philosophy.

_____

Thomas D. Hurley, Ph.D., Chair

_____

Zhong–Yin Zhang, Ph.D.

Doctoral Committee

_____

Millie M. Georgiadis, Ph.D.

July 2, 2013

_____

Jian–Ting Zhang, Ph.D.

Dedication

I dedicate my thesis to four important people of my life.

- My father Mr. Bedlal Parajuli, who has been more of a friend than a parent to me. He has taught me almost everything he has known in his life and has helped me take the right decisions in right time. I will always be indebted to the compromises and sacrifices that he has made for me. Without his support and encouragement, I would not have come so far in my life.
- My mother Mrs. Radha Parajuli, who has been so kind all these years. Despite her willingness to keep me close to her eyes, she has made this sacrifice to let me travel 7000 miles to pursue my dreams. I cannot go to the past and make it not happen, but will surely give the best I can in my life to make her proud for the decision she took. I really have no words to describe love and support that she has given to me.
- My brother Bijay Parajuli, who has been a great friend of mine. I would like to thank him from the bottom of my heart for all those wonderful midnight conversations that we had all these years. Thanks for giving me updates from home.
- My sweetheart Kriti Acharya, who has been on my side at all times. I must say that I am pleased to have you in my life and looking forward to spending a more exciting life with you.

Acknowledgements

I would like to start by thanking everyone who played a part in the completion of my PhD thesis. Firstly, I would like to thank IBMG program for providing me this opportunity. I would like to thank my mentor Dr. Thomas D. Hurley, for providing me with an opportunity to do research with him and for being such a wonderful mentor and a friend. Despite having no early experiences, he trusted me and let me handle this project independently. I would always be grateful to him for giving me so much of learning opportunity that has given me confidence and has helped me learn enzymology, structural biology and many other things that came along with this project. I would like to recognize and thank my committee members: Dr. Zhong–Yin Zhang, Dr. Millie Georgiadis and Dr. Jian–Ting Zhang for their advice and constructive criticism over the course of my PhD. I would especially like to recognize the Chemical Genomics Core Facility, especially Dr. Lan Chen, for providing access to the chemical libraries and their facility to perform high throughput screening. I am also thankful to the people from Argonne National Laboratory, who have provided me access to their facility to perform crystallographic experiments. The Argonne National Laboratory is operated by the University of Chicago Argonne, LLC, for the United States Department of Energy Office of Biological and Environmental Research under Contract DE–AC02–06CH11357. I am also thankful to the NIH for its grant support. This research was supported by the U.S. National Institute of Health [Grants R01AA018123, R01AA019746] to TDH; and an IUSM Core Pilot grant to TDH.

I thank Dr. Maureen Harrington for providing access to cell culture facility, former members of Dr. Hurley's laboratory: Dr. Sulochanadevi Baskaran and Dr. Samantha

Perez Miller for getting me started in the lab; Dr. Hina Younus, Dr. May Khanna, Lanmin Zhai, Cindy Morgan, Dr. Vimbai Chikwana, Dr. Ann Kimble Hill, Cameron Buchman and Krishna Kishore Mahalinghan for their friendship and support. I could not have asked for a better group of colleagues to work with. I would like to thank Dr. Melissa L. Fishel for teaching me cell culture work and Dr. Tax Georgiadis from Indiana University Chemical Synthesis core facility. I want to thank all my friends for support, encouragement and much needed distraction from work especially Dr. Kentaro Yamada and his family, Dr. Tsuyoshi Imasaki, Dr. Sergio Chai and Dr. Jing Ping Lu.

I want to thank my family, both here and in Nepal, for encouraging me and believing in my potential. Most importantly, I want to acknowledge my mother Radha Parajuli and my father Bedlal Parajuli. Our everyday conversations, the time you spent here with me have been invaluable. I am so grateful to you for believing in me and letting me pursue my dreams. The person I am today is because of you. To my dear uncle and my aunt Khem Kandel and Laxmi Kandel: your support and friendship has been such a help during this time. Lastly, to my sweetheart Kriti Acharya, your love and support provided me with the strength to persevere through the tough times and the long distances. Thanks for being there for me.

Abstract

Bibek Parajuli

IDENTIFICATION, KINETIC AND STRUCTURAL CHARACTERIZATION OF SMALL MOLECULE INHIBITORS OF ALDEHYDE DEHYDROGENASE 3A1 (ALDH3A1) AS AN ADJUVANT THERAPY FOR REVERSING CANCER CHEMO-RESISTANCE

ALDH isoenzymes are known to impact the sensitivity of certain neoplastic cells toward cyclophosphamides and its analogs. Despite its bone marrow toxicity, cyclophosphamide is still used to treat various recalcitrant forms of cancer. When activated, cyclophosphamide forms aldophosphamide that can spontaneously form the toxic phosphoramide mustard, an alkylating agent unless detoxified by ALDH isozymes to the carboxyphosphamide metabolite. Prior work has demonstrated that the ALDH1A1 and ALDH3A1 isoenzymes can convert aldophosphamide to carboxyphosphamide. This has also been verified by over expression and siRNA knockdown studies. Selective small molecule inhibitors for these ALDH isoenzymes are not currently available. We hypothesized that novel and selective small molecule inhibitors of ALDH3A1 would enhance cancer cells' sensitivity toward cyclophosphamide. If successful, this approach can widen the therapeutic treatment window for cyclophosphamides; permitting lower effective dosing regimens with reduced toxicity. An esterase based absorbance assay was optimized in a high throughput setting and 101, 000 compounds were screened and two new selective inhibitors for ALDH3A1, which have IC_{50} values of 0.2 µM (CB7) and 16 µM (CB29)

were discovered. These two compounds compete for aldehyde binding, which was validated both by kinetic and crystallographic studies. Structure activity relationship dataset has helped us determine the basis of potency and selectivity of these compounds towards ALDH3A1 activity. Our data is further supported by mafosfamide (an analog of cyclophosphamide) chemosensitivity data, performed on lung adenocarcinoma (A549) and glioblastoma (SF767) cell lines. Overall, I have identified two compounds, which inhibit ALDH3A1's dehydrogenase activity selectively and increases sensitization of ALDH3A1 positive cells to aldophosphamide and its analogs. This may have the potential in improving chemotherapeutic efficacy of cyclophosphamide as well as to help us understand better the role of ALDH3A1 in cells. Future work will focus on testing these compounds on other cancer cell lines that involve ALDH3A1 expression as a mode of chemoresistance.

Thomas D. Hurley Ph.D., Chair

Table of Contents

List of tables

List of figures

List of abbreviations

A.....Alanine

Å..... Angstroms, 10^{-10} m

ALDH .....Aldehyde Dehydrogenase

ALDH1A1..... Aldehyde Dehydrogenase class 1 A1 (cytosol)

ALDH2 ..... Aldehyde Dehydrogenase class 2 (mitochondria)

ALDH3A1..... Aldehyde Dehydrogenase class 3 A1 (cytosol)

Apo.....enzyme in the absence of cofactor

BME.....Beta–mercaptoethanol

bp.....Base pair

C.....Cysteine

ºC..... Degree centigrade

CB ..... ChemBridge library

CD..... ChemDiv library

CGCF .....Chemical Genomics Core Facility

CP.....Cyclophosphamide

DMSO.....Dimethyl sulfoxide

DNA..... Deoxyribonucleic acid

DTT.....Dithiotheritol

DMEM .....Dulbecco's Minimal Essential Medium

E .....Glutamic acid

E. coli .....Escherichia coli

EDTA..... Ethylene diamine tetra–acetic acid

EtOH ..... Ethanol

FBS ..... Fetal Bovine Serum

GABA ..... Gamma–aminobutyric acid

H ..... Histidine

Holo ..... enzyme in the presence of cofactor

HEPES ..... N–2–hydroxythylpoperazine–N'–ethanesulfonic acid

H_2O_2 ..... Hydrogen peroxide

HRP ..... Horse Radish Peroxidase

HTS ..... High–throughput screening

IPTG ..... Isopropyl–β–D–thiogalactopyranoside

IC_{50} ..... Inhibition Concentration 50%

IUSC ..... Indiana University Synthetic Core facility

K ..... Lysine

L ..... Liter

M ..... Molar

mg ..... Milligrams

Mg^{2+} ..... Magnesium

mL ..... Milliliter

mM ..... Millimolar

MTT ..... Tetrazole 3–[4, 5–Dimethylthiazol–2–yl]–2,5–diphenyl tetrazolium bromide

N ..... Asparagine

NAD^+ ..... Nicotinamide adenine dinucleotide

$NADP^+$ ..... Nicotinamide adenine dinucleotide phosphate

NADH ..... Nicotinamide adenine dinucleotide (reduced)

NADPH ..... Nicotinamide adenine dinucleotide phosphate (reduced)

NaCl ..... Sodium Chloride

nm ..... Nanometer

nM ..... Nanomolar

PBS ..... Phosphate buffered saline

RA ..... Retinoic acid

RAR ..... Retinoic acid receptor

RT ..... Room temperature

SDS ..... Sodium dodecyl sulfate

siRNA ..... Small–interfering RNA

SLS ..... Sjogren–Larson syndrome

TBS ..... Tris buffered saline

TBST ..... Tris buffered saline with Tween 20 buffer

U ..... Units

V ..... Volts

Y ..... Tyrosine

W ..... Tryptophan

I. Introduction

A. Overview

1. Aldehydes: Sources, reactivity and metabolism

Aldehydes are highly reactive compounds that are produced as a consequence of many exogenous and endogenous processes. Endogenous sources of aldehydes include lipid peroxidation products and metabolites of neurotransmitters and amino acids. Over 200 aldehyde species are generated from the oxidative degradation of cellular membrane lipids, also known as lipid peroxidation products such as 4–hydroxynonenal and malondialdehyde (Esterbauer et al., 1991). Amino acid catabolism generates several aldehyde intermediates, including glutamate γ–semialdehyde, while neurotransmitters, such as gamma–aminobutyric acid (GABA), serotonin, noradrenaline, adrenaline, and dopamine, also give rise to aldehyde metabolites during oxidative deamination (Vasiliou et al., 2004; Marchitti et al., 2007). Exogenous sources include food, ethanol which generates acetaldehyde, nicotine and cyclophosphamide metabolites (Lindahl, 1992). Various aldehydes, including formaldehyde, acetaldehyde and acrolein, are also ubiquitous in the environment and are present in smog, cigarette smoke and motor vehicle exhaust. Aldehydes are also produced in various industries in the production of resins, polyester plastics. Numerous dietary aldehydes, including citral and benzaldehyde, are approved additives in various foods where they provide flavor and odor (Marchitti et al., 2008). Table 1 shows the list of aldehydes generated from various endogenous and exogenous sources.

Table 1. Aldehydes and its sources. Aldehydes generated from various exogenous and endogenous sources via metabolism of amino acids, fatty acids and ethanol (Extracted from Lindahl, 1992).

Endogenous source	Aldehyde
Choline metabolism	Betaine aldehyde
Corticosteroid catabolism	21–Dihydrocorticosteroids
Dopamine catabolism	3, 4–Dihydroxyphenylacetaldehyde
GABA metabolism	Succinic semialdehyde
Lipid peroxidation	Malondialdehyde, 4–Hydroxynonenal, Hexanal
Proline biosynthesis	Glutamic–γ–semialdehyde
Putrescine catabolism	γ–amino butyraldehyde
Serotonin metabolism	5–Hydroxyindoleacetaldehyde
Threonine catabolism	Acetaldehyde
Vitamin A metabolism	Retinal

Exogenous source	Aldehyde
Codeine	Formaldehyde
Combustion	Formaldehyde, acetaldehyde, acrolein
Cyclophosphamide	Aldophosphamide, acrolein
Ethanol	Acetaldehyde
Foods	Benzaldehyde, lipid aldehydes, acrolein, glyoxal, methylglyoxal, crotonaldehyde
Nicotine	γ–3–Pyridyl–γ–methylaminobutyraldehyde

While some aldehydes play important roles in normal physiological processes including vision, embryonic development and neurotransmission, many aldehydes are carcinogenic and cytotoxic (Yokoyama et al., 2001). Aldehydes show high reactivity due to their highly reactive carbonyl group. Unlike free radicals, aldehydes are relatively long lived and not only react with cellular components near the site of their formation, but also affect targets some distance away as a consequence of diffusion or transport (Esterbauer

et al., 1991). They show a strong tendency to form adducts with nucleic acids, glutathione (GSH) and proteins leading to impaired cellular homeostasis, enzyme inactivation, DNA damage and cell death. If their levels are not minimized, aldehydes cause damage that can cause cancer and several other complications (Lindahl, 1992).

In order to minimize the amount of aldehyde in the body, several mechanisms of elimination exist. Aldehydes are detoxified primarily through reductive and oxidative Phase I enzyme–catalyzed reactions (Figure 1), including the non–P450 enzyme systems alcohol dehydrogenase (ADH), aldo–keto reductase (AKR), short chain dehydrogenase/ reductase (SDR), aldehyde oxidase (AOX), and aldehyde dehydrogenase (ALDH).

Alcohol dehydrogenase

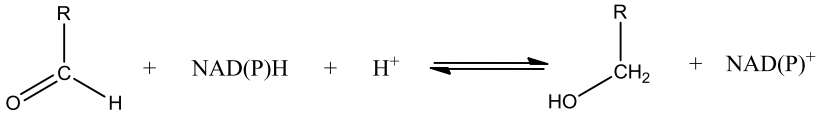

Aldehyde dehydrogenase

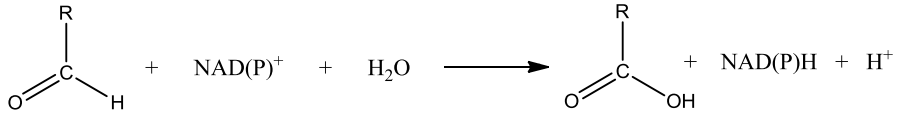

Aldehyde oxidase

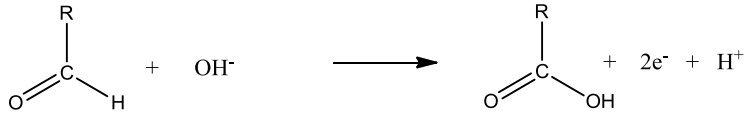

Aldose reductase

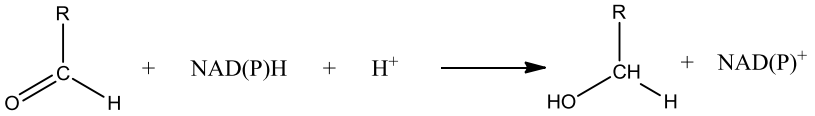

Figure 1. Enzymes involved in aldehyde detoxication and their mechanisms. Figure shows reaction mechanism of four classes of enzymes that metabolize aldehydes and ketones.

The aldo–keto reductase superfamily reversibly reduces a variety of aldehydes and ketones to their corresponding alcohols. The conversion, however, strongly depends on the NADPH/ $NADP^+$ ratio. Aldehyde reductase shows broad specificity and prefers negatively charged aldehydes (Jez et al., 1997). It has also been involved in various diseased states such as diabetes (Lee et al., 1995; Suzen and Buyukbingol, 2003), lung cancer (Fukumoto et al., 2005), abnormal metabolism of male and female sex hormones (Penning and Byrns, 2009) and bile acid deficiency (Lemonde at al., 2003). Alcohol dehydrogenases catalyze the oxidation of alcohols to aldehydes and ketones, but can also catalyze the reverse reaction. The direction of the reaction, however, strongly depends on the NAD^+/ NADH ratio (McMahon, 1982). Aldehyde oxidase on the other hand catalyzes the oxidation of aldehydes into carboxylic acid. It also catalyzes the hydroxylation of some heterocycles and aromatic aldehydes that arise from metabolism of biogenic amines (Beedham et al., 1995). Similarly, another enzyme, glutathione S–transferase, is known to be important for elimination of lipid peroxidation products via conjugation to glutathione (Srivastava et al., 1998). The role of these enzymes in aldehyde metabolism is relatively small compared to that of aldehyde dehydrogenase.

Aldehyde dehydrogenases are $NAD(P)^+$ dependent enzymes that catalyze the irreversible oxidation of a broad range of aliphatic and aromatic aldehydes generated from various exogenous and endogenous precursors to their corresponding carboxylic acids (Lindahl, 1992; Vasiliou et al., 2000). The human genome contains 19 members of the ALDH superfamily where each member exhibits unique chromosomal locations (Vasiliou et al., 2005) (Table 2). A nomenclature system based on divergent evolution and amino acid identity was established for the ALDH superfamily over 12 years ago and

is based on the P450 nomenclature system (Vasiliou et al., 1999). ALDH isozymes are found in all cellular compartments including cytosol, mitochondria, endoplasmic reticulum and nucleus, with several found in more than one compartment. ALDH isozymes found in organelles other than the cytosol possess leader or signal sequences that allow their translocation to specific subcellular regions (Braun et al., 1987). After translocation or import, these leader sequences may be removed. Mutations and polymorphisms in *ALDH* genes are associated with distinct phenotypes in humans and rodents (Vasiliou et. al., 2000). These include Sjögren–Larsson syndrome (Rizzo et al., 2005), type II hyperprolinemia (Onenli–Mungan et al., 2004), γ–hydroxybutyric aciduria (Akaboshi et al., 2003), pyridoxine–dependent seizures (Mills et al., 2006), hyperammonemia (Baumgartner et al., 2000), alcohol–related diseases (Enomoto et al., 1991), cancer (Yokoyama et al., 2001) and late onset of Alzheimer's disease (Kamino et al., 2000). In addition to clinical phenotypes, studies on transgenic knockout mice have suggested a pivotal role of ALDHs in physiological functions and processes such as embryogenesis and development as well (Niederreither et al., 1999; Dupe et al., 2003).

Besides aldehyde detoxication, ALDHs are also able to catalyze ester hydrolysis (Sydow et al., 2004) and can act as binding proteins for various endogenous (e.g., androgen, cholesterol and thyroid hormone) and exogenous compounds (acetaminophen) (Vasiliou et al., 2004). ALDH enzymes also have important antioxidant roles including the production of NAD(P)H (Pappa et al., 2003; Lassen et al., 2006), the absorption of UV light (Estey et al., 2007; Lassen et al., 2007).

Table 2. ALDH genes, their loci, localization, PDB ID, substrates and phenotypes.

New name	ALDH1A1	ALDH1A2	ALDH1A3	ALDH1B1
Common name	ALDH1A1	RALDHII	ALDH6 RALDHIII	ALDH5
Chr. Loc.	9q21.13	15q22.1	15q26.3	9p11.1
Tissue location	ubiquitous	embryonic trunk, forebrain	stomach, kidney, saliva	liver, kidney muscle heart
Substrates	aliphatic alde-hyde, retinal, CP	retinal	Aliphatic aldehyde retinal	Aliphatic aldehyde acetaldehyde
Comments	Inducible KO mice have cataracts	KO mice die shortly after birth	KO mice lethal	Unknown
Oligomer	tetramer	tetramer	tetramer	Tetramer
PDB ID	1BXS (sheep)	1BI9 (rat)	NA	NA

New name	ALDH1L1	ALDH2	ALDH3A1
Common name	10FTDH	ALDH2	ALDH3
Chr. Loc.	3q21.2	12q24.2	17p11.2
Tissue location	cytoplasm	liver, various tissues, mitochondria	cornea, lung stomach, liver
Substrates	folate metabolism	acetaldehyde	aromatic aldehydes lipid peroxidation products
Comments	KO mice infertile, less folate	Alcoholism, cocaine addiction, myocardial infarction	KO mice have cataracts, CP metabolism
Oligomer	Unknown	Tetramer	Dimer
PDB ID	NA	1O02	3SZA

Information extracted from www.aldh.org

New name	ALDH3A2	ALDH3B1	ALDH3B2	ALDH4A1
Common name	FALDH ALDH10	ALDH7	ALDH8	GGSDH, ALDH4 P5CDH
Chr. Loc.	17p11.2	11q13.2	11q13.2	1p36.13
Tissue location	liver, heart muscle (ER)	kidney, lungs, microsome	parotid microsomal	liver, kidney, mitochondria skeletal muscle,
Substrates	fatty aldehyde, aromatic membrane lipid	aliphatic, aromatic	Unknown	gamma–semialdehyde
Comments	Sjogren Larsson syndrome	Linked to schizophrenia	Unknown	Type II hyperprolinemia
Oligomer	dimer	dimer	NA	dimer
PDB ID	NA	NA	NA	102O

New name	ALDH5A1	ALDH6A1	ALDH7A1	ALDH9A1
Common name	SSDH	MMSDH	ANTQ1	ALDH9
Chr. Loc.	6p22.2	14q24.3	5q31	1q23.1
Tissue location	brain, liver heart, mitochondria	kidney, liver, heart, mitochondria	cochlea, ovary eye, heart, liver kidney	liver, kidney brain, muscle, cytoplasm
Substrates	succinic semialdehyde	Methylmalonate semialdehyde		GABA
Comments	gamma–hydroxybutyric aciduria	developmental delay	pyridoxine dependent seizures	
Oligomer	tetramer	tetramer		tetramer
PDB ID	NA			1A4S

ALDH enzymes share a large number of highly conserved residues necessary for catalysis and cofactor binding. Sequence alignment of 145 ALDHs demonstrates a very limited number of conserved residues. The catalytic cysteine Cys302, Glu268, Gly299 and Asn169 are all essential for catalysis (numbering based on the mature human ALDH2 protein) (Steinmetz et al., 1997; Liu et al., 1997; Hempel et al., 1997; Perozich et al., 2001). Gly245 and Gly250 are essential residues within the ALDH Rossman fold (GxxxxG) and are necessary for cofactor binding. Also, residues Lys192, Glu399 and Phe401 are important for proper cofactor positioning and, thus, impact catalysis. Crystal structures of mammalian ALDH enzymes have shown that each subunit has a $NAD(P)^+$ binding domain, a catalytic domain and an oligomerization domain (Steinmetz et al., 1997; Liu et al., 1997).

Crystallographic structures have also helped us understand the basic catalytic mechanism of ALDH (D'Ambrosio et al., 2006; Hammen et al., 2002; Hurley et al., 1999). Briefly, $NAD(P)^+$ binding in the Rossmann fold of the enzyme activates the catalytic cysteine (Cys302) nucleophile (Hammen et al., 2002). Cys302 then performs a nucleophilic attack on the carbonyl carbon of the aldehyde. This forms a thiohemiacetal intermediate that facilitates hydride transfer to the cofactor. This results in the formation of a thioacylenzyme intermediate. Hydrolysis of the thioacylenzyme and release of the carboxylic acid product takes place via Glu268, which acts as a general base to activate the hydrolytic water after hydride transfer. The activated water performs a nucleophilic attack on the carbonyl carbon displacing the carbon–sulfur bond and releasing the reduced cofactor NAD(P)H and product carboxylic acid. The order of product release is believed to be the product acid followed by reduced cofactor (Sohling et al., 1993) (Figure 2).

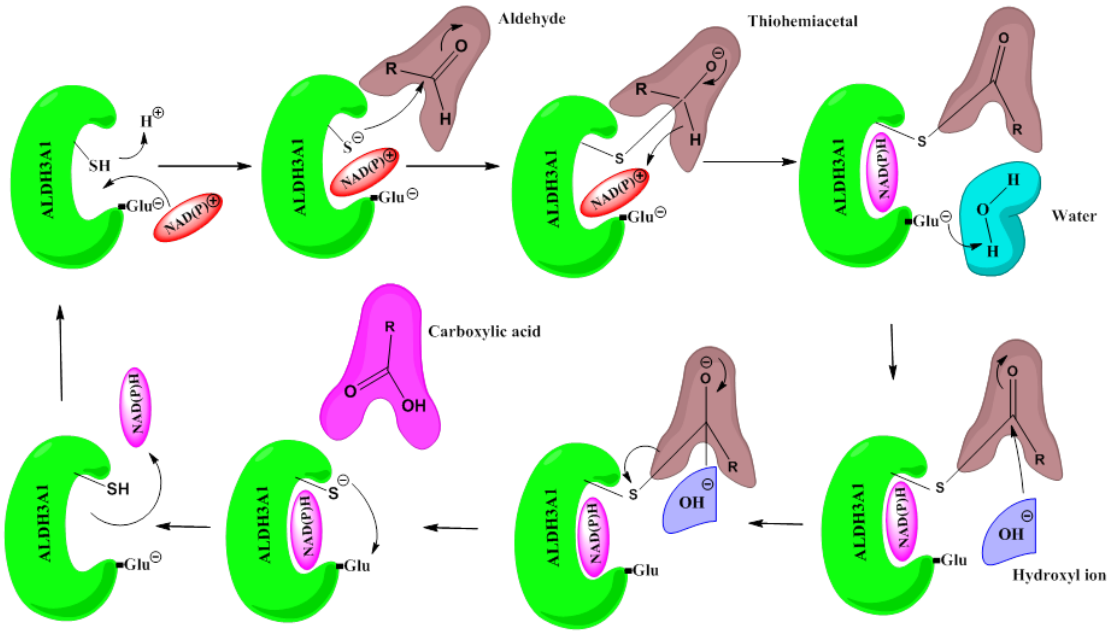

Figure 2. General reaction mechanism for aldehyde dehydrogenase. Figure shows detailed kinetic mechanism of conversion of aldehydes to carboxylic acid by ALDH3A1 in the presence of $NAD(P)^+$ and water.

2. Important aldehyde dehydrogenase family members

Structural, kinetic and knockout studies of several human aldehyde dehydrogenase isozymes have been performed over the years to understand their biological function. These studies have become important since lot of these enzymes show similarity in terms of structural packing, substrate preferences, catalytic residues and expression levels in cells despite being involved in completely different physiological processes or pathogenesis. Hence, a proper understanding of each of these isozymes is necessary for characterizing their function with respect to different physiological processes. Some of the enzymes that have been extensively studied include ALDH1A1 (RALDH1), ALDH1A2

(RALDH2), ALDH1A3 (RALDH3), ALDH1B1, ALDH2 and ALDH3A1. All these isozymes show broad tissue distribution, constitutive or inducible expression and oxidize a variety of aldehydes.

ALDH1A1 is a tetrameric, cytosolic enzyme expressed in the adult epithelium of various organs including testis, brain, eye lens, liver, kidney, lung and retina (King et al., 1997; Zhai et al., 2001). It is a highly conserved enzyme that can catalyze the oxidation of the retinol metabolite, retinaldehyde to retinoic acid (Zhao et al., 1996; Wang et al., 1996). It has high affinity for the oxidation of both all–*trans* and 9–*cis*–retinal (Yoshida et al., 1992). Retinoic acid regulates gene expression by serving as a ligand for nuclear retinoic acid receptors and retinoid X receptors. It is important for normal growth, differentiation, development and maintenance of adult epithelia in vertebrate animals (Ross et al., 2000). During embryogenesis, ALDHs have shown to exhibit differential expression patterns especially in retinoid dependent cells, indicating that retinoic acid signaling is essential for embryogenesis (Haselbeck et al., 1999; Niederreither et al., 2002; Marlier et al., 2004; Dickman et al., 1997; Duester et al., 2000). ALDH1A1 knockout mice (*Aldh1a1*$^{-/-}$) are viable and have normal retina morphology. However, later during their life, they display reduced retinoic acid synthesis and increased retinal levels in serum after retinol treatment (Fan et al., 2003; Molotkov et al., 2003). *Aldh1a1*$^{-/-}$ mice are protected against diet–induced obesity and insulin resistance, suggesting that retinal may transcriptionally regulate the metabolic response to high–fat diets. Hence, ALDH1A1 may be a candidate for therapeutic targeting (Ziouzenkova et al., 2007). In cultured hepatic cells, suppression of *ALDH1A1* gene reduced both omega oxidation of free fatty acids and the production of reactive oxygen species (Li et al., 2007). Retinoid X Receptor alpha

knockout (*RXRα*$^{-/-}$) mice display decreased liver ALDH1A1 levels, suggesting that retinoic acid binding is an activating factor in *ALDH1A1* gene expression (Gyamfi et al., 2006). Retinoic acid is required for testicular development, and *ALDH1A1* is absent in genital tissues of humans with androgens receptor–negative testicular feminization (Yoshida et al., 1993; Yoshida et al., 1998; Pereira et al., 1991).

ALDH1A1 is also highly expressed in dopaminergic neurons that require retinoic acid for their development and differentiation (Galter et al., 2003; Jacobs et al., 2007). In these neurons, ALDH1A1 expression is under the control of the transcription factor, Pitx3, which regulates the specification and maintenance of distinct populations of dopaminergic neurons through *ALDH1A1* up–regulation (Chung et al., 2005). Decreased levels of ALDH1A1 occur in dopaminergic neurons of the substantia nigra in Parkinson's disease (PD) patients and in dopaminergic neurons of the ventral tegmental area in schizophrenic patients (Galter et al., 2003; Mandel et al., 2005). In the central nervous system, monoamine oxidase (MAO) metabolizes dopamine to its aldehyde form 3, 4–dihydroxyphenylacetaldehyde (DOPAL). DOPAL may be neurotoxic, and its accumulation may lead to cell death associated with neurological pathologies such as Parkinson's disease. ALDH1A1 plays a critical role in maintaining low intraneuronal levels of DOPAL by catalyzing its metabolism to 3, 4–dihydroxyphenylacetic acid (DOPAC) (Galter et al., 2003).

ALDH1A1 is involved in metabolism of the acetaldehyde, a metabolite of ethanol. Acetaldehyde is toxic at high concentrations in cells (Ueshima et al., 1993). Low activity of ALDH1A1 accounts for alcohol sensitivity in Caucasian populations (Ward et al., 1994; Yoshida et al., 1989). Decreased levels of ALDH1A1 reported in *RXRα*$^{-/-}$ mice are

susceptible to alcoholic liver injury (Gyamfi et al., 2006). ALDH1A1 also plays a key role in the cellular defense against oxidative stress by oxidizing lipid peroxidation products–derived aldehydes. These include 4–HNE, hexanal, and malondialdehyde (MDA) (Manzer et al., 2003).

ALDH1A1 also plays an important role in cancer. ALDH1A1 activity has been reported to decrease the effectiveness of some oxazaphosphorine anticancer drugs, such as cyclophosphamide (CP) and ifosfamide, by detoxifying their major active aldehyde metabolite, aldophosphamide (Sladek et al., 1999). Indeed, inhibition of ALDH1A1 activity leads to increased toxicity of the major metabolite of CP, 4–hydroperoxycyclophosphamide (Moreb et al., 2007). Patients with low breast tumor ALDH1A1 levels have been reported to respond to cyclophosphamide–based treatment significantly more often than those with high levels, indicating that ALDH1A1 may be a predictor of the drug's therapeutic effectiveness (Sladek et al., 2002). Various non–cancerous cells, such as hematopoietic progenitor cells, express relatively high levels of ALDH1A1 and hence are relatively resistant to oxazaphosphorine–induced toxicity (Sladek et al., 1994). ALDH1A1 has also been shown to bind to certain anticancer drugs such as daunorubicin (Banfi et al., 1994) and flavopiridol (Schnier et al., 1999).

Recent studies have shown that increased ALDH activity is a hallmark of cancer stem cells (CSC) that can be detected through the Aldefluor assay (Storms et al., 1999). The Aldefluor assay quantifies ALDH activity by measuring the conversion of BODIPY aminoacetaldehyde to the fluorescent reaction product BODIPY aminoacetate. Addition of the ALDH inhibitor diethylaminobenzaldehyde (DEAB) reduces fluorescence that confirms that ALDH positive cells are correctly identified. This assay was developed by suc-

cessful isolation of viable hematopoietic stem cells from human umbilical cord blood and was reported to be specific for ALDH1A1 (Storms et al., 1999). However, while ALDH isoforms show substrate specificity, they also have cross–reactivity that makes it likely that the assay is detecting the ALDH activity of other ALDH isoforms as well. A recent ALDH1A1 knockout study showed that ALDH1A1 expression was not required for hematopoietic and neural stem cell function (Levi et al., 2008). Despite not having ALDH1A1 expression, these stem cells did not show reduction in aldefluor activity, suggesting that additional factors are responsible for aldefluor activity (Levi et al., 2008). Instead authors detected expression of ALDH2, ALDH3A1 and ALDH9A1 in the ALDH1A1–deficient hematopoietic cells that implies that one or more of these isoforms are responsible for the Aldefluor activity (Levi et al., 2008). In another study conducted in prostate cancer cell lines, high expression of ALDH7A1 was found with much lower expression of ALDH1A1 (van den Hoogen et al., 2010). These cells, however, showed very high Aldefluor activity suggesting that ALDH7A1 might be a contributor for Aldefluor activity as well (van den Hoogen et al., 2010). Another study with breast cancer patient tumor samples isolated for Aldefluor positive and Aldefluor negative tumor cells shows that at least for breast cancer stem cells, ALDH1A1 expression is not the primary determinant of Aldefluor activity (Marcato et al., 2011). Indeed, a proper correlation of ALDH1A3 and Aldefluor activity was seen in these cells. Expression and quantification of all 19 forms of ALDH in breast cancer cell lines revealed that ALDH1A3 expression correlated best with the ALDH activity. Only knockdown of ALDH1A3 reduced ALDH activity in all three Aldefluor positive breast cancer cells (Marcato et al., 2011). However, it still leaves a possibility that other ALDH isoforms including ALDH1A1 have a po-

tential to promote Aldefluor activity in breast cancer cells if expressed at sufficient levels. Based on all these studies, it becomes clear that ALDH isoforms responsible for Aldefluor activity vary depending on cancer type and tissue of origin.

ALDH1A2 is another cytosolic isozyme that plays an important role in retinoid synthesis during embryonic development. Knockout studies have shown that it is the major retinoic acid–synthesizing enzyme during early embryogenesis (Haselbeck et al., 1999). ALDH1A2 knockout mice induced lethal defects in heart and forebrain development (Ribes et al., 2006). Transgenic mice lacking ALDH1A2 expression die at mid–gestation without undergoing axial rotation. They also show shortened anterioposterior axis and do not form limb buds. Their heart consists of single, medial, distal cavity and their frontonasal region is truncated (Niederreither et al., 1999). A recent study has shown that ALDH1A2 is expressed in normal prostrate epithelia but is down–regulated in prostate cancer (Kim et al., 2005). Thus ALDH1A2 may function as a tumor suppressor in prostate cancer (Kim et al., 2005). This also leaves a possibility of a role for retinoids in the prevention or treatment of prostate cancer.

ALDH1A3 is a cytosolic homotetramer that is expressed at low levels in organs and tissues. Its expression in salivary gland, stomach and kidney are much higher than other tissues in body (Hsu et al., 1994). It is also differentially activated during early embryonic head and forebrain development. Studies showed that ALDH1A3 knockout mice have reduced retinoic acid synthesis that cause malformations restricted to ocular and nasal regions are similar to that observed in Vitamin A–deficient mutants or retinoid receptor mutants (Dupe et al., 2003). ALDH1A3 knockout causes choanal atresia (nasal blockage

by soft tissue) that is responsible for the respiratory distress and resulting death of the mice (Dupe et al., 2003).

ALDH1B1 is mitochondrial homotetramer that is known to be expressed in liver, testis, kidney, skeletal muscle and fetal tissues (Hsu et al., 1991). It exhibits ~72% sequence homology to ALDH2 and is insensitive to inhibition by disulfiram.

ALDH2 is an important mitochondrial enzyme that is constitutively expressed in a variety of tissues including liver, kidney, heart, lung and brain (Goedde et al., 1990). It is the primary enzyme responsible for oxidation of acetaldehyde during ethanol metabolism (Klyosov et al., 1996). To date, several ALDH2 mutants have been reported, including the most widely studied ALDH2*2 allele (single base pair mutation G/ C→ A/ T) that results in an E487K or E504K mutation. Glu487, located in the bridging domain, maintains a stable scaffold and facilitates catalysis by linking together the cofactor–binding and catalytic domains through its interaction with Arg–264 and Arg–475 (Larson et al., 2005; Larson et al., 2007). Since ALDH2 functions as a homotetramer, when ALDH2*2 allele is dominant, heterotetrameric ALDH2 proteins containing even one ALDH2*2 subunit are enzymatically inactive (Crabb et al., 1989). The ALDH2*2 allele is found in approximately 40% of individuals of Asian descent (Goedde et al., 1992). It causes alcohol induced toxicity in those who drink alcohol primarily due to acetaldehyde accumulation (Wall et al., 1999; Peng et al., 2007). This is one of the reasons for lower alcoholism rate in Asian populations (Luczak et al., 2002). Studies have shown the association of *ALDH2*2* with an increased risk for various cancers, including esophageal, stomach, colon, lung, head, and neck cancers (Muto et al., 2000). Alcoholic *ALDH2*2* individuals display increased levels of acetaldehyde–derived DNA adducts, indicating a potential

mechanism of DNA damage and cancer development (Matsuda et al., 2006). ALDH2*2 has been associated with alcoholic liver disease and cirrhosis in Asian individuals, even with moderate alcohol intake (Enomoto et al., 1991). ALDH2*2 allele may also be a risk factor for increased DNA damage in workers exposed to polyvinyl chloride, a carcinogen that is metabolized to the ALDH2 substrate chloroactaldehyde, which produces DNA crosslinks and strand breaks (Wong et al., 1998; Spengler et al., 1988).

In addition to acetaldehyde metabolism, ALDH2 is the principle enzyme responsible for the first step in the bioactivation of nitroglycerin, a long used treatment for angina and heart failure (Chen et al., 2002). The *ALDH2*2* allele is associated with lack of nitroglycerin efficacy in Chinese patients (Li et al., 2006), increased myocardial damage following infarction in Korean patients (Jo et al., 2007) and hypertension in Japanese patients (Hui et al., 2007). *Aldh2*$^{-/-}$ mice display increased alcohol toxicity correlating with increased brain and blood acetaldehyde levels (Isse et al., 2005; Isse et al., 2005) and increased urinary 8–hydroxdeoxyyguanosine and DNA–acetaldehyde adducts after exposure to acetaldehyde or oral ethanol administration (Ogawa et al., 2006, Ogawa et al., 2007). The results were not seen in mice with normal ALDH2 expression.

ALDH2 is reported to be associated with hepatotoxicity in alcoholics, late onset of Alzheimer's and Parkinson's disease. Hepatotoxicity in alcoholics occurs due to competition of lipid peroxidation product–derived aldehydes with acetaldehyde for ALDH2–mediated metabolism. ALDH2 is involved in the metabolism of LPO–derived aldehydes, including 4–HNE and malondialdehyde (MDA) (Vasiliou et al., 2004). ALDH2 specifically seems to be responsible for 4–hydroxynonenal elimination in hepatic and Kupffer cells (Reichard et al., 2000; Luckey et al., 2001). ALDH2 activity is activated in the cere-

bral cortex of Alzheimer's disease patients, which may be a protective mechanism against high 4–HNE levels (Picklo et al., 2001). *In vitro,* ALDH2–deficient cells are highly vulnerable to 4–HNE induced apoptosis (Ohsawa et al., 2003). ALDH2*2 is associated with elevated risk for the late onset of AD in Chinese population (Wang et al., 2008). It is involved in metabolism of the neurotoxic aldehyde metabolite of dopamine, DOPAL; and hence deficiency of ALDH2 may contribute to the onset of Parkinson's disease (Maring et al., 1985).

ALDH3A1 is another cytosolic 55 KDa homodimer expressed in various tissues including cornea, stomach, esophagus and lung. It is believed to be an important enzyme involved in cellular defense against oxidative stress (Estey et al., 2007). It catalyzes the oxidation of various LPO–derived aldehydes including α, β–hydroxyalkenals (Pappa et al., 2003). ALDH3A1 also functions as corneal crystallin and is highly expressed in corneal epithelium, accounting for as much as 50% of the total water–soluble protein (Estey et al., 2007; Pappa et al., 2001). *Aldh3a1*$^{-/-}$ mice show clear corneal tissue, but when exposed to UV light, these mice show cataract formation and corneal opacification (Nees et al., 2002; Lassen et al., 2007). *Aldh3a1*$^{-/-}$ mice show increased levels of 4–HNE and MDA–protein adducts (Lassen et al., 2007). Low expression of ALDH3A1 is associated with corneal disease (Pei et al., 2006) while overexpression in human corneal epithelial cells makes these cells less sensitive to UV light and UV associated cytotoxicity (Pappa et al., 2003). Enzymatic action of ALDH3A1 may also generate NADPH, which is critical for GSH maintenance and antioxidant retention (Kirsch et al., 2001). *In vitro,* ALDH3A1 prevents UV–induced protein inactivation and, *in vivo,* UV light inactivates

ALDH3A1 while other metabolic enzymes are unaffected, suggesting that ALDH3A1 may function to absorb UV–light as part of a suicide response (Downes et al., 1993).

ALDH3A1 also influences cell proliferation and the cell cycle. Cell lines expressing high levels of ALDH3A1 are more resistant to the anti–proliferative effects of lipid peroxidation derived aldehydes and ALDH3A1 deficiency or ALDH3A1 inhibition reduces cellular growth rates through aldehyde accumulation (Canuto et al., 1999, Muzio et al., 2003). *In vitro*, ALDH3A1 has been shown to prevent DNA damage and reduce apoptosis from various toxins including hydrogen peroxide and etoposide, indicating that ALDH3A1–mediated cell cycle delay and subsequent decreased cell growth is associated with resistance to DNA damage (Lassen et al., 2006). ALDH3A1 has also been identified as a potential diagnostic marker for non–small–cell lung cancer (Kim et al., 2007) and as a candidate gene in the pathogenesis of esophageal squamous cell carcinoma (Huang et al., 2000). Interestingly, while ALDH3A1 is expressed at low levels in normal liver, its expression in hepatoma cells increases in direct correlation with the growth rate of the tumor (Canuto et al., 1994). *ALDH3A1* is induced in other neoplastic tissues and cell lines (Sreerama et al., 1997), and its expression is differentially affected by hormones such as progesterone and cortisone, suggesting a potential role in hormone dependent tumors (Stephanou et al., 1999). *ALDH3A1* expression is also induced by various xenobiotics, including polycyclic hydrocarbon (PAHs) and 3–methylcholanthrene (Reisdorph et al., 2007).

3. ALDH3A1 and its importance in cancer chemoresistance

ALDH3A1 was originally designated as the tumor ALDH, as it was found highly expressed in some human tumors such as hepatoma, lung adenocarcinoma, myeloma, breast cancer as well as in stem cell populations (Sreerama et al., 1993, Sreerama et al., 1997). ALDH3A1 is known to catalyze the metabolic inactivation of oxazaphosphorines such as cyclophosphamide and its analogs and contribute to drug resistance in various tumor types (Figure 3) (Manthey et al., 1990; Sreerama et al., 1993). Differential expression of ALDH3A1 may account for the variable clinical responses to cyclophosphamide treatment in certain cancers (Sreerama et al., 1997; Sladek et al., 2002). In support of this hypothesis, ALDH3A1 knockdown increases cellular sensitivity to cyclophosphamide and its metabolite, 4–hydroperoxycyclophosphamide (Moreb et al., 2007), and transfection of *ALDH3A1* into normal human peripheral blood hematopoietic progenitor cells results in increased resistance to cyclophosphamide (Wang et al., 2001). ALDH3A1 can also be expressed in certain tumor cells by inducing these cells with catechol. MCF–7 cells induced with 30 μM catechol for 5 days (MCF–7/ CAT) show much higher levels of cytosolic class–3 aldehyde dehydrogenase (ALDH3A1) than control cells (MCF–7). As a result of ALDH3A1 expression, MCF–7/ CAT cells are >35–fold more resistant to oxazaphosphorine treatment as compared to control (MCF–7) cells (Sreerama et al., 1995). Cellular levels of ALDH–3 activity were also increased when a number of other human tumor cell lines, e.g. breast adenocarcinoma MDA–MB–231, breast carcinoma T–47D and colon carcinoma HCT 116b, were cultured in the presence of catechol (Sreerama et al., 1995). The cultured human colon carcinoma cell line, Colon C has elevated cytosolic ALDH3A1 expression and shows intrinsic cellular resistance to mafosfamide (Ganaganur

et al., 1994). Colon C cells were found to be 10–fold less sensitive to mafosfamide than were two other cultured human colon carcinoma cell lines, RCA and HCT 116b, that do not express ALDH3A1 (Ganaganur et al., 1994). RCA and HCT 116b cell lysates had 200–fold less aldehyde dehydrogenase activity ($NADP^+$ dependent benzaldehyde oxidation) as compared to colon C cells. Interestingly, the three cell lines were equally sensitive to phosphoramide mustard, the final cross linking product of cyclophosphamide activation that cannot be detoxified by ALDH3A1. The relative insensitivity of Colon C cancer cells to mafosfamide was not seen in the presence of the competitive substrates benzaldehyde, or 4–diethylaminobenzaldehyde, since these substrates compete with mafosfamide binding and its detoxication. Sensitivity of HCT 116b and RCA cells to both mafosfamide and phosphoramide mustard was unaffected when drug exposure was in the presence of the same substrates (Ganaganur et al., 1994). Similarly, another study performed with putative ALDH3 inhibitors (NPI–2)–[(4–chlorophenyl) sulfonyl–[2–(methylpropan–2–yl) oxycarbonyl] amino] acetate and (API–2)–1–(4–chlorophenyl) sulfonyl–1–methoxy–3–propylurea sensitized MCF–7/ 0/ CAT cells to mafosfamide treatment; the LC_{50} decreased from >2mM to 175 µM and 200 µM, respectively (Ganaganur et al., 1998). MCF–7 cells electroporated with ALDH3A1 were 16–fold less sensitive toward mafosfamide than control cells (Sreerama et al., 1995).

Some antineoplastic agents induce apoptosis in cancer cells by producing oxidative stress through generation of lipid peroxidation products. ALDH3A1 can detoxify the products of lipid peroxidation and hence facilitate drug resistance. In fact, a recent study has shown that *ALDH3A1* is one of the downstream targets of metadherin (*MTDH),* an important contributor toward multidrug chemoresistance (Hu et al., 2009). LM2 cells en-

gineered to express an inducible shRNA against *ALDH3A1* for conditional knockdown were more sensitive to chemotherapeutic agents such as paclitaxel, doxorubicin and 4–hydroxycyclophosphamide when ALDH3A1 was knocked down. Also constitutive over-expression of *ALDH3A1* in LM2 cells was able to partially rescue the chemoresistance to paclitaxel, doxorubicin and 4–hydroxycyclophosphamide (Hu et al., 2009). These studies highlight the role of ALDH3A1 in a broad–spectrum of cancer chemoresistance and support the development of selective, potent small molecule inhibitors.

4. Cyclophosphamide and its mechanism of cytotoxicity

Cyclophosphamide and related oxazaphosphorines are clinically important antineoplastic and immunosuppressive agents. Even today, 52 years after their initial synthesis, it is still widely used as a chemotherapeutic agent and in the mobilization and conditioning regimens for blood and marrow transplantation. Reviewing the chemistry and pharmacology of cyclophosphamide is crucial for understanding its wide therapeutic applicability. Cyclophosphamide is, in fact, a prodrug activated by cytochrome P450 to produce an equilibrium mixture of aldophosphamide and its tautomeric isomers, *cis* and *trans* 4–hydroxycyclophosphamide (Figure 3). Aldophosphamide undergoes a non–enzymatic β–elimination reaction to give the active antineoplastic agent phosphoramide mustard (Sladek et al., 2002). Phosphoramide mustard acts as an alkylating agent that cross links DNA and renders target cells nonviable (Figure 3) (Sladek et al., 2002).

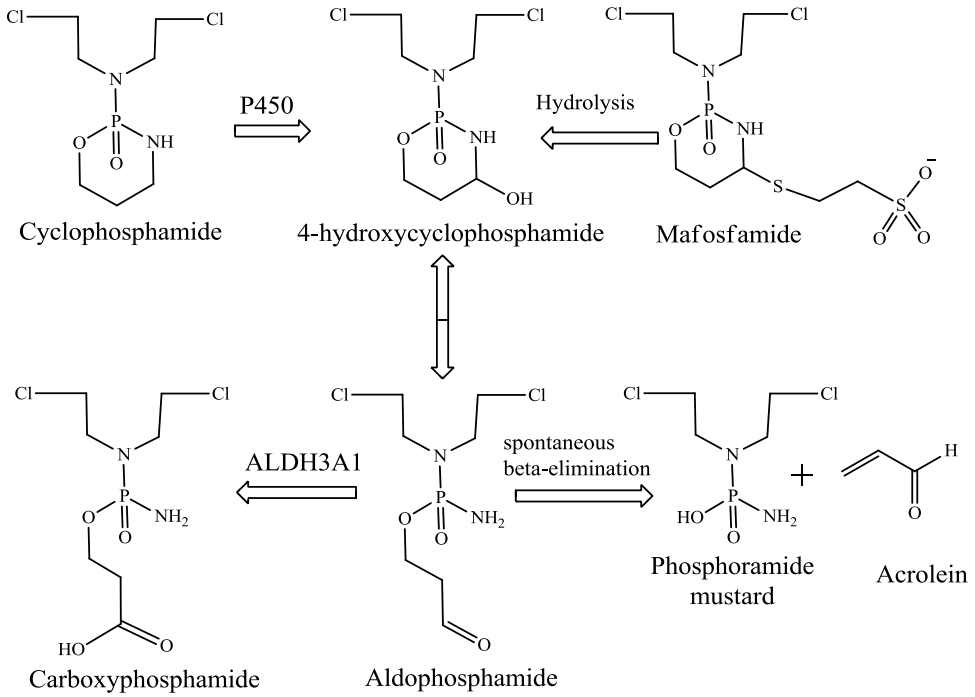

Figure 3. Metabolic pathway for cyclophosphamide. Figure shows the metabolic activation of cyclophosphamide by P450 or spontaneous activation of mafosfamide to form 4–hydroxycyclophosphamide that eventually from phosphoramide mustard. ALDH3A1 acts on one of the intermediate aldophosphamide to form inactive carboxyphosphamide.

5. Cytotoxic action of phosphoramide mustard

The cytotoxic action of phosphoramide mustard is closely related to the reactivity of the 2–chloroethyl groups attached to the central nitrogen atom. Under physiological conditions, phosphoramide mustard undergoes an intramolecular cyclization through elimination of chloride forming a cyclic aziridinium cation. This highly unstable cation is readily attacked by several nucleophiles, including the N9 nitrogen in guanine residues in nucleic acids. This reaction releases the nitrogen of the alkylating agent and makes it

available to react with the second 2–chloroethyl group, facilitating the formation of a second covalent linkage with another nucleophile. By forming an interstrand DNA cross-link the target cell is rendered non–viable (Figure 4) (Sladek et al., 2002).

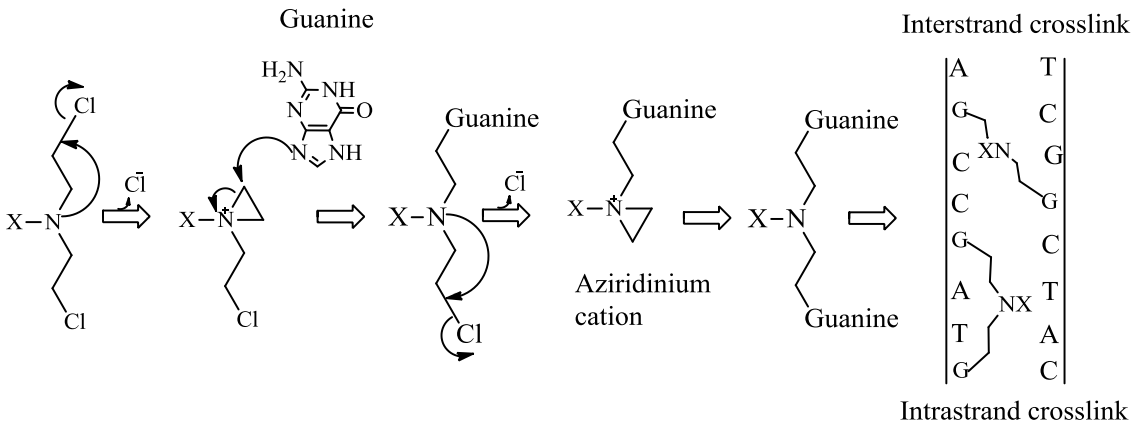

Figure 4. Phosphoramide mustard and its mechanism of DNA cross linking. Figure represents how phosphoramide mustard forms intrastrand and interstrand cross–links between guanine bases from DNA.

B. Hypothesis and approaches

Hypothesis

Since ALDH3A1 is involved in metabolism of aldophosphamide (activated form of cyclophosphamide), we hypothesized that inhibition of catalytic activity of ALDH3A1 using a small molecule inhibitor will increase cyclophosphamide chemosensitivity in cells that express ALDH3A1 as a mode of cyclophosphamide chemoresistance.

Approaches

The overall goal of this work is to identify and characterize selective inhibitors of ALDH3A1 that can enhance the sensitivity of chemotherapeutic agents such as cyclophosphamide as well as tease out the contributions to aldophosphamide metabolism in tumor cells. Several approaches have been used to accomplish the objectives of research: (1) *In vitro* high throughput screen for inhibitor identification (2) Steady state competition assays for determining mode of inhibition (3) X–ray crystallographic studies of enzyme inhibitor complexes (4) Site directed mutagenesis for locating residues crucial for interaction (5) Structure Activity Relationship experiments to map out the basis of selectivity and potency (6) Chemosensitivity experiments in cancer cells that do or do not express ALDH3A1.

II. Materials and Methods

Materials

Chemicals and reagents for the experiments were purchased from Bio–Rad Laboratories (Hercules, CA), Corning Costar (Cambridge, MA), Fisher (Pittsburg, PA), GE Healthcare (Piscataway, NJ), Gibco BRL Technologies (Gaithersburg, MD), Hyclone (Logan, UT), Invitrogen (Carlsbad, CA), Sigma Aldrich (St. Louis, MO), Roche Applied Science (Indianapolis, IN), Santa Cruz Biotechnology Inc. (Santa Cruz., CA), Thermo Scientific (Rockford, IL). PEG3350 was purchased from Hampton Research (Laguna Niguel, CA). Compounds for high–throughput screening were purchased from ChemBridge Corporation and ChemDiv Corporation. Lead compounds were purchased from Enamine Corporation (Kiev, Ukraine) and through the Indiana University Chemical Synthesis Core.

Methods

A. Purification of ALDH3A1

The full–length cDNA for human ALDH3A1 was purchased from Open Biosystems and subcloned into the pET–28a expression plasmid and used to transform *E. coli* BL21 (DE3). The resulting cells were grown in LB medium in the presence of kanamycin (50 μg/ mL final concentration) at 37°C until absorbance at 600 nm reached 0.6. At that point, isopropyl β–thiogalactopyranoside (IPTG; 0.1 mM final concentration) was added to induce the synthesis of ALDH3A1, and the cells were incubated for an additional 16 hours at 16°C, and collected by centrifugation. The cell pellets were resuspended in Buffer A (20 mM sodium HEPES, 300 mM NaCl pH 7.8, 2 mM benzamidine, 1 mM beta–

mercaptoethanol) and lysed by passage through a French Press operated at 13, 000 psi. The lysate was clarified by centrifugation at 100, 000xG for 45 minutes at 4°C in a Beckman Ti45 rotor. The lysate supernatant was loaded onto a nickel–NTA column, and the fractions were eluted using gradient elution of Buffer B (20 mM sodium HEPES, 300 mM sodium chloride, 500 mM imidazole pH 7.8, 2 mM benzamidine, 1 mM betamercaptoethanol). The eluted fractions from the nickel–NTA column were analyzed by SDS gel to confirm the presence of ALDH3A1 protein. Those fractions containing protein were pooled and dialyzed against two changes of Buffer C (10 mM sodium HEPES pH 7.8, 1 mM benzamidine, 1 mM sodium EDTA, and 1 mM dithiothreitol) at 4°C. The dialyzed fractions were loaded onto a Q–sepharose column equilibrated in Buffer C and were eluted using Buffer D (10 mM sodium HEPES, 250 mM NaCl, pH 7.8, 1 mM benzamidine, 1 mM EDTA and 1 mM dithiothreitol). Fractions containing the ALDH3A1 protein were once again pooled and dialyzed against Buffer E (10 mM sodium HEPES pH 7.8, 1 mM dithiothreitol) at 4°C. The dialyzed protein was concentrated using a protein concentrator (Amicon Ultra–0.5 Centrifugal Filter Devices) operated with 30, 000 Dalton molecular weight cutoff membranes. The concentrated protein was filtered, and its concentration and specific activity were determined before flash freezing aliquots in liquid nitrogen and storing at −80°C. ALDH1A1 and ALDH2 protein was purified and kindly provided by Lanmin Zhai.

B. Activity assays for ALDH1A1, ALDH2 and ALDH3A1

The activity of ALDH3A1 was measured using two different methods–oxidation of benzaldehyde and hydrolysis of para–nitrophenylacetate. The dehydrogenase activity

was assayed spectrophotometrically on a Beckman DU–640 by monitoring the increase in absorbance at 340 nm due to NADPH formation (molar extinction coefficient of 6, 220 M^{-1} cm^{-1}) in a solution containing 6.8 nM of ALDH3A1, 1 mM benzaldehyde and 1.5 mM $NADP^+$ in 100 mM sodium phosphate buffer, pH 7.5 (Figure 5). The esterase activity was assayed spectrophotometrically by monitoring the formation of para–nitrophenol at 405 nm (molar extinction coefficient of 18, 000 M^{-1} cm^{-1}) in a solution containing 180 nM ALDH3A1, and 0.8 mM para–nitrophenylacetate in 25 mM sodium HEPES buffer, pH 7.0 (Figure 5).

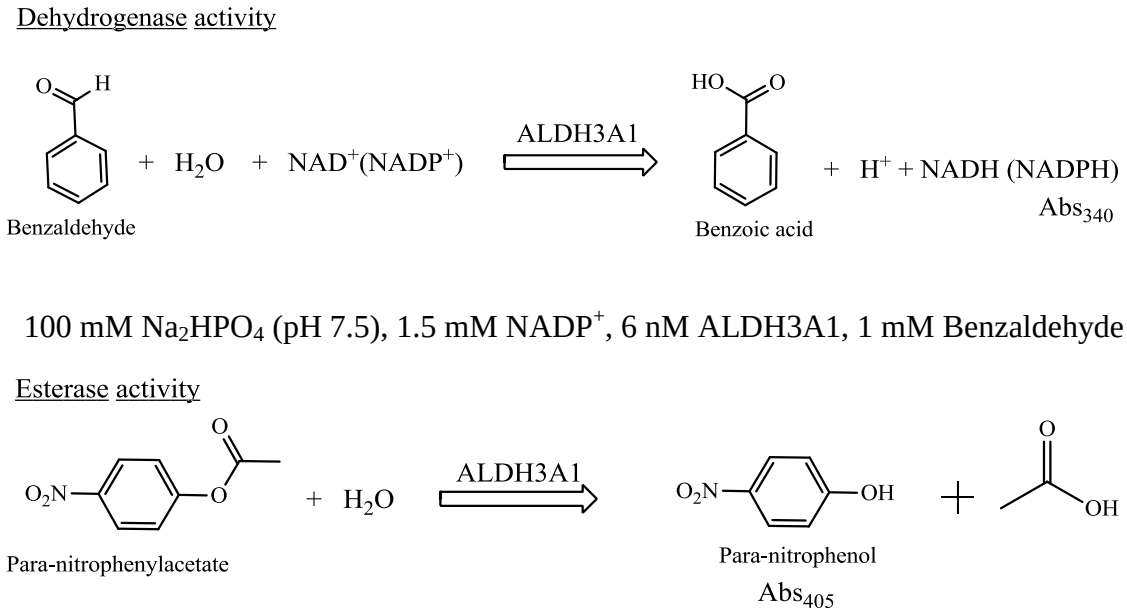

Figure 5. Catalysis of benzaldehyde and para–nitrophenylacetate by ALDH3A1. Figure showing the reaction mechanisms of dehydrogenase and esterase assay catalyzed by ALDH3A1. The standard condition for a 15 minute linear reaction is also shown.

ALDH2 and ALDH1A1 based activity was assayed spectrophotometrically on a Beckman DU–640 by monitoring the increase in absorbance at 340 nm due to NADH formation (molar extinction coefficient of 6, 220 M^{-1} cm^{-1}) in a solution containing 100 nM of ALDH1A1/ ALDH2, 1 mM propionaldehyde and 1.5 mM NAD^+ in 100 mM BES, pH 7.5. All assays were initiated by the addition of substrate, following a preincubation with inhibitors for 2 minutes.

C. High Throughput Screening (HTS) assay

1) Reagent preparation and principle of assay

High–throughput screening was carried out using the esterase assay. This assay is more suitable for screening because the spectral properties of para–nitrophenol do not overlap with the absorbance and fluorescence characteristics of most compounds in the library. The substrate 4 mM para–nitrophenylacetate is prepared by adding 0.0725 grams of substrate powder in 6 mL of 100 % DMSO solvent. The substrate volume is then increased to 100 mL by adding 94 mL of water. Enzyme is diluted to a concentration of 0.045 mg/ mL using buffer 10 mM HEPES, pH 7.5, 10 µM DTT. Aldi–3 stock for the experiment was prepared such that final solution had 10 µM compound contained in 2% DMSO.

2) Z' Factor Measurement

A standard statistical value known as the Z' factor, which reflects the reliability of the screen, was calculated before initiating the high–throughput screen. A Z' factor value between 0.5 and 1.0 is an indication of an excellent assay, and a value between 0 and 0.5 is

an indication of a poor assay (Zhang et al., 1999). To calculate the Z' factor measurement, positive and negative control reactions were carried out in 384 well plates. The control reaction included 800 µM para–nitrophenylacetate, 0.009 mg/ mL of ALDH3A1 contained in 25 mM HEPES, pH 7.0 (2% DMSO) in a 50 µL reaction volume. The inhibition reaction included all the above mentioned components as well as 10 µM of Aldi–3 (Khanna et al., 2011). Aldi–3 is a covalent inhibitor of aldehyde dehydrogenase that forms adduct with the active site cysteine (Cys243) of ALDH3A1 and inhibits it activity (Khanna et al., 2011). The assay was carried out for 15 minutes and then the rates of the control and inhibition reactions (384 points for each set of reactions) were used to calculate the Z' factor using the following formula:

$$Z' \text{ factor} = 1 - \frac{3(\delta p + \delta n)}{(\mu p - \mu n)}$$

Where δp= standard deviation of the control reaction, δn= standard deviation of the inhibition reaction, µp= average of the points in the control reaction and µn=average of the points in the inhibition reaction (Zhang et al., 1999).

3) HTS assay to identify potential inhibitors of ALDH3A1

Library of diverse drug–like compounds that follow Lipinski's rule (Lipinski et al., 2004) were screened at the Indiana University Chemical Genomics Core Facility. The chemical library was composed of 101, 000 compounds, among which 64, 000 were from ChemDiv Corp. and 37, 000 were from ChemBridge Corp. All the compounds were present in 10 µL aliquots in 2% DMSO at 50 µM concentration in a 384 well plate format. The Genesis (Tecan) Workstation 150, TeMo with a 96–channel pipetting head was used to make all the reagent additions. Screening was done on 384 well clear bottom plates

using the esterase assay by monitoring the absorbance of para–nitrophenol at 405 nm wavelength in a 50 µL assay containing 180 nM ALDH3A1, 0.8 mM para–nitrophenylacetate, 10 µM library compound, 2% DMSO and 25 mM sodium HEPES buffer, pH 7.5 (all final concentrations) on a Spectromax Plus 384 plate reader over a 10–minute period. The reaction was initiated by the addition of substrate (para–nitrophenylacetate). Every assay plate included one column each for the positive and negative control for the assay. The negative control lane contained the enzyme with no inhibitors but 2% DMSO whereas the positive lane contained 5 µM Aldi–3 incubated with ALDH3A1. DMSO (2%) had no effect on ALDH3A1 activity under this condition. The rates of reaction were used to determine percent inhibition, and the rate of reaction for ALDH3A1 protein without inhibitors was considered as the 100% control. Subsequent inhibition by compounds was considered relative to that of the control.

$$\% \text{ activity} = \frac{rate\ of\ reaction\ with\ inhibitor}{rate\ of\ reaction\ without\ inhibitor} * 100$$

Compounds that showed more than 60% inhibition in the primary screen were taken for secondary screening to validate the inhibition. Compounds whose inhibition could be reproduced were further tested for their ability to inhibit the dehydrogenase, assayed with the Beckman DU–640 UV–Vis spectrophotometer. Basic selectivity for the inhibitors was tested using purified recombinant ALDH1A1 and ALDH2 enzymes. ALDH1A1 and ALDH2 activities were assayed spectrophotometrically by monitoring the absorbance at 340 nm in a solution containing 1.5 mM NAD^+, 200 µM propionaldehyde, 10 µM inhibitors, 0.16 µM of enzyme, in 25 mM sodium BES buffer, pH 7.5 (Weiner et al., 1976; Parajuli et al., 2011; Perez Miller et al., 2003). Compounds that

strongly inhibited ALDH3A1 and only minimally inhibited ALDH1A1 and ALDH2 were selected for IC_{50} determination.

IC_{50} values were further determined against propionaldehyde oxidation (for ALDH1A1 and ALDH2) or benzaldehyde oxidation (for ALDH3A1). This was performed spectrophotometrically on a Beckman DU–640 by monitoring NAD(H) or NAD(P)H formation (molar extinction coefficient of 6220 $M^{-1}cm^{-1}$ at 340 nm) over time at various concentrations of inhibitors ranging from 50 nM to 250 µM following a 1 minute pre–incubation. All reactions were initiated by the addition of the aldehyde substrate. The inhibition curves were fit to the Logistic four parameter IC_{50} equation using the sigma plot (v11, StatSys). All data represent the average of three independent sets of experiments with each set of experiments performed twice.

D. Structural classification of compounds

A series of compounds that independently emerged from the screen had similarity in their molecular structures in at least 50% of their atomic positions. These compounds were all classified under different categories based on these similarities. Some of the compounds, however, had no similarities with each other at all. IC_{50} values were determined for ALDH3A1, ALDH2 and ALDH1A1 based dehydrogenase assay for all these related analogs. Specificity of these compounds was tested as well against ALDH1A1 and ALDH2.

E. Steady–state kinetic characterization

We characterized the mode of inhibition using steady–state kinetics through covariation of inhibitor and substrate concentrations. However, before doing that K_m (con-

centration required for half maximal velocity) values were determined for both benzaldehyde and $NADP^+$. The steady state kinetic measurements were then performed in 100 mM Na_2HPO_4 buffer, pH 7.5. The reaction mixture contained 10 nM ALDH3A1, varied $NADP^+$ (50 µM–1 mM; fixed benzaldehyde, 1 mM) or varied benzaldehyde (50 µM–800 µM; fixed $NADP^+$, 1.5 mM) and varied inhibitor concentrations. In all cases including the control reactions lacking inhibitors, the final reaction mixture contained 2% (v/ v) DMSO. The reaction was initiated by addition of substrate, and the initial rate of formation of product was determined on a Beckman DU–640. All data were fitted to selected kinetic expressions for competitive, non–competitive, mixed–type non–competitive and uncompetitive inhibition. Appropriateness of the inhibition model was determined through analysis of goodness–of–fit and the residuals of those fits. Lineweaver–Burke plots were created using Sigma Plot (v11, StatSys) to visualize the inhibition patterns. All data represent the average of three independent experiments utilizing duplicate assays at each concentration point.

F. Search for structurally related analogs

A structural search was performed using Pubchem (Kaiser et al., 2005) and Scifinder software in order to identify commercially available analogs with at least 90% structural similarity on their atomic positions with the lead compounds CB7 and CB29. Several compounds were purchased from ChemBridge Corp. and ENAMINE Ltd., Kiev, Ukraine and Indiana University Chemical Synthesis and Organic Drug Lead Development Core. The purity of the compounds according to the vendor was >95%. Compounds were dissolved and diluted in 100% DMSO and stored at -20ºC. The analogs were tested

for their selectivity against ALDH1A1 and ALDH2 and ALDH3A1 at 100 µM concentrations. IC_{50} values were determined for the analogs with significant selectivity. The first class of compounds had N–[4–{(4–(methylsulfonyl)–2–nitrophenyl) 4amino} phenyl] acetamide group as a basic pharmacophore. Analogs related to this group were named as follows: A1– (ChemBridge Corp.– 5119656), A18– (ENAMINE– T5477155), A57– (ChemBridge Corp.– 6809058), B1– (ENAMINE– T56333437), B2– (ENAMINE– T5477154), B4– (ENAMINE–T5395179), B5– (ENAMINE–T5237743), B6– (ENAMINE–T05126153), B9– (ENAMINE– T5804455), B10– (ENAMINE– T5662523), B11– (ENAMINE– T5655673), B13– (ENAMINE– T6245968), B15– (ENAMINE– T6241917), B16– (ENAMINE– T6053724), B17– (ENAMINE– T6036772), B18– (ENAMINE– T6032083), B19– (ENAMINE– T6266966), B21– (ENAMINE– T6560452), B22– (ENAMINE– T6536700), IUSC–12415, IUSC–12416 and IUSC–12417. The second class of compounds had 1–{(4–fluorophenyl) sulfonyl}–2–methyl–1H–benzo[d]imidazole group as a basic pharmacophore. Analogs related to this group were named as follows:

Compounds	Vendors with ID numbers
A3	(ChemBridge Corp.–5172826)
A5	(ChemBridge Corp.–5172831)
A6	(ChemBridge Corp.–5175600)
A10	(ChemBridge Corp.–5215982)
A13	(ChemBridge Corp.–5231103)
A16	(ChemBridge Corp.–5243439)
A20	(ChemBridge Corp.–5260321)
A21	(ChemBridge Corp.–5264371)
A22	(ChemBridge Corp.–5284379)

A24	(ChemBridge Corp.–5510049)
A30	(ChemBridge Corp.–5607189)
A38	(ChemBridge Corp.–5648440)
A39	(ChemBridge Corp.–5651872)
A40	(Vitas M. Laboratories.–STK354007)
A47	(ChemBridge Corp.–6104618)
A53	(ChemBridge Corp.–6382505)
A62	(ChemBridge Corp.–7224032)
A64	(ChemBridge Corp.–7289639)
A67	(ChemBridge Corp.–7567094)
A70	(ChemBridge Corp.–7928260)
B27	(Vitas M. Laboratories.–STK454495)
B36	(ChemDiv Corp. 6529–0359)
B37	(ChemDiv Corp. K783–5471)
CB7	(ChemBridge Corp.–5613645)

G. Site directed mutagenesis

In order to characterize the binding pattern of CB7 to the catalytic site of ALDH3A1, two important mutations were made. Point mutations of ALDH3A1 were performed using QuickChange (Qiagen) mutagenesis. ALDH3A1 mutants were constructed using forward primer 5'–CTT CAA CCT CAC CAT CGC GCC CAT GGT GGG CGCC–3' and complement for Q122A and forward primer 5'–CCT TCA ACC TCA CCA TCT GGC CCA TGG TGG GCG CCA TC–3' and complement for Q122W mutant. These two mutant proteins were purified exactly the same way as was ALDH3A1. Mutants were frozen in 50mM NaCl. However, the yield was significantly decreased as compared to WT protein. Q122A was stored at 0.9 mg/ mL concentration

and Q122W was stored at 0.4 mg/ mL concentration at -80ºC. Kinetic experiments were performed exactly the same way as WT enzyme.

H. Preparation and crystallization of ALDH3A1 with compounds

ALDH3A1 crystals were grown in solution containing 0.2 M potassium acetate, 20% PEG 3350 at a temperature of 25ºC. The enzyme concentration was 3–3.5 mg/ mL, in 10 mM HEPES buffer, pH 7.5. Various crystal morphologies form under these conditions. CB29–ALDH3A1 complex crystal was obtained in P1 space group (triclinic crystal), CB25–ALDH3A1 co–crystal was obtained in $P2_12_12_1$ space group (orthorhombic crystal) and CB7–NAD^+–ALDH3A1 co–crystal was obtained in $P2_1$ space group (monoclinic crystal). Crystal of different morphologies were obtained for each complexes because CB29–ALDH3A1 complex crystal was obtained by soaking experiment, CB25–ALDH3A1 complex crystal was obtained by co–crystallization and CB7–ALDH3A1 was obtained in the presence of NAD^+. The triclinic ALDH3A1 crystals were initially soaked with 2% DMSO for 24 hours followed by another 24 hour soak with 500 µM CB29 [2% (v/ v) DMSO final]. Initial soak with DMSO was performed because direct soaking with 500 µM CB29 in 2% (v/ v) DMSO cracked the apo–crystals. Crystal for CB25–ALDH3A1 was obtained using co–crystallization method by using 500 µM CB25 co–crystallized with 4 mg/ mL of ALDH3A1 using the sitting drop method. These crystals were orthorhombic plates. The third crystal structure of CB7 bound to ALDH3A1 along with NAD^+ were obtained using 1 mM NAD^+, 1000 µM CB7 and 4 mg/ mL of ALDH3A1. The drop size was 8 µL with 1000 µLs of mother liquor. All these crystals were obtained using the sitting drop method. Crystals were directly frozen without using

any cryoprotectant. Datasets were collected at a wavelength of 0.9869 Å and at 100 K at the Advanced Photon Source using the GM/ CA–CAT beamline 23–ID located at Argonne National Laboratory. The diffraction data was indexed, integrated and scaled using the HKL3000 program (Minor et al., 2006). All refinements were performed using the program package REFMAC5 as implemented in the CCP4 program suite (Minor et al., 2006) and model inspection and building was accomplished using COOT (Emsley et al., 2004). All these structures were solved by performing molecular replacement using the apo–form of ALDH3A1 structure as the search model (RCSB code 3SZA). Molecular replacement was performed using MolRep program provided by CCP4 Interface software. Initial maps showed clear electron density for the corresponding ligand bound on the active site of each monomer in the asymmetric unit. Atomic co–ordinates of bound ligands were included in later stages of refinement. Water molecules were added after the addition of ligands in order to obtain an unbiased map for ligands. Ligand maps were sketched in Sketcher (provided by CCP4). This structure was used to create library description file (cif file– defining the bond angle, bond lengths, etc.) and a coordinate file for the ligand, which were later used for refinement.

I. Cell culture

Lung adenocarcinoma (A549), SF767 and CCD13–Lu cell lines were provided by Dr. Hua Lu, Dr. X. Charlie Dong, Dr. Karen Pollok and Dr. Melissa L. Fishel respectively. A549, HEK–293 and CCD13Lu cells were cultured in 1X DMEM (Cellgro, Mediatech Inc, Manassa, VA) supplemented with 10% fetal bovine serum (FBS) (Gibco, Invitrogen Company, Grand Island, NY), 100 units/ mL of penicillin and 10 µg/ mL of strep-

tomycin. SF767 cell lines were cultured in 1X IMDM (Gibco, Invitrogen Company, Grand Island, NY) supplemented with 10% fetal bovine serum (FBS) (Gibco, Invitrogen Company, Grand Island, NY), 100 Units/ mL penicillin and 10 µg/ mL streptomycin. The multiple myeloma (MM) cells U266, H929 and RPMI–8226 were kindly provided by Dr. Attaya Suvannasankha. These cell lines were cultured in RPMI 1640 media (Gibco, Invitrogen Company, Grand Island, NY) and supplemented with 10% heat–inactivated fetal bovine serum (FBS) (Gibco, Invitrogen Company, Grand Island, NY), 100 units/ mL penicillin and 10 µg/ mL streptomycin. Cell viability as assessed by tryphan blue exclusion was consistently >95%. Cells were passaged after every 80–90% confluence.

J. Cell lysate activities in the presence and absence of ALDH3A1 inhibitors

Cells (A549, HEK–293, SF767 and CCD13Lu) were washed with ice cold PBS to remove residual media. 400 µL of RIPA buffer (Cell signaling technologies) containing 1 mM PMSF (Sigma Aldrich) was added to each 10 cm dish. Plates were incubated on ice for 5 minutes. Plates were scraped and lysates were collected. Lysates were centrifuged for 10 minutes at 16, 000xG in a micro–centrifuge at 4°C. Protein concentrations of the supernatant were measured using the Bradford reagent (Biorad Laboratories). 50 µg of cell lysate was used in the activity assay. We calculated the activity of cell lysates using 1.5 mM $NADP^+$ (co–factor) and 1 mM benzaldehyde (substrate) and reaction buffer (100 mM Na_2HPO_4, pH 7.5). Reaction was blanked with cell lysate containing 1 mM benzaldehyde and reaction buffer (100 mM Na_2HPO_4, pH 7.5) without $NADP^+$. This was performed to blank any ALDH associated activity that could be contributed by NAD^+ that is present in cell lysates. ALDH3A1 activity in cell lysates were measured in 100 mM

Na_2HPO_4 buffer at pH 7.5, with 1.5 mM $NADP^+$ and 1 mM benzaldehyde. Activity assay was also performed with 1 µg of recombinant ALDH3A1 in the presence and absence of ALDH3A1 inhibitors. This was performed to normalize the amount of ALDH3A1 present in cell lysates from cancer cells. All assays contained 1% (v/ v) DMSO. Lysates were treated with these compounds for 1 minute before the substrate was added and measurements were taken.

K. Western blot analysis

Cells (A549, HEK–293, SF767 and CCD13Lu) cells were washed with ice cold PBS to remove the residual media. 400 µL of RIPA buffer (Cell signaling technologies) containing 1 mM PMSF (Sigma Aldrich) was added to each 10 cm dish. Plates were incubated on ice for 5 minutes, scraped and lysates were collected. Lysates were subjected to sonication for 30 seconds and centrifuged for 10 minutes at 16, 000xG in a micro–centrifuge at 4°C. Protein concentrations were measured using the Bradford reagent (Bio-rad Laboratories). A549, HEK–293, SF767 and CCD13Lu cell lysates were resolved by 10% SDS–PAGE. Protein was transferred to 0.2 µm nitrocellulose membrane (Schleicher & Schuell, Keene, NH) and subsequently blocked with 5% (w/ v) nonfat dry milk dissolved in TBS–T (20 mM Tris/ HCl (pH 7.9), 150 mM NaCl, and 0.05% Tween 20) solution for 1 hour at 25 ºC. This was followed by an overnight incubation at 4º C with primary antibody specific for ALDH3A1 (Santa Cruz Biotechnology, sc–67310) at a dilution of 1: 5000 in 5% (w/ v) nonfat dry milk. ALDH1A1 was detected using primary antibody (ab–23375, Abcam) at a dilution of 1: 1000 in 5% (w/ v) nonfat dry milk overnight at 4º C. Blots were washed with TBS–T three times, 15 minutes each and were sub-

sequently incubated with secondary antibody (sc–2054 for ALDH3A1 and ab6721 for ALDH1A1) at a dilution of 1: 5000 for 1 hour at 4º C. GAPDH was taken as a loading control. GAPDH was blocked with 1.25% of filtered milk solution. GAPDH was detected using primary antibody (ab9484 diluted in 1.25% filtered milk in a ratio of 1: 5, 000) followed by secondary antibody (ab6728 diluted in 1.25% filtered milk in a ratio of 1: 5000). Proteins bound to antibodies were visualized using HRP chemiluminescence immunoblot detection solution prepared in lab. HRP chemiluminescence solution is made up of mixture of solution 1 and solution 2 in a ratio of 1: 1. Solution 1 contains (50 µL of 2500 mM Luminol, 22 µL of 90 mM Coumaric acid, 0.5 mL of 1M Tris pH 8.5, and 4.46 mL of deionized water. Similarly, solution 2 contains 3 µL of hydrogen peroxide dissolved in 0.5 mL of 1M Tris pH 8.5, and 4.5 mL of deionized water. The mixed HRP solution was incubated for a minute before adding it to the nitrocellulose blot incubated with primary and secondary antibody. All experiments were performed in triplicates.

L. MTT assay to evaluate cell proliferation

The MTT assay was used to measure the extent of mafosfamide chemosensitivity. Mafosfamide was used for this study primarily because it is an analog of cyclophosphamide that does not require cytochrome P450 for its activation, which is ideal for cell based studies (Blaney et al., 2005). The MTT assay was optimized for each cell line such that the number of cells utilized for the experimental treatments corresponded to the linear range of the assay measurements. The results of these standardization measurements indicated that 5000 cells/ well was optimal for A549 and CCD13Lu and 10, 000 cells/ well was optimal for the HEK–293 and SF767 cell line. An optimization trial was per-

formed for lung adenocarcinoma (A549), glioblastoma (SF767), human embryonic kidney (HEK–293) and lung fibroblast (CCD13Lu) cell line to find the approximate ED_{50} value of mafosfamide (Niomech– IIT GmbH, Bielefeld, Germany); 125 μM for A549 cells, 150 μM for SF767 cells, 80 μM for HEK–293 and 40 μM for CCD13Lu cell line (Figure 28). Following optimization, A549 (5, 000 cells/ well), HEK–293 (10, 000 cells/ well), SF767 (10, 000 cells/ well) and CCD13Lu (5000 cells/ well) cells were seeded in 96 well plates. After 29 hours, A549 and SF767 cells were treated with ALDH3A1 inhibitors in the absence or in the presence of 125 μM mafosfamide. HEK–293 and CCD13Lu cells were treated with ALDH3A1 inhibitors in the absence or in the presence of 80 μM and 40 μM mafosfamide respectively. The MTT assay was carried out following 19 hours of incubation with the inhibitors and/ or mafosfamide. To visualize cellular proliferation, 0.01 mL of MTT (Millipore CT01–5, 50 mg/ mL in PBS) was added to each well, and the cells were incubated for 2–3 hours at 37º C to allow for the reduction of MTT. Isopropanol with 0.04 N HCl (100 μL each) was added and mixed thoroughly for color development. After an additional hour of incubation, the absorbance was measured at 570 nm using a reference wavelength at 630 nm. For the calculation, absorbances measured at 570 nm were corrected through background subtraction using the absorbance at 630 nm. The relative percentage of cell proliferation was calculated in comparison to DMSO (0.25%) treated controls. The time points for treatment were chosen based on similar experiments performed earlier (Khanna et al., 2011).

III. Results

A. Protein purification

His–tagged ALDH3A1 was cloned onto pET28a vector by our lab member Dr. Sulochanadevi Baskaran. ALDH3A1 protein was purified using Ni–NTA affinity followed by Q–sepharose column. Upon IPTG induction (50 µg/ mL), we saw expression of ALDH3A1 (Figure 6A). Protein was loaded to a Ni–NTA column and was eluted using an imidazole gradient as shown below. These fractions were run on a 10% SDS–PAGE gel to analyze the fractions that had ALDH3A1 (Figure 6B). Fractions that showed maximal expression of ALDH3A1 with minimal contamination of other proteins (fractions 12–18) were pooled together and dialyzed against Buffer C (10 mM sodium HEPES pH 7.8, 1 mM benzamidine, 1 mM sodium EDTA, and 1 mM dithiothreitol) at 4°C.

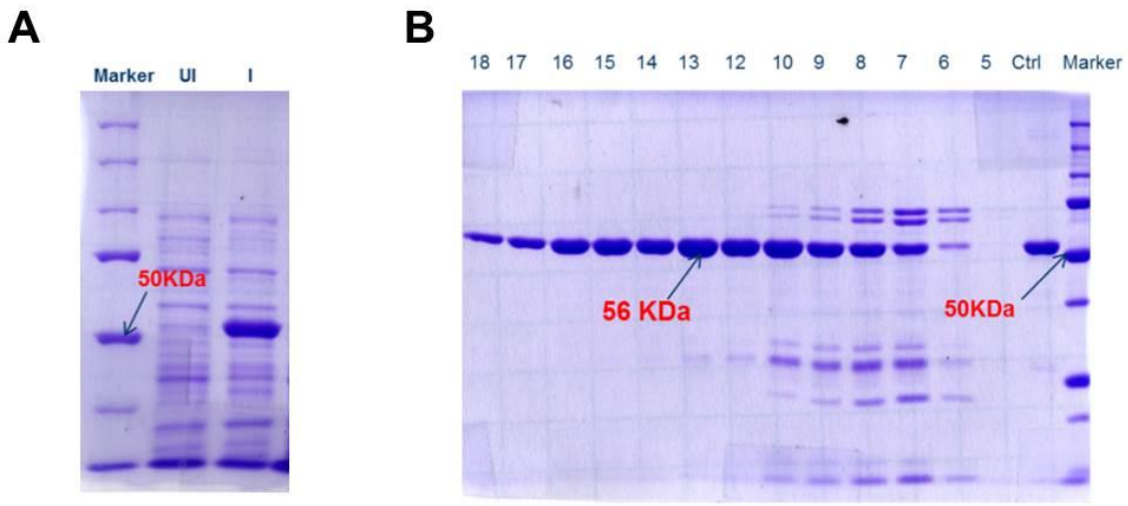

Figure 6. SDS–PAGE for Ni–column fractions. (A) ALDH3A1 expression after induction with IPTG. **(B)** Fractions of ALDH3A1 ran on SDS PAGE gel after running it through the nickel column.

The dialyzed fractions were loaded onto a Q–sepharose column equilibrated in Buffer C and then eluted using gradient of Buffer D (10 mM sodium HEPES, 250 mM NaCl, pH 7.8, 1 mM benzamidine, 1 mM EDTA and 1 mM dithiothreitol). Several fractions were collected from the Q column and again run on 10% SDS–PAGE gel to analyze the fractions that had ALDH3A1 (Figure 7). Proteins eluted from the Q–column showed almost no contamination of any other protein except for ALDH3A1. Pure protein (fraction 15–23) were pooled together, concentrated up to 4 mg/ mL and stored at -80ºC. Standard activity assay conditions were optimized for ALDH3A1 activity.

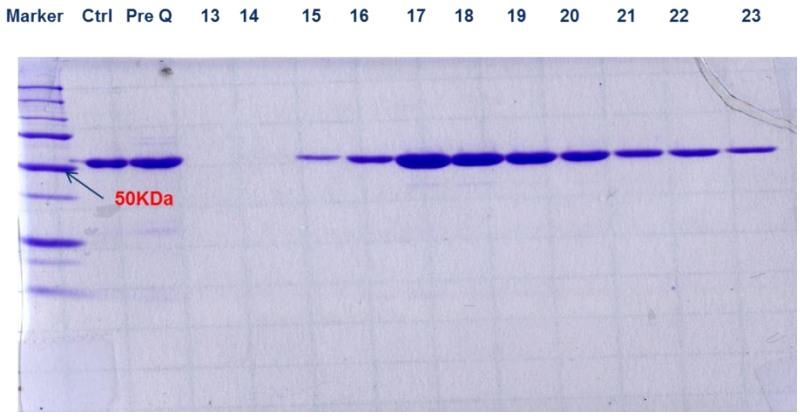

Figure 7. SDS–PAGE for Q–column fractions. ALDH3A1 fractions collected after running it through Q column fractions were pure with optimal specific activity (32 U/ mg).

Assay condition for determining the activity of ALDH3A1

	Final conc.	Volume
100mM Na_2HPO_4, pH 7.5	100 mM	920 µL
75 mM $NADP^+$	1.5 mM	20 µL
25 mM Benzaldehyde	2.5 mM	40 µL
ALDH3A1	15 nM	20 µL

B. Z' score calculation

For high throughput screening, we used an assay system based on the inherent esterase activity of ALDH3A1. The esterase assay was selected for the primary screening assay because the absorbance of para–nitrophenol at 405 nm has minimal spectral overlap with the absorbance characteristics of the majority of compounds in the chemical library. In addition, the catalytic requirements for ester hydrolysis overlap with those required for propionaldehyde oxidation. Several optimization trials were performed before the screen. An assay condition containing 800 μM para–nitrophenylacetate, 0.009 mg/ mL of enzyme in 25 mM BES, pH 7.5 with 2 μM DTT was optimal for screening. 10 μM Aldi–3 was added to the solution as a positive control. DTT was essential for the reaction since it is a reducing agent and keeps active site Cys302 in a reduced condition. Reactions that had no DTT showed ~40–50% less activity than the ones with DTT. Under this condition, the reaction was linear for 30 minutes and <10% of substrate was used. Using this assay condition, a Z' experiment was conducted using 384 plate systems. Z' is a measure that tells us how good a screen is. A score of more than 0.5 is equivalent to a separation of 12 standard deviations between μp and μn. Our Z' score was 0.56 under these conditions (Figure 8).

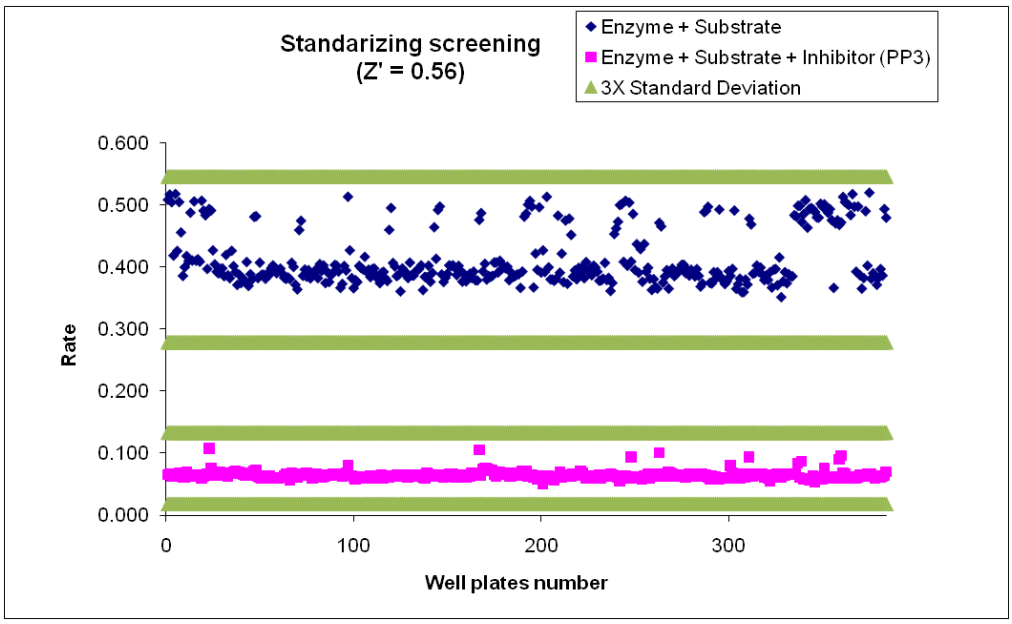

Figure 8. Z' score calculation. Experiment for optimization of Z' score before conducting high throughput screen. Enzyme substrate activity in the presence and absence of inhibitor Aldi–3 (covalent inhibitor of ALDH3A1) was calculated which did not show overlap up to 12 standard deviations.

C. High throughput screen results

I performed a primary screen of 101, 000 compounds available from two commercial libraries (ChemDiv and ChemBridge). We had 64, 000 compounds available from ChemDiv library and 37, 000 compounds available from ChemBridge library. For our initial screen, we considered a compound as a hit if it showed an inhibition greater than 60% as compared to the control. Screening was performed in 384 well plates that had 16 rows and 24 columns. The first 22 columns in 384 well plates had 10 micromolar concentration of compound stock solution which was tested for inhibition of ALDH3A1

activity. An example of one of the 384 screening well plate screened is shown below (Figure 9).

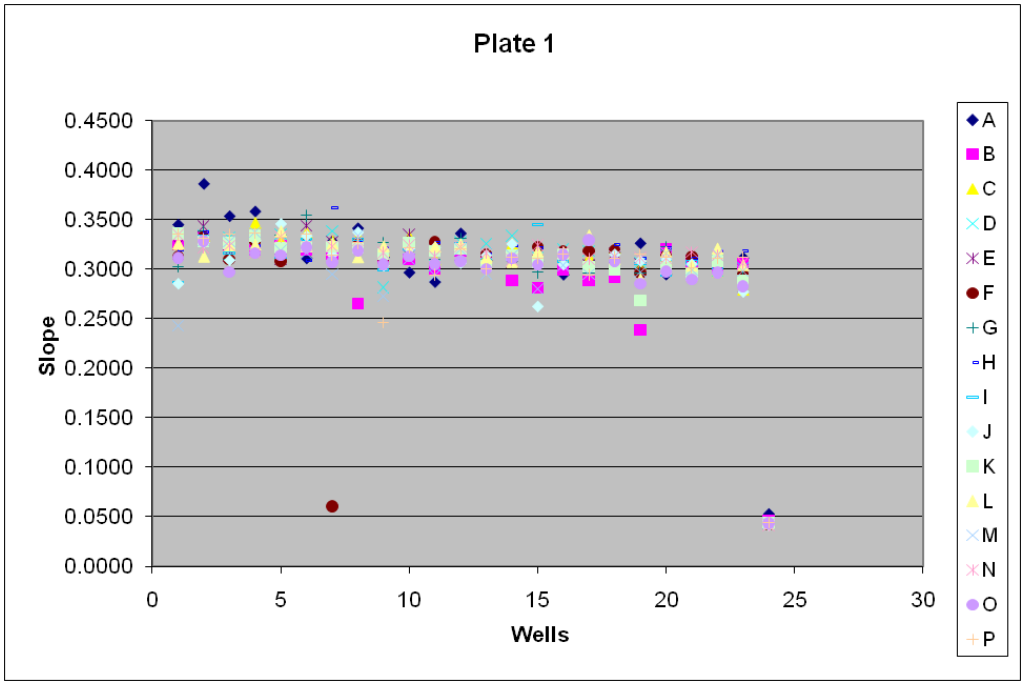

Figure 9. Screening result from one of the 384 well plates screened. X axis shows the corresponding column number in 384 well plates and Y axis shows the activity. Brown dot at F7 position shows a hit. Column 24 shows positive control for inhibition by Aldi3.

In the first round of screening, 436 compounds were identified as potential inhibitors. These compounds were cherry–picked from master plates and rescreened. Only 71 compounds reproduced the inhibitory potency on our second round of assay. Rescreening of these compounds using benzaldehyde oxidation as the assay yielded 55 inhibitors that inhibited ALDH3A1 in both assays. All of the active compounds had molecular masses ranging between 300 and 600 Da; some sharing the same core structures. The independ-

ent identification of compounds with similar core structure provides confidence that our screen has identified genuine ALDH3A1 inhibitors. These 55 compounds were classified into 11 different categories based on their structures, though some compounds were unique and lacked structural homologs in the initial inhibitor list. We determined IC_{50} values for both the benzaldehyde oxidation and ester hydrolysis reactions for the best inhibitor prototype within each class of inhibitor. To assess the potential selectivity of these inhibitor compounds, we tested their ability to inhibit aldehyde oxidation of both ALDH1A1 and ALDH2. Steps for screening are summarized by Figure 10.

S. No.	Steps for screening	Compounds
1	In–vitro kinetic screen using esterase assay	101, 000
2	Compounds with >60% inhibition	436
3	Secondary screen by cherry–picking the initial hits	71
4	Validation of inhibitors using dehydrogenase assay	55
5	Structural classification of compounds	55
6	Testing specificity against ALDH1A1 and ALDH2	55
7	IC_{50} determination	3
8	Selective inhibitors	2

Figure 10. Various steps for high throughput screen. Different steps of high throughput screening for identification and validation of selective inhibitors of ALDH3A1.

Out of the two screens we looked at, we were not able to get isozyme selective inhibitor for ALDH3A1 from the ChemDiv library (64, 000 compounds). Therefore, we screened ChemBridge library (37, 000 compounds) to look for isozyme selective inhibitors. Overall, a variety of structures were obtained from our screen (Figure 11 and Figure 12).

		IC_{50} (micromolar)		
		ALDH1A1	ALDH2	ALDH3A1
CD4	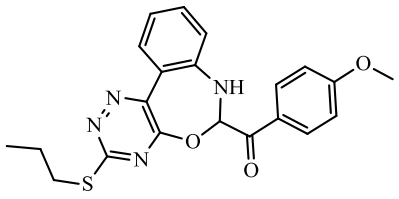	21.2	1.4	2.5
CD5	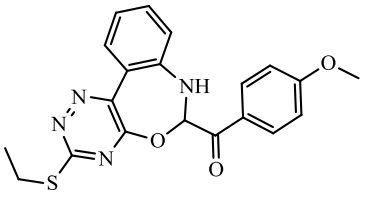	8.2	1.2	1.5
CD7	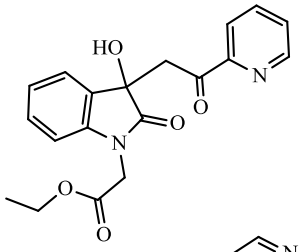	0.7	NI	25.5
CD8	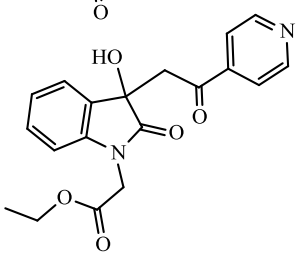	0.8	11.1	6.3
CD10	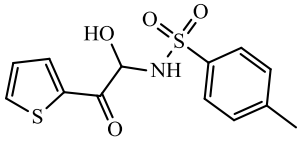	4.0	2.2	3.4
CD11	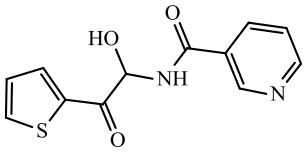	5.9	6.5	10.2
CD12	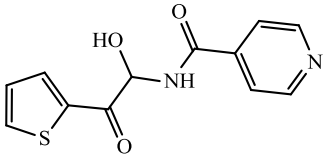	4.2	5.3	5.6

Figure 11. Structure of inhibitors that emerged from ChemDiv screen. Lot of the compounds that emerged as inhibitors from the screen showed structural similarity with each other.

		IC_{50} (micromolar)		
		ALDH1A1	ALDH2	ALDH3A1
CD3	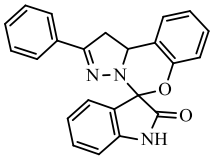	6.5	41.8	38.5
CD13	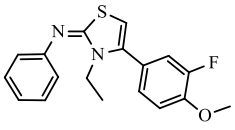	6.3	7.3	60
CD14	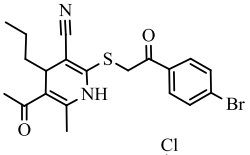	10.4	13.7	71.5
CD20	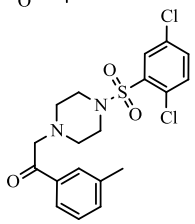	33	NI	41

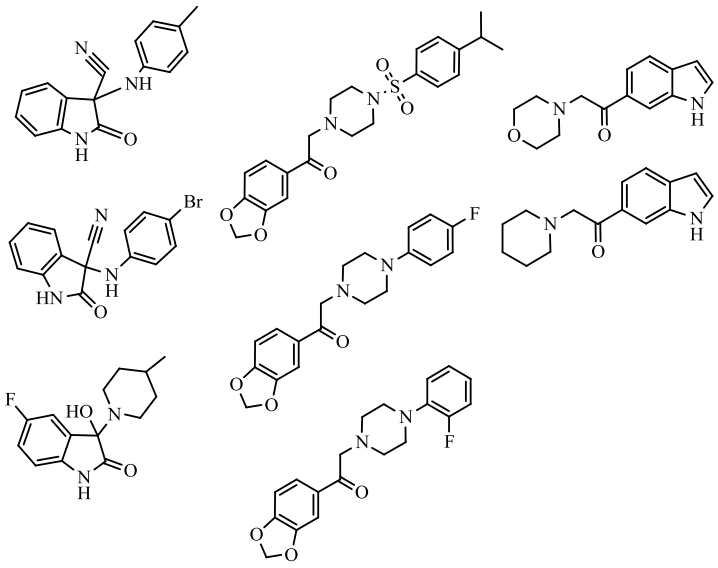

Figure 11 (Continued). Structure of inhibitors that emerged from ChemDiv screen. Lot of the compounds that emerged as inhibitors from the screen showed structural similarity with each other.

		Inhibition patterns		
		% inhibition @ 10 micromolar concentration		
		ALDH1A1	ALDH2	ALDH3A1 IC_{50} (micromolar)
CB1	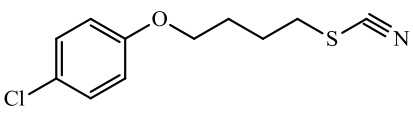	>50%	NI	3.7
CB2	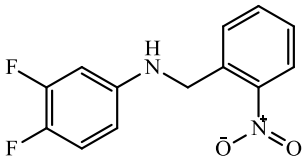	<20%	NI	5.2
CB7	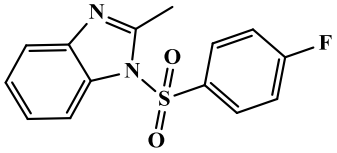	**NI**	**NI**	**0.2**
CB12	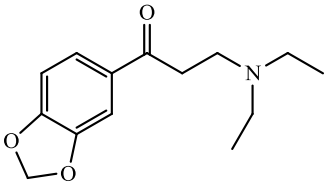	NI	>50%	3.2
CB13	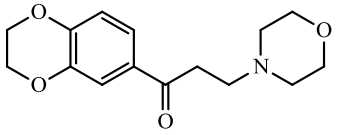	<20%	NI	11.7
CB29	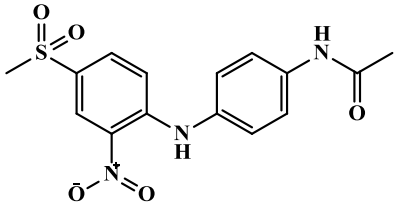	**NI**	**NI**	**4.0**

Figure 12. Structure of inhibitors that emerged from ChemBridge screen. Chem-Bridge screen, despite having less number of compounds (37,000) than ChemDiv screen (64,000), provided us more hits and gave us two selective ALDH3A1 inhibitors CB7 and CB29 shown above.

		% inhibition @ 10 micromolar conc.		(IC_{50} micromolar)
		ALDH1A1	ALDH2	ALDH3A1
CB15	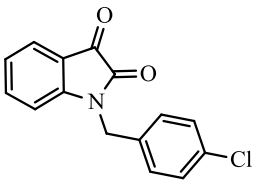	>50% Inh	NI	1.5
CB20	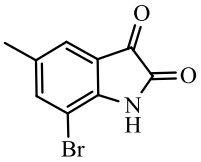	>50% Inh	>50% Inh	0.8
CB34	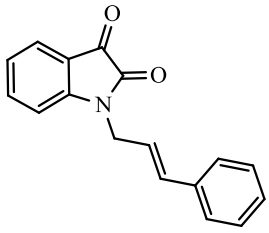	>50% Inh	NI	0.4
CB22	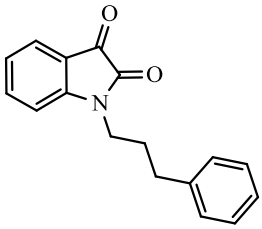	>50% Inh	NI	0.8
CB25	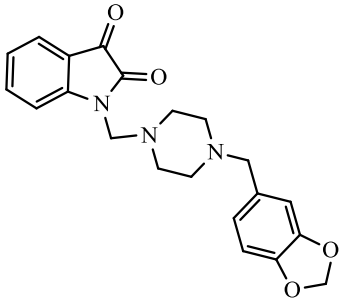	20	NI	4.5

Figure 12 (Continued). Structure of inhibitors that emerged from ChemBridge screen. A family of compounds having indole–2,3–dione group emerged as ALDH inhibitors, which showed varying degree of ALDH1A1 and ALDH3A1 inhibition based on minor substitutions at various positions.

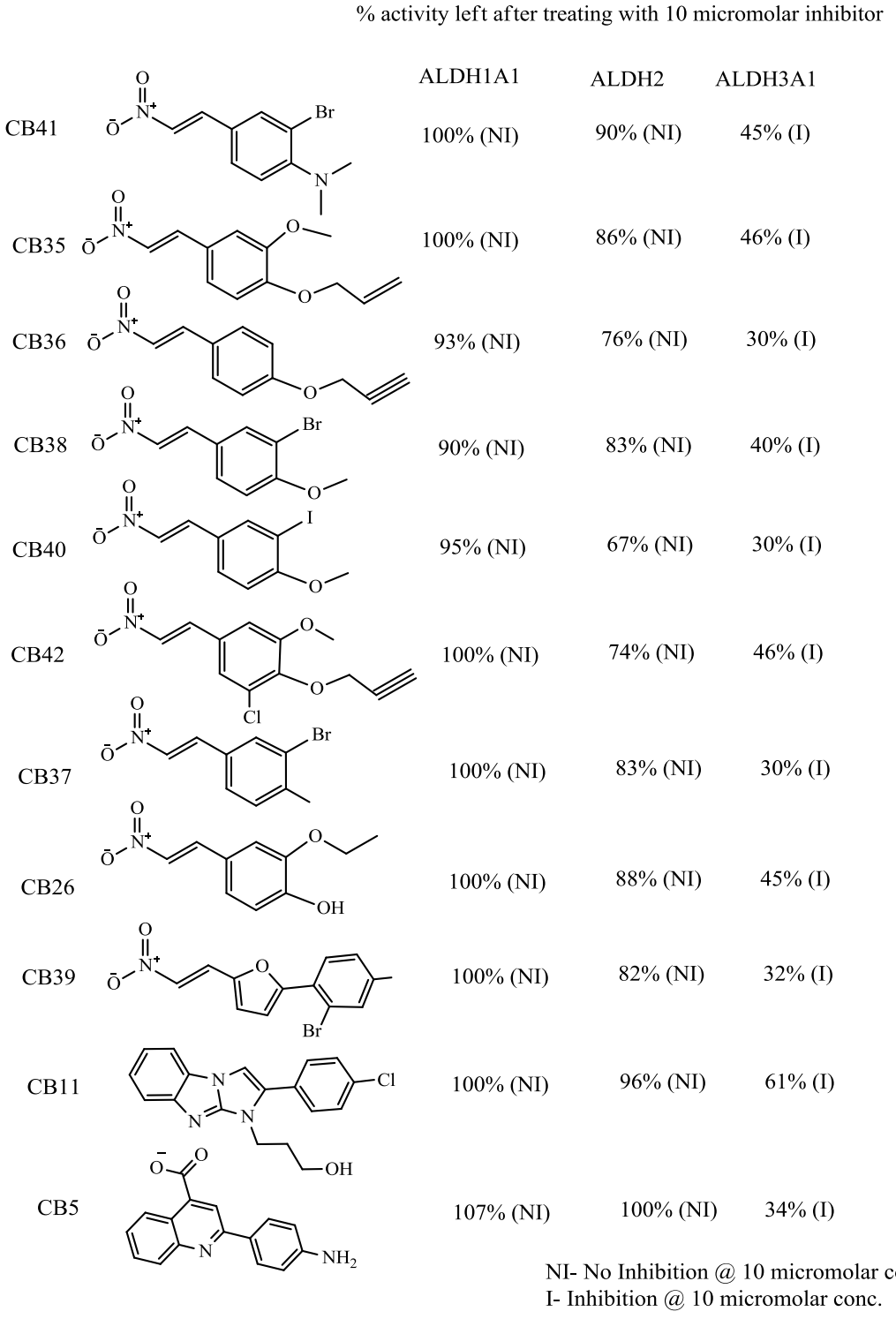

Figure 12 (Continued). Structure of inhibitors that emerged from ChemBridge screen. Class of inhibitors with nitro subgroup inhibited ALDH3A1 but this class was not pursued since these compounds were not greatly potent.

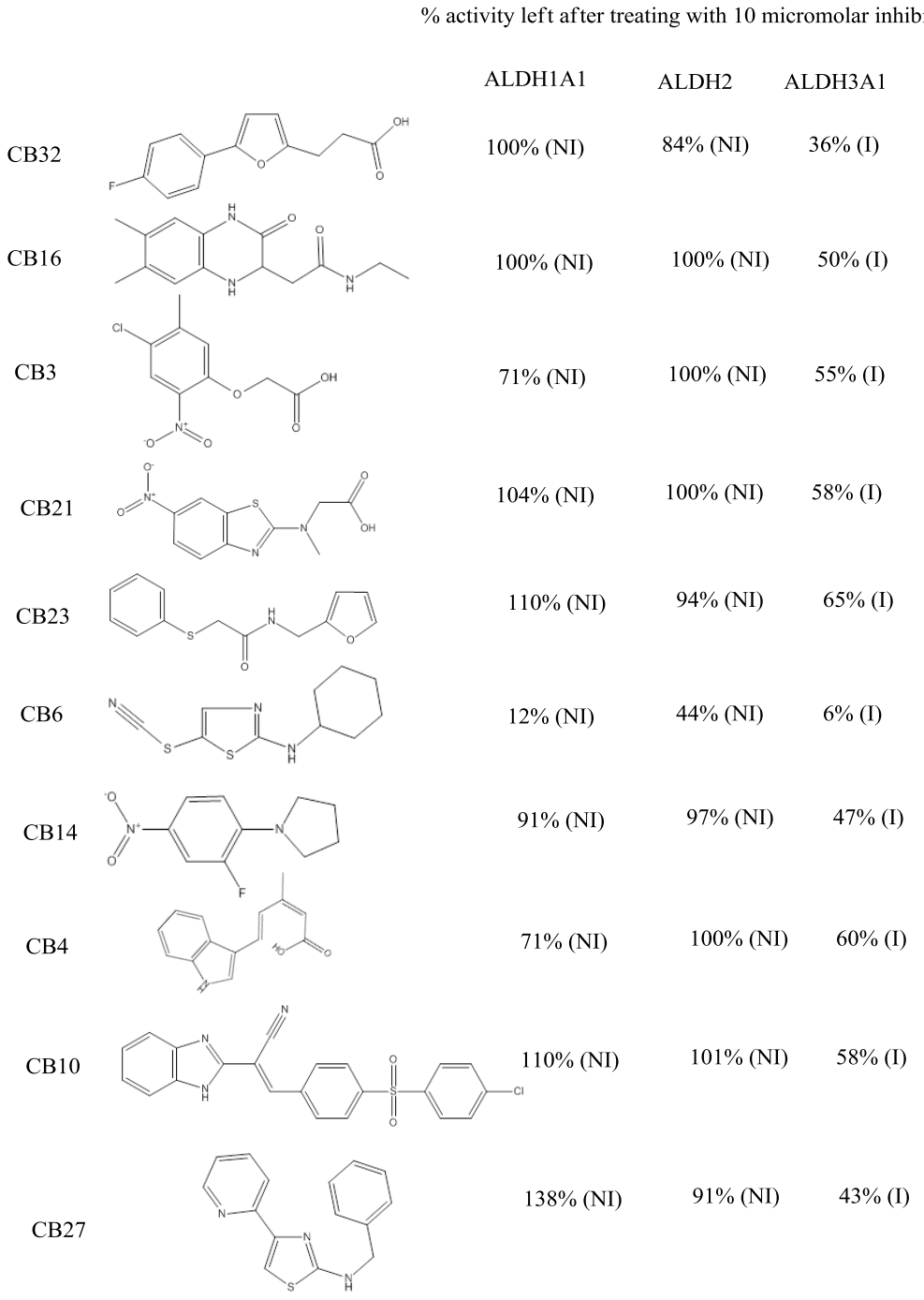

Figure 12 (Continued). Structure of inhibitors that emerged from ChemBridge screen. These inhibitors were not pursued since they had weak potency and no specific selectivity pattern.

Two inhibitors (CB7 and CB29) from the ChemBridge collection showed high ALDH3A1 inhibition but no inhibition to ALDH1A1 and ALDH2 activity. Another compound CB25 showed greater inhibition to ALDH3A1 but had minor inhibition of ALDH1A1 activity at 10 μM concentration. Chart showing selectivity and potency of CB7, CB25 and CB29 is shown below in Figure 13.

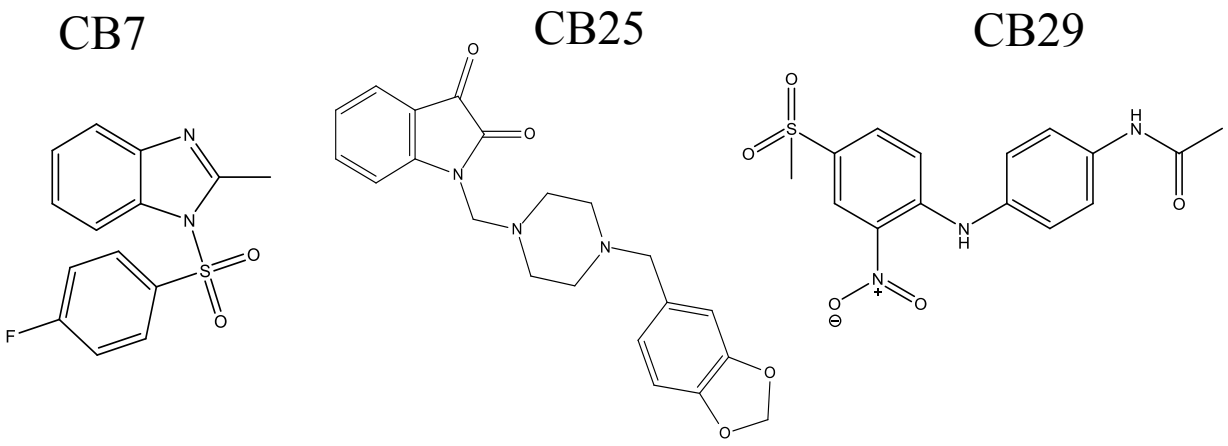

Isozymes	CB7 (IC_{50})	CB25 (IC_{50})	CB29 (IC_{50})
ALDH1A1	> 250 μM	20.0 μM	> 250 μM
ALDH2	> 250 μM	> 250 μM	> 250 μM
ALDH3A1	0.20 μM	1.80 μM	16.0 μM

Figure 13. Three hit compounds CB7, CB25 and CB29 with their IC_{50} values. CB7, CB29 and CB25 are three hit compounds that emerged from the screen. CB7 and CB29 are selective inhibitors for ALDH3A1 whereas CB25 inhibits ALDH1A1 and ALDH3A1 but still exhibits ~10 fold higher selectivity to ALDH3A1.

D. Steady state kinetic characterization

We characterized the mode of inhibition using steady–state kinetics through co–variation of inhibitor and substrate concentrations. The steady–state kinetic measurements were performed in 100 mM Na_2HPO_4 buffer, pH 7.5. Initial studies showed that $NADP^+$ had a K_m value of 260 μM whereas benzaldehyde had a K_m value of 200 μM (Figure 14). Steady state competition experiments showed a competitive mode of inhibition for CB7 with respect to benzaldehyde with a K_i of 0.082 μM and non–competitive mode against $NADP^+$ with a K_i of 0.11 μM (Figure 15). CB29 showed a competitive mode of inhibition with respect to both benzaldehyde and $NADP^+$ with K_i values of 4.7 μM and 3.9 μM respectively (Figure 16). CB25 showed a non–competitive mode of inhibition with respect to both benzaldehyde and $NADP^+$ with K_i values of 0.70 and 1.4 μM, respectively (Figure 17).

(A)

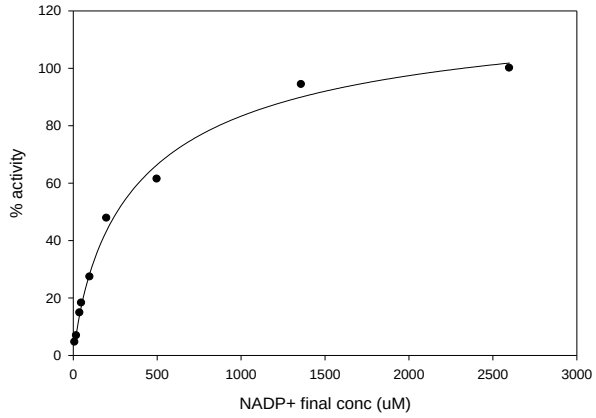

$K_m = 260 \pm 20\ \mu M$

(B)

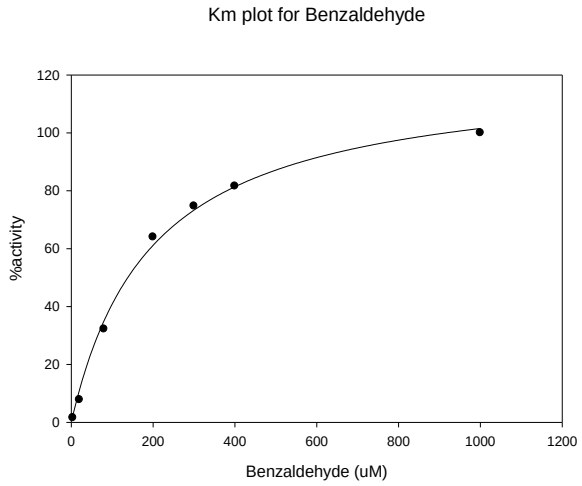

$K_m = 200 \pm 12\ \mu M$

Figure 14. K_m for $NADP^+$ and benzaldehyde for ALDH3A1 activity. (A) Determination of K_m for $NADP^+$ for ALDH3A1. **(B)** Determination of K_m for benzaldehyde.

(A)

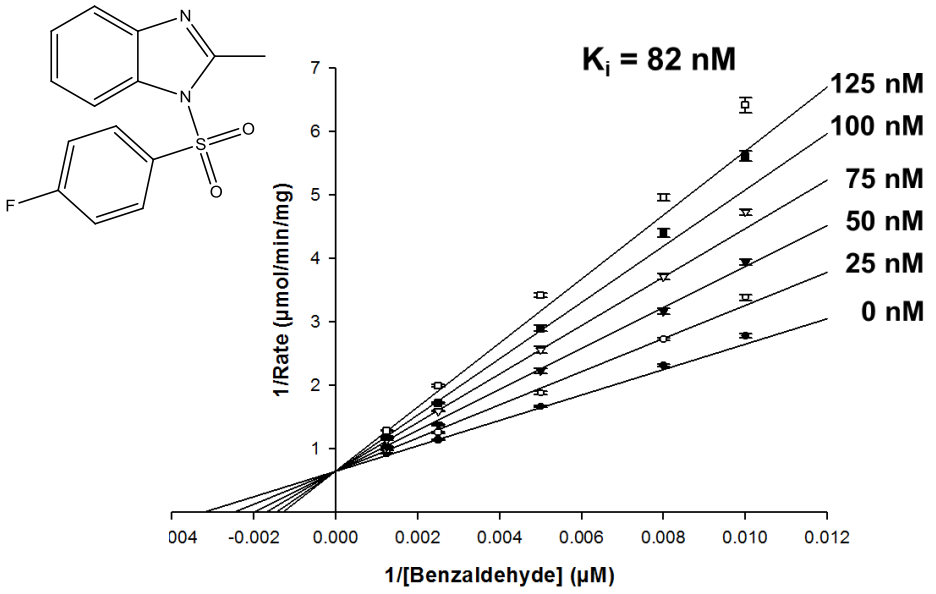

(B)

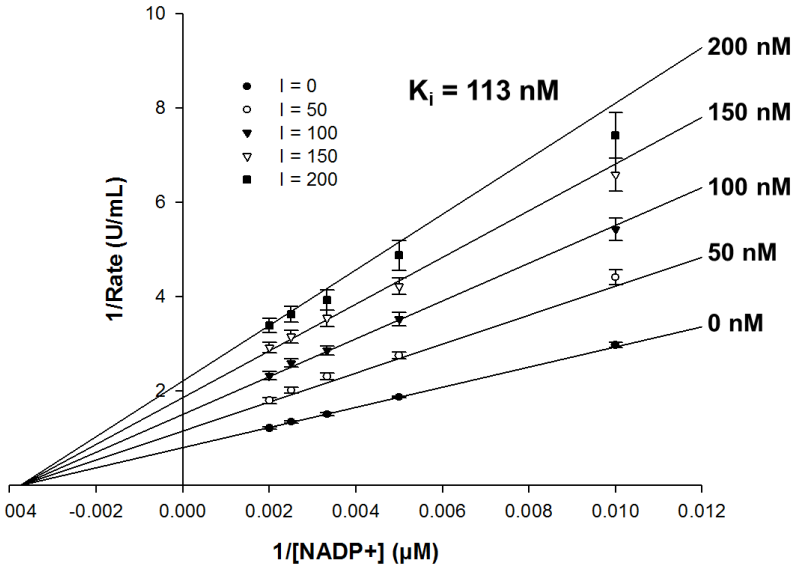

Figure 15. Competition experiments of CB7 with benzaldehyde and $NADP^+$. Competition experiment showing the mode of inhibition of CB7 with respect to **(A)** benzaldehyde and **(B)** $NADP^+$.

(A)

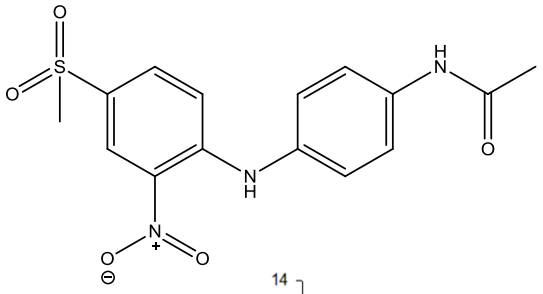

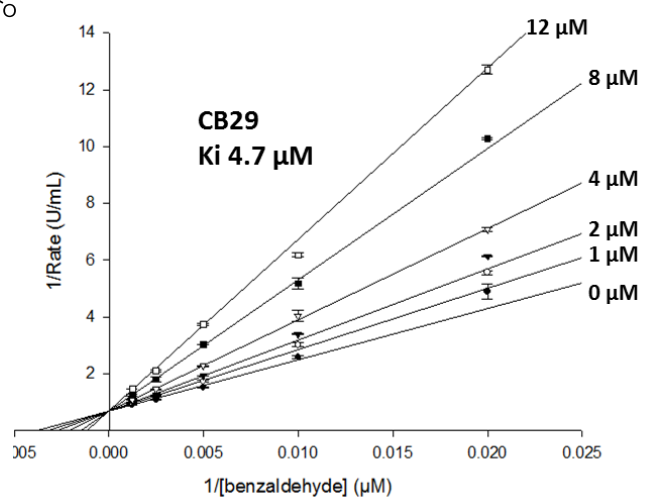

(B)

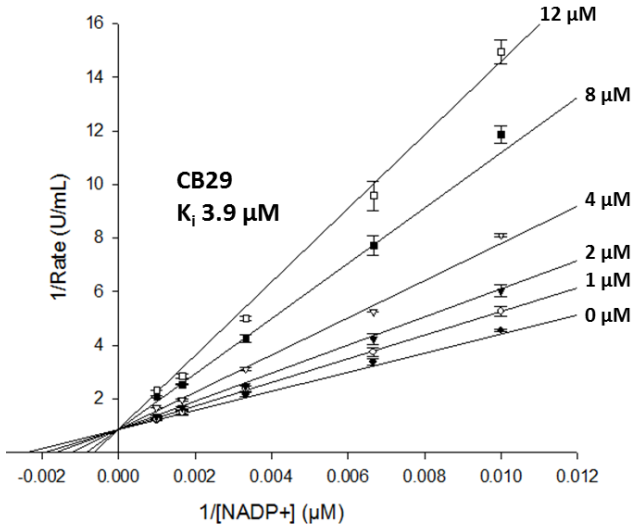

Figure 16. Competition experiments of CB29 with benzaldehyde and NADP$^+$. Competition experiment showing the mode of inhibition of CB29 with respect to **(A)** benzaldehyde **(B)** NADP$^+$.

(A)

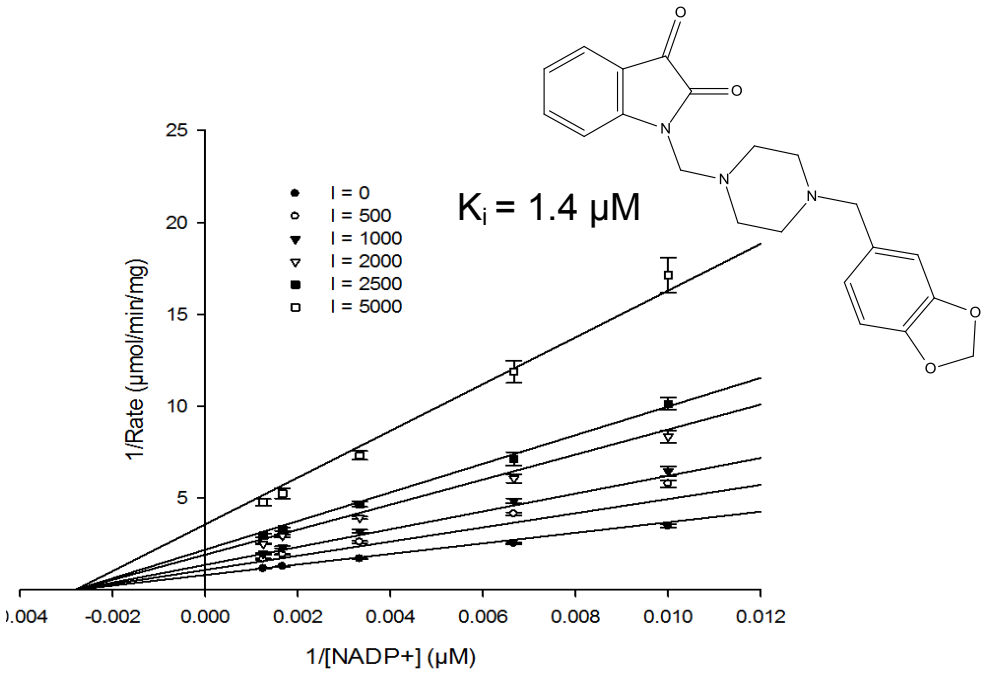

(B)

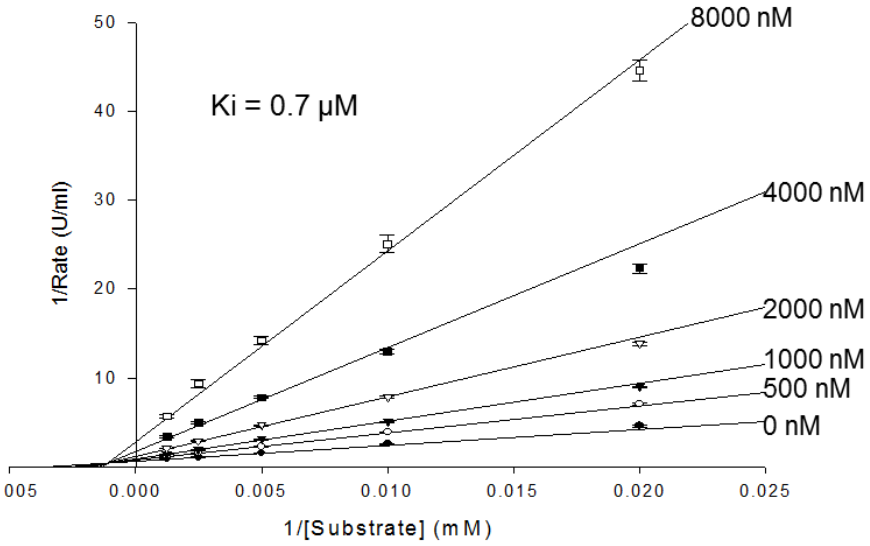

Figure 17. Competition experiments of CB25 with benzaldehyde and NADP$^+$. Competition experiment showing the mode of inhibition of CB25 with respect to **(A)** NADP$^+$ **(B)** benzaldehyde.

E. Structure Activity Relationship

1. SAR by CB29 class of compounds

We purchased 64 different compounds that showed at least 90% structural similarity in their atomic positions with CB29 and tested their selectivity for ALDH1A1, ALDH2 and ALDH3A1 (Table 3A and 3B). Our results showed that only those CB29 derivatives with smaller subgroups, such as methyl or methylamine, at the R1 position were inhibitory toward ALDH3A1 (Table 3A). Substitution of the R1 position with larger substituent, such as diethylamine or morpholine, eliminated inhibitory potency for ALDH3A1, but showed weak activation of ALDH1A1 activity [Table 3A, compare CB29 (IC_{50} = 16 μM) with B6 (NI) and B2 (IC_{50} = 26 μM) with B5 (NI) and B18 (NI)]. Since larger substitutions were deleterious to potency, we examined whether substitution of the CH_3 with CF_3 improved potency. Replacement of the methyl group with a tifluoromethyl group (CF_3) at the R1 position generated an equally potent compound [Table 3A, compare CB29 (IC_{50} = 16 μM) with 12415 (IC_{50} = 17 μM)]. We concluded that a methyl substituent was optimal at the R1 position. Next, we examined analog with a methyl sulfonyl group at R3 position. Our SAR result showed that this substitution leads to both lower solubility (by more than 5–fold) and lower potency of compound [Table 3A, compare CB29 (IC_{50} = 16 μM) with 12416 (IC_{50} = 40 μM)]. In addition, this compound was less selective and inhibited both ALDH1A1 and ALDH3A1. Based on these results, we believe that the nitro group is advantageous for solubility and selectivity. Since CB29 had a substituted aniline group at the R2 position (Table 3B), we explored a number of different substituted anilines to test their contribution to the potency and selectivity of CB29. Our results showed that an aniline at the R2 position was required for inhibition of ALDH3A1 [Table 3B, compare A1

(NI), A57 (NI) with CB29 (IC_{50} = 16 μM), B1 (IC_{50} = 27 μM) and B4 (IC_{50} = 30 μM)]. Even the substitution of an ether linkage greatly reduced potency [Table 3B, compare CB29 (IC_{50} = 16 μM) with 12417 (IC_{50} = 100 μM)]. We evaluated a series of anilines at the R2 position with substitutions at the ortho, meta and para positions. Compounds with substituents at the ortho position (R4/R8) lost all activity toward ALDH3A1 [Table 3A, B17 (NI)]. Compounds with substitutions at the meta positions (R5/R7) showed similar potencies to CB29 [Table 3A, B15 (IC_{50} = 10 μM) and B21 (IC_{50} = 26 μM)]. Finally, we examined substitutions at the para (R6) position. Since our parent compound CB29 had an acetamide at this position, we looked for analogs with an ester instead of amide linkage at the corresponding position (A18 and B11). This substitution yielded compounds with similar potencies [A18 (IC_{50} = 31 μM), B11 (IC_{50} = 24 μM)], which rules out a possibility of hydrogen bond formation by this nitrogen to the enzyme. We next looked larger amide substitutions at the R6 position. Here a surprising pattern was seen, when the acetamide was substituted with isobutyramide (B13) or isopentanamide (B16), these two compounds were inhibitory towards both ALDH1A1 and ALDH3A1 (Table 3A). In addition, analogs with larger amides at the R6 position and larger substitutions at the R1 position (B22) showed greater potency toward ALDH1A1 than toward ALDH3A1 (Table 3A). In contrast, as mentioned above when the acetamide group was held constant and the larger morpholine was introduced at the R1 position (B6), the compound lost all inhibitory potency toward either ALDH1A1or ALDH3A1.Compounds having aniline at the R2 position with its meta and para position substituted with electronegative subgroups seemed to activate ALDH1A1 activity at 100 μM concentration (B21, B15, B2, B18, B11) by about 30%–50%.

Table 3. (A) SAR for CB29 analogs. SAR study for analogs having aniline at R3 position but with ortho, meta and para substitutions at various positions (R4, R5, R6, R7 and R8). Also included are compounds with substitutions at R1 and R3 positions. Shaded in yellow are the residues of ALDH3A1 that are in close proximity with of CB29.

Table 3A

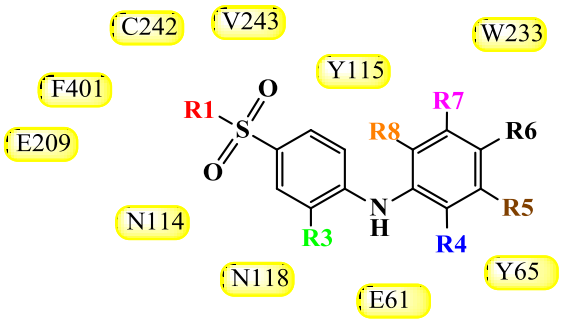

Name	R1	R3	R4	R5	R6	R7	R8	IC_{50} (uM) ALDH3A1	ALDH2	ALDH1A1
CB29	CH_3	NO_2	H	H		H	H	16 (0.5)	NI	NI
B6		NO_2	H	H		H	H	NI	NI	NI
B2	$NHCH_3$	NO_2	H	H	F	H	H	26 (1.2)	NI	NI
B18		NO_2	H	H	F	H	H	NI	NI	WA
B5		NO_2	H	H	CH_2CH_3	H	H	NI	NI	WA
12415	CF_3	NO_2	H	H		H	H	17 (0.8)	WA	NI
12416	CH_3	SO_2CH_3	H	H	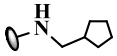	H	H	40	NI	32 (3)
B17	CH_3	NO_2	CH_3	H	H	CH_3	H	NI	NI	WA
B15	CH_3	NO_2	H	F	CH_3	H	H	10.8 (0.1)	NI	WA
B21		NO_2	H		H	H	H	26.3 (4)	NI	WA
A18	$NHCH_3$	NO_2	H	H	OCH_3	H	H	31.7 (2.6)	NI	NI
B11	$NHCH_3$	NO_2	H	H	$OCHF_2$	H	H	24.7 (1.2)	NI	NI
B13	CH_3	NO_2	H	H		H	H	19.6 (3.3)	NI	16.8 (2)
B16	$NHCH_3$	NO_2	H	H	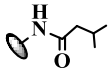	H	H	42.3 (1.5)	NI	11.6 (6)
B22		NO_2	H	H		H	H	100	NI	8.3 (3)

Table 3. (B) SAR for CB29 analogs. SAR showing the effect of first set of analogs that had substitutions other than aniline at R3 position (such as halogen, glycine and ethers). Values in parentheses are S.D. for three independent assays. NI stands for no inhibition at 100 µM inhibitor concentration. WA represents (30–50) % activation shown by 100 µM compound to respective enzymes.

Table 3B

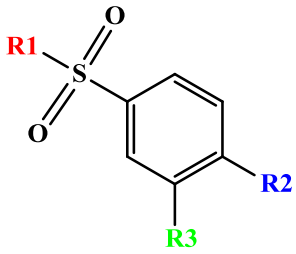

Name	R1	R2	R3	IC_{50} (uM) ALDH3A1	ALDH2	ALDH1A1
A1	CH_3	Br	NO_2	NI	NI	NI
A57	CH_3	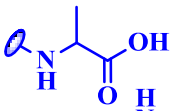	NO_2	NI	NI	50 (6.6)
CB29	CH_3	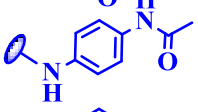	NO_2	16 (0.5)	NI	NI
B1	CH_3	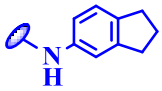	NO_2	26.9 (6)	NI	NI
B4	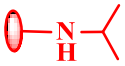	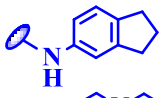	NO_2	30.5 (3.5)	NI	NI
B9	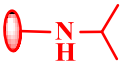	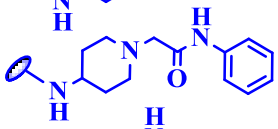	NO_2	25.6 (2.3)	NI	NI
12417	CF_3	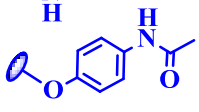	NO_2	100	NI	NI

2. SAR by CB7 class of compounds

We evaluated 118 different structurally related analogs of CB7 with at least 95% structural similarity for their inhibitory potency toward ALDH3A1 and selectivity versus ALDH1A1 and ALDH2 using the dehydrogenase assay. Substitutions were made at several different positions. Representative compounds with their selectivity and potency pattern in respective enzymes are shown in Table 4. We initially looked at the contribution of the methyl group at R1 position to see if any other substitutions in this region would make this compound more potent. Our SAR study showed that methyl substitution at R1 position is optimal [compare A20 (IC_{50} 0.3 μM) with A21 (IC_{50} 1.5 μM) and A10 (IC_{50} 0.7 μM) with A3 (IC_{50} 50 μM)]. However, aromatic or bigger substitutions were not tolerated [compare A6 (IC_{50} >100 μM) and A13 (IC_{50} >100 μM) with A20 (IC_{50} 0.3 μM), A21 (IC_{50} 1.5 μM), B36 (IC_{50} 1.2 μM) and B37 (IC_{50} 1 μM)]. Next, compounds modified in the R2 and R3 position were tested for their selectivity and potency. Our study showed that compounds having even a methyl substitution at R2 or R3 position showed no inhibition on ALDH3A1 activity (A38 and A47). One interesting feature of CB7 is the presence of fluorine atom at R6 position. We looked at analogs with different charges and sizes at the R6 position. Analogs with hydrogen, methyl, isobutyl, acetamide substitution at this position do not inhibit ALDH3A1 whereas fluorine or chlorine substitution was able to inhibit ALDH3A1 [compare A5 (IC_{50} >50 μM), A3(IC_{50} ~50 μM), A16 (IC_{50} >100 μM) and A67 (IC_{50} >100 μM) with A21 (IC_{50} >1.5 μM) and A24 (IC_{50} >2.1 μM)]. Since chlorine and fluorine are two strong electron withdrawing atoms, we believe that these two halogens enhance the hydrophobic interactions with the surrounding residues whereas an acetamide is electron donating and has the opposite effect [compare A20

(IC_{50} 0.3 μM) with A22 (IC_{50} >100 μM)]. It could also be possible due to the steric effect since halogens are smaller subgroups whereas an acetamide is a bigger subgroup. Next, we looked at compounds with substitution at either the R4 or R8 position. Compounds with methoxy or halogen substitution at these two positions were not inhibitory to ALDH3A1 activity [compare A30 (IC_{50} >100 μM) with A20 (IC_{50} 0.3 μM), A39 (IC_{50} >100 μM) with A24 (IC_{50} 2.1 μM) and A40 (IC_{50} >100 μM) with CB7 (IC_{50} 0.2 μM)]. Even methyl substitutions at these two positions were not tolerated. Substitutions at either R5 or R7 were not greatly deleterious, but still showed some drop in their inhibitory potency [compare A53 (IC_{50} 0.7 μM) and A64 (IC_{50} 0.9 μM) with A20 (IC_{50} 0.3 μM) and A70 (IC_{50} 0.9 μM) with CB7 (IC_{50} 0.2 μM)]. Since all the analogs we tested had higher IC_{50} values than the CB7, we concluded that the commercially available analogs were not able to improve the potency of CB7.

Table 4. SAR for CB7 analogs. Values in parentheses represent standard error. NI stands for no inhibition and NI(A) stands for no inhibition but very weak activation (~20% at 100 μM). Residues of ALDH3A1 that are in close contact with CB7 are shown in yellow boxes.

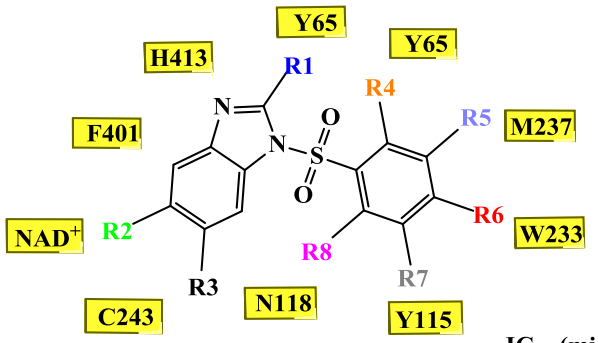

Cmpd	R1	R2	R3	R4	R5	R6	R7	R8	IC_{50} (micromolar conc.) ALDH1A1	ALDH2	ALDH3A1
A5	H	H	H	H	H	H	H	H	NI	NI	>50
A3	H	H	H	H	H	CH_3	H	H	NI	NI	~50
A16	H	H	H	H	H	$NHCOCH_3$	H	H	NI	NI	>100
A67	H	H	H	H	H		H	H	NI	NI	>100
A21	H	H	H	H	H	Cl	H	H	NI	NI	1.5(0.5)
A24	H	H	H	H	H	F	H	H	NI(A)	NI	2.1 (0.4)
A10	CH_3	H	H	H	H	CH_3	H	H	NI	NI	0.7 (0.2)
A20	CH_3	H	H	H	H	Cl	H	H	NI	NI	0.3 (0.06)
A22	CH_3	H	H	H	H	$NHCOCH_3$	H	H	NI	NI	>100
B36	NH_2	H	H	H	H	Cl	H	H	NI(A)	NI	1.2 (0.2)
B37	$COCH_3$	H	H	H	H	Cl	H	H	NI	NI	1.0 (0.1)
A6		H	H	H	H	Cl	H	H	NI	NI	>100
A13		H	H	H	H	Cl	H	H	NI	NI	>100
A38	H	NO_2	H	H	H	OCH_3	H	H	NI	NI	>100
A47	H	CH_3	CH_3	H	H	F	H	H	NI	NI	>100
A39	H	H	H	OCH3	H	F	H	H	NI	NI	>100
A30	CH_3	H	H	Br	H	Cl	H	H	NI	NI	>100
B27	H	H	H	H	F	F	H	H	NI	NI	4.2 (1.2)
A53	CH_3	H	H	H	CH_3	Cl	H	H	NI(A)	NI	0.7 (0.1)
A62	CH_3	H	H	H	CH_3	OCH_3	H	H	NI	NI	2.0 (0.4)
A64	CH_3	H	H	H	OCH_3	Cl	H	H	NI	NI	0.9 (0.06)
A70	CH_3	H	H	H	OCH_3	F	H	H	NI	NI	0.9 (0.2)
A40	CH_3	H	H	H	H	F	H	OCH_3	NI	NI	>100
CB7	CH_3	H	H	H	H	F	H	H	NI	NI	0.2 (0.05)

F. Crystal structures of inhibitors with ALDH3A1

1. Crystal structure of ALDH3A1 with CB29

In order to understand target specificity and provide a structural context for the kinetic results, we determined the crystal structure of CB29 bound to ALDH3A1. CB29 was chosen because it had very high solubility in water, had reasonable potency (K_i = 4 μM) and showed good selectivity amongst its analogs. Since our analogs shared > 90% structural similarity to CB29, it also serves as a good starting point upon which to build the SAR on this series. Triclinic crystals were obtained that had unit cell dimensions of a = 89.1 Å, b = 95.4 Å, c = 117.2 Å and diffracted up to 2.5 Å resolution. Four dimers are present in one asymmetric unit. Figure 18(A) shows one of the four independent dimers. The presence of CB29 within the active site of ALDH3A1 was confirmed through examination of the original figure–of–merit, σ_A–weighted, electron density maps (Figure 18B). The active site of all eight subunits of ALDH3A1 were fully occupied by CB29 (Figure 18B). Detailed refinement statistics are provided in Table 5. In the Ramachandran plot, 97% of all residues are in the most favored regions. There are four residues Cys243, Val244, Glu61 and Asn114 that contribute hydrogen bonding interactions with CB29 (Figure 19). The two sulfonyl oxygens and the amino group linking the two benzene rings mediate these hydrogen bonds whereas the terminal benzene and acetamide moieties contribute mostly hydrophobic and van der Waals interactions (Figure 19). One of the sulfonyl oxygens forms a hydrogen bond with the peptide nitrogen of Val244. The second sulfonyl oxygen is positioned similar to the oxyanion formed during catalysis and lies in proximity to the peptide nitrogen of Cys243 and the side chain amide nitrogen of Asn114. The nitrogen linking the two substituted benzene rings in CB29 donates a hy-

drogen bond to the peptide carbonyl oxygen of Glu61. The remainder of the interactions between CB29 and the active site are hydrophobic and van der Waals contacts. The methyl associated with the sulfonyl group forms a hydrophobic interaction with Phe401 and the nitro–benzene ring forms hydrophobic pi–stacking interactions with Tyr115. The side chains of Ile394 and Thr242 also contribute hydrophobic interactions with the nitro–benzene ring. The second aromatic ring forms hydrophobic interactions with Tyr65 and Thr395 on one side, while the opposing face interacts with the Cβ and Cγ side chain atoms of Glu61 and the side chain of Met237. The terminal acetamide group is within van der Waals contact distance to Tyr65, Trp233, Thr395, Val 392 and Arg441 (Figure 19).

(A)

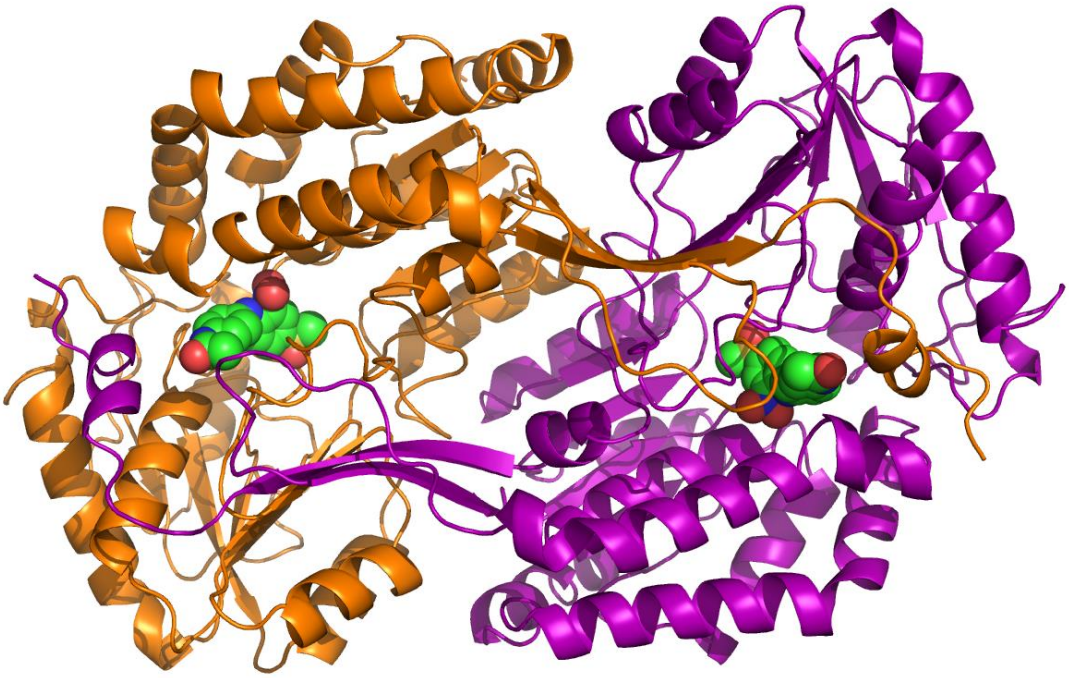

Figure 18. (A) CB29 binding in ALDH3A1 pocket. A cartoon representation of one of the four independent dimers present in one asymmetric unit of ALDH3A1–CB29 complex crystal structure. The individual subunits are colored orange and magenta. CB29 is shown using van der Waals spheres.

(B)

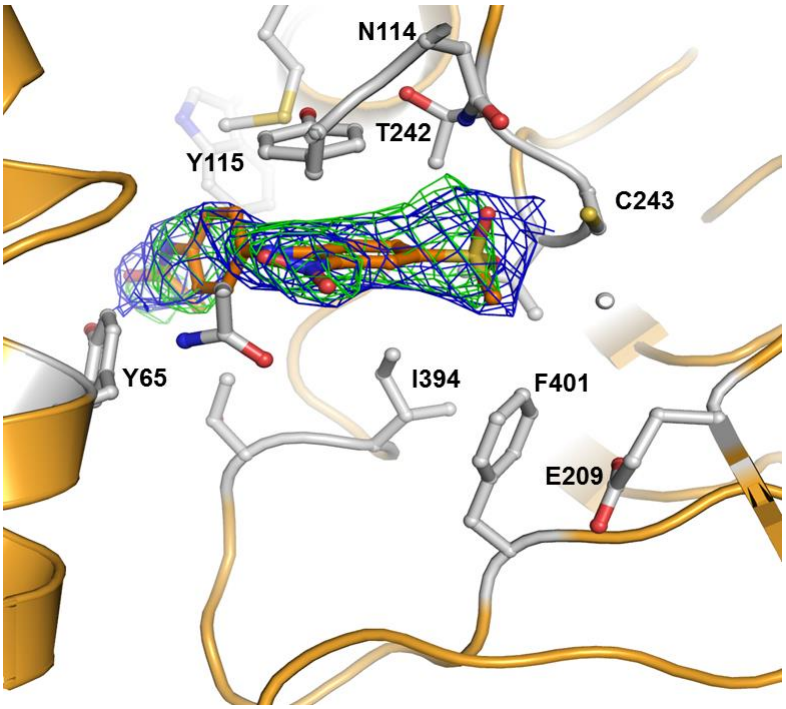

Figure 18. (B) Electron density of CB29 bound to active site of ALDH3A1. The electron density maps displayed are the original figure of merit (σ–A weighted) F_o-F_c map contoured at 2.5 standard deviations (blue) and the original figure–of–merit weighted $2F_o$-F_c map contoured at 1 standard deviation (green) superimposed on the final refined model of CB29 bound in the enzyme active site.

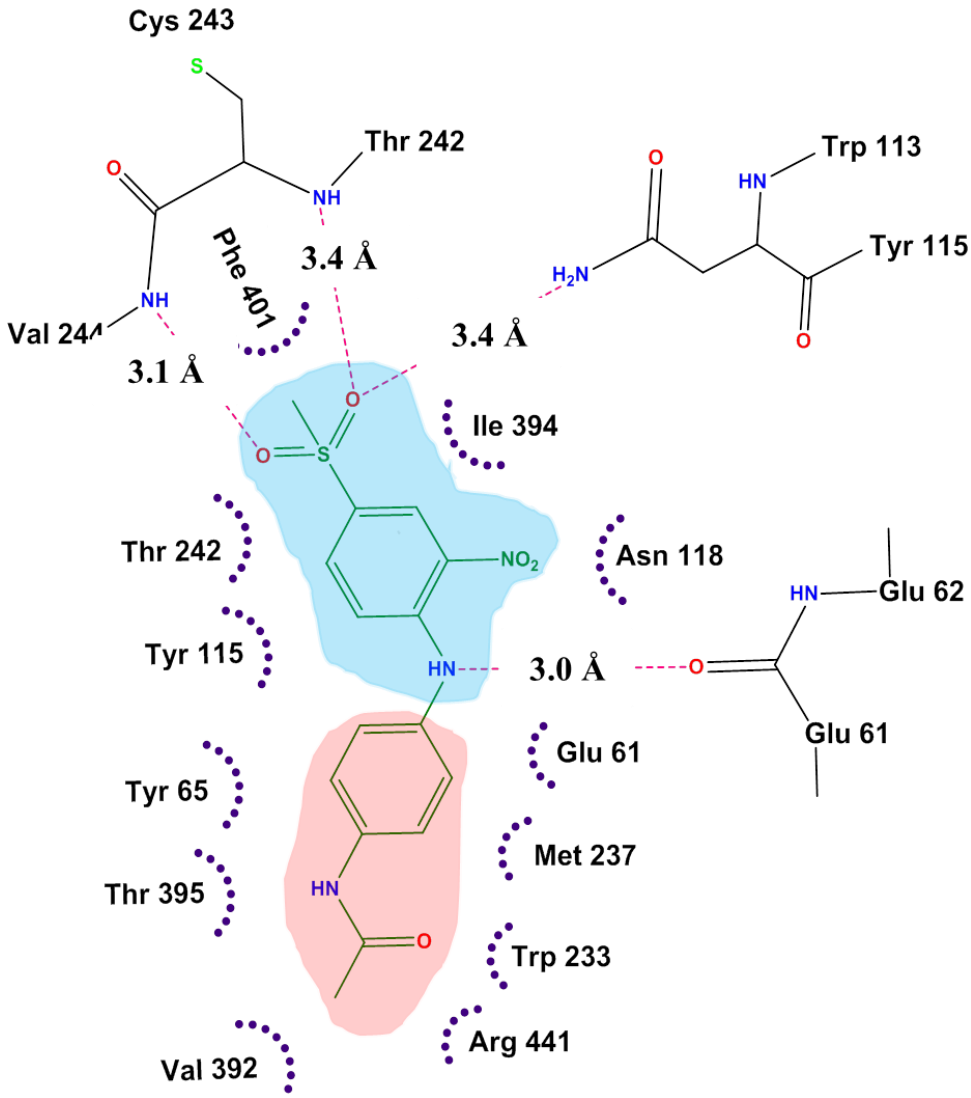

Figure 19. Two dimensional map showing CB29 binding in ALDH3A1 pocket. Two dimensional representation of the important contacts between CB29 and residues within the active site of ALDH3A1. Pink dotted lines represent potential hydrogen bonding interactions. The distance shown is the average of the distances observed in the eight subunits of the asymmetric unit. Hydrophobic contacts are represented by purple arcs radiating towards the ligand. Regions that contribute hydrogen bonds are shaded green and those that contribute hydrophobic contacts are shaded red.

Table 5. Refinement statistics for CB29 bound to ALDH3A1.

	ALDH3A1 (CB29 soak)
Data collection	
Space group	P_1
Cell dimensions	a = 89.1 Å, b = 95.4 Å, and c = 117.2 Å
	α = 112.4 °, β = 91.7 °, and γ = 91.0 °
Resolution (Å)	50–2.50 (2.54–2.5)
R_{merge}	0.067 (0.25)
I/σ_I	10.4 (3.1)
Completeness	93.6 % (72.5%)
Redundancy	2.2 (2.0)
Refinement	
Resolution (Å)	50.0–2.50
No. of reflections	109, 547
R_{work}/ R_{free}	0.23/ 0.25
No. of atoms	
Protein	28003
Ligand/ Ion	192
Water	218
B–factor (overall)	25.2
RMSD	
Bond angles (°)	1.15 °
Bond lengths (Å)	0.008 Å

2. Crystal structure of ALDH3A1 with CB7

The structure of ALDH3A1 with CB7 proved more difficult to obtain and required the presence of the cofactor NAD^+ in order to obtain the complex. CB7 was chosen among all of these compounds because it was the most potent compound (Ki = 0.1 μM), exhibited very good solubility, and shared > 95% structural similarity to the other analogs. Monoclinic crystals were obtained that belonged to space group $P2_1$ with unit cell dimensions of a = 95.2, b = 90.9, c = 117.9 and diffracted up to 1.9 Å resolution. Structure was determined by performing molecular replacement using the apo–form of ALDH3A1 structure as the search model (RCSB code 3SZA). Molecular replacement was performed using MolRep program provided by CCP4 Interface software. The presence of CB7 within the active site of ALDH3A1 was confirmed through examination of the original figure–of–merit, σ_A–weighted, electron density maps (Figure. 20). There are four subunits in one asymmetric unit arranged as two independent dimers. The active site is fully occupied by CB7 in two out of four subunits (Figure 20). The third and fourth subunit showed partial occupancy of CB7 in its catalytic site. Our structure also showed the presence of NAD^+ inside the Rossmann pocket of all four subunits with full occupancy (Figure 21A and 21B). Detailed refinement statistics are provided in Table 6. In the Ramachandran plot, 97.3 % of all residues are in the most favored regions. Interestingly, no hydrogen bonding interactions were observed between CB7 and ALDH3A1. However, we observed numerous hydrophobic and van der Waals interactions between CB7 and ALDH3A1 (Figure 22). The benzene ring from benzimidazole forms hydrophobic contact with Phe401, Tyr115, Leu119 and Cys243. The imidazole ring forms a strong hydrophilic interaction with His 413 and Ile 394. The methyl group associated with imidazole

ring forms hydrophobic interaction with Tyr65 and Ile394. One of the sulfonyl oxygen forms van der Waals interactions with Tyr65, Glu62 and Asn118. The other sulfonyl oxygen forms van der Waals interactions with Tyr115, Glu62 and Asn118. Benzene ring attached to fluorine form hydrophobic interactions with two tyrosine residues, Tyr65 and Tyr115 as well as with Thr395 and Glu61. The sulfonyl and attached fluorobenzene subgroup lie symmetrically between Tyr115 and Tyr65, creating almost an equivalent hydrophobic interaction between two Tyrosine residues (Tyr65 and Tyr115). Hydrophobic contacts are also seen between fluorine and Ile391, Trp233 and Met237.

In addition to CB7 binding, in our crystal structure we also see the presence of the cofactor NAD^+. NAD^+ binds to ALDH3A1 through numerous hydrogen bonding interactions. The amide nitrogen from the nicotinamide group forms a hydrogen bond with carbonyl oxygen from Leu210. The two hydroxyl groups from the nicotinamide ribose ring form two hydrogen bonding interactions with the two carboxyl oxygens of Glu333. Four oxygens from the two phosphates form four hydrogen bonds with Thr112, Trp113, His289 and Ser188, respectively. The two hydroxyl groups from the adenosine ribose ring form two more hydrogen bonds with carboxyl oxygens of Glu140. All of these hydrogen bonding interactions tightly bind NAD^+ in its Rossmann fold. In addition, several hydrophobic interactions are also present. A detailed two dimensional map for NAD^+ binding is shown in Figure 23.

We compared interaction between NAD^+ and ALDH3A1 with interaction pattern between NAD^+ and ALDH2 (Perez–Miller et al., 2003). The NAD^+ conformation in CB7 bound ALDH3A1 structure exhibits a hydride transfer conformation in terms of binding partners and the types of interactions it forms with ALDH3A1. In ALDH2 structure, in

hydride transfer conformation (PDB code 1o00), amide nitrogen from nicotinamide group forms a hydrogen bond with Leu269. In ALDH3A1, we see hydrogen bond between amide nitrogen and Leu210. In ALDH2, we see two hydroxyl groups from the nicotinamide ribose ring forming two hydrogen bonding interactions with the two carboxyl oxygens of Glu399. In our structure, we see two similar hydrogen bonds between hydroxyl groups from the nicotinamide ribose ring and Glu333. Hydrogen bonds shown by two phosphate groups in ALDH2 are however not identical in ALDH3A1 structure. In ALDH2 structure, four oxygens from the two phosphates form hydrogen bonds with a Magnesium ion, Ser246 and Trp168. In ALDH3A1, we see interaction of four oxygens with Ser188, Trp113, Thr112 and His289 but not magnesium ion. In ALDH2, the two hydroxyl groups from the adenosine ribose ring form three hydrogen bonds with Ile166, Lys192 and Glu195. In ALDH3A1, these hydroxyl groups form hydrogen bond with terminal carboxylic oxygens from Glu140. The adenine ring is not bonded to any residue but water in both ALDH2 and ALDH3A1. Overall, we see a lot of structural similarity in terms of binding both in NAD^+–ALDH2 as well as NAD^+–ALDH3A1 structure in their hydride transfer conformation.

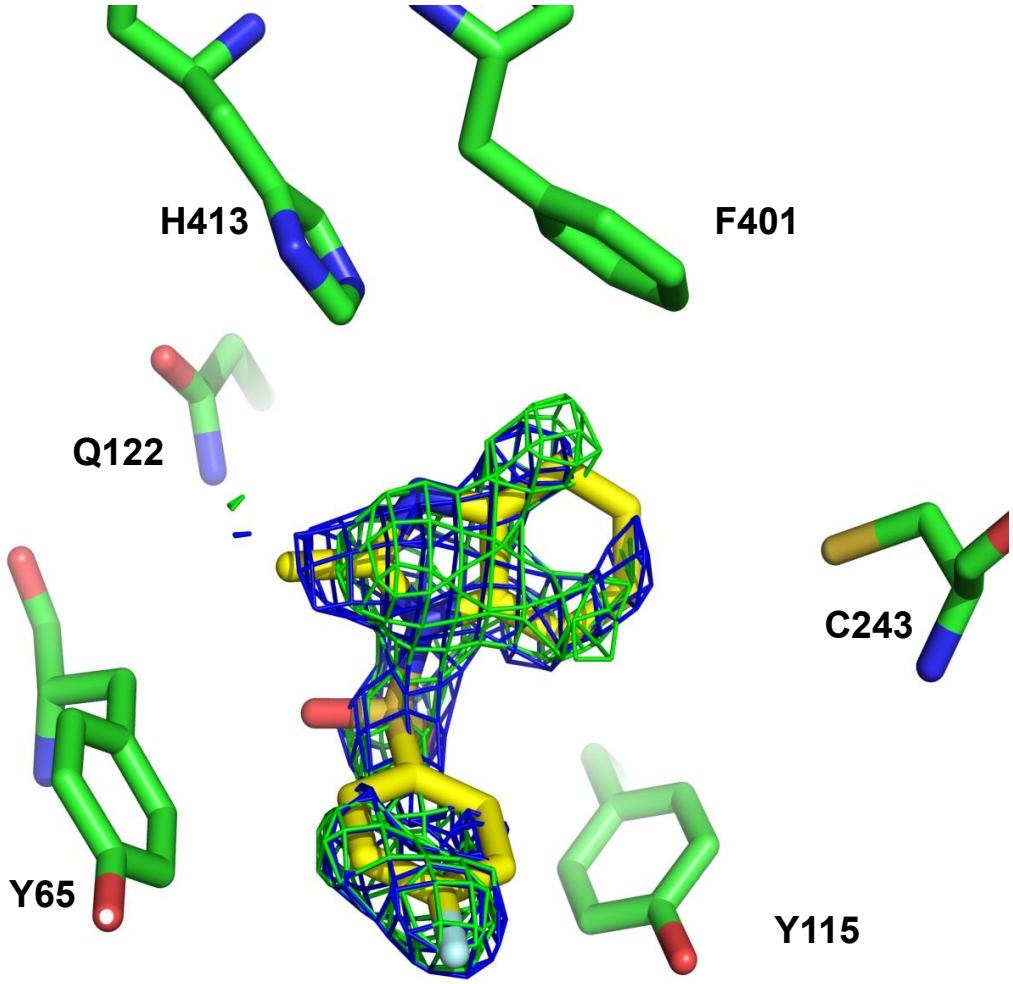

Figure 20. Density map showing CB7 bound to ALDH3A1. The electron density maps displayed are the original figure of merit (σ–A weighted) F_o-F_c map contoured at 2.5 standard deviations (green) and the original figure–of–merit weighted $2F_o$-F_c map contoured at 1 standard deviation (blue) superimposed on the final refined model of CB7 bound in the enzyme active site. Residues that contribute to hydrophobic interactions within a distance of 3.4–4.0 Å are represented as sticks.

(A)

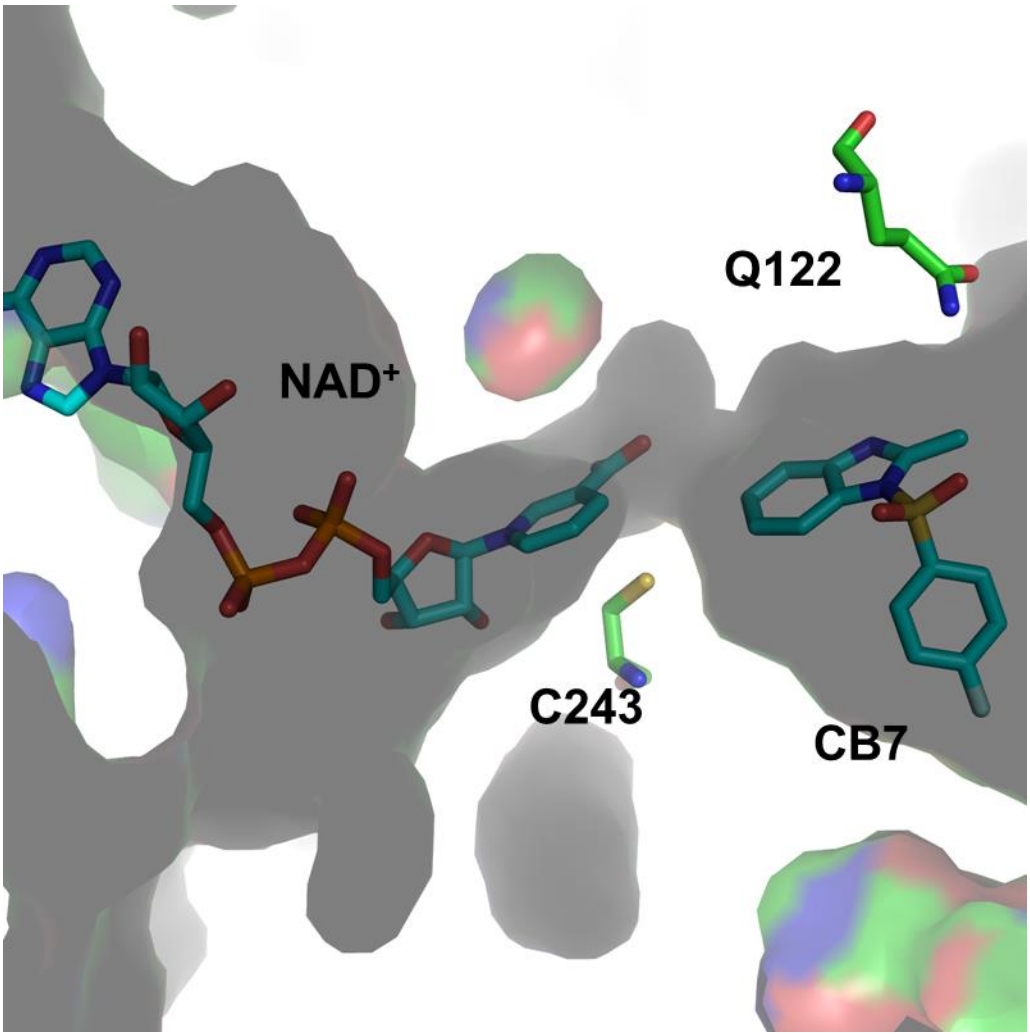

Figure 21. (A) Map showing NAD^+ binding to ALDH3A1 in the presence of CB7. Surface representation of the catalytic and $NAD(P)^+$ binding site of ALDH3A1. NAD^+ is bound on one pocket followed by binding of CB7 into the catalytic pocket. Bound ligands are represented as sticks.

(B)

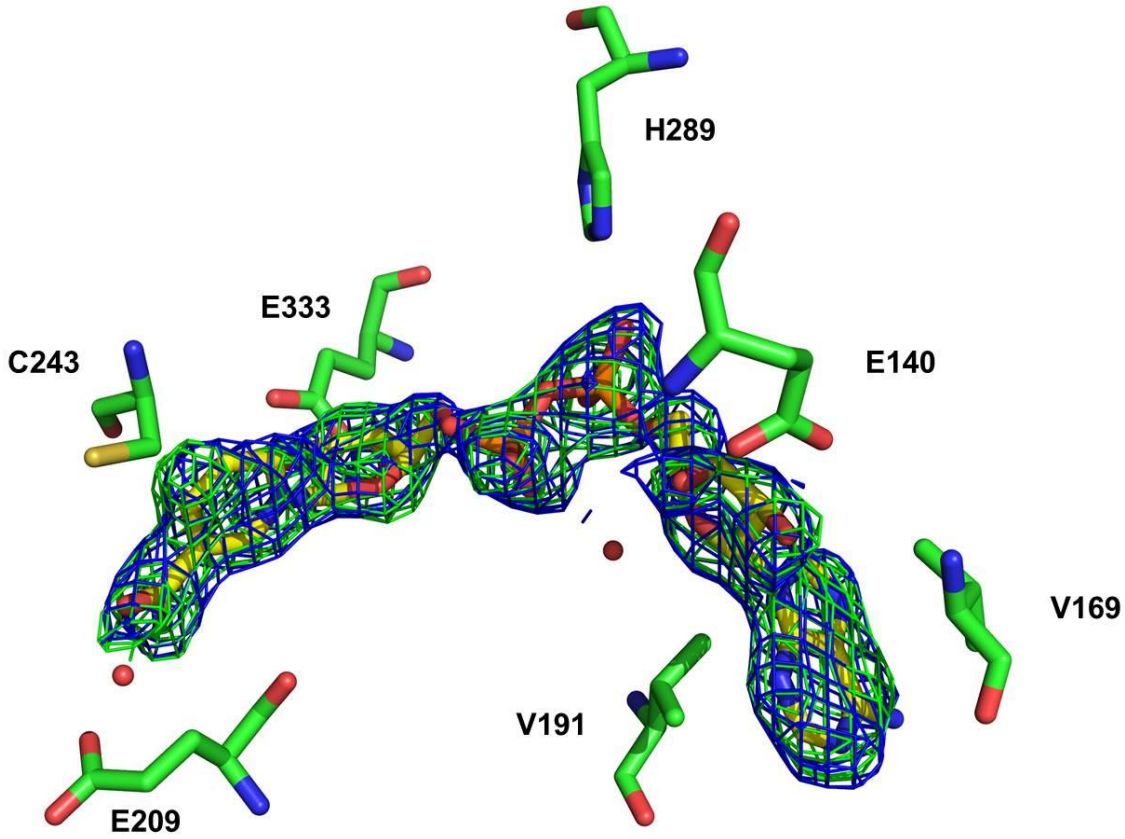

Figure 21. (B) Electron density of NAD^+ bound to ALDH3A1. The electron density maps displayed are the original figure of merit (σ–A weighted) F_o-F_c map contoured at 2.5 standard deviations (green) and the original figure–of–merit weighted $2F_o$-F_c map contoured at 1 standard deviation (blue) superimposed on the final refined model of NAD^+ bound. Residues involved in catalysis; Cys243 and E209 and shown in sticks.

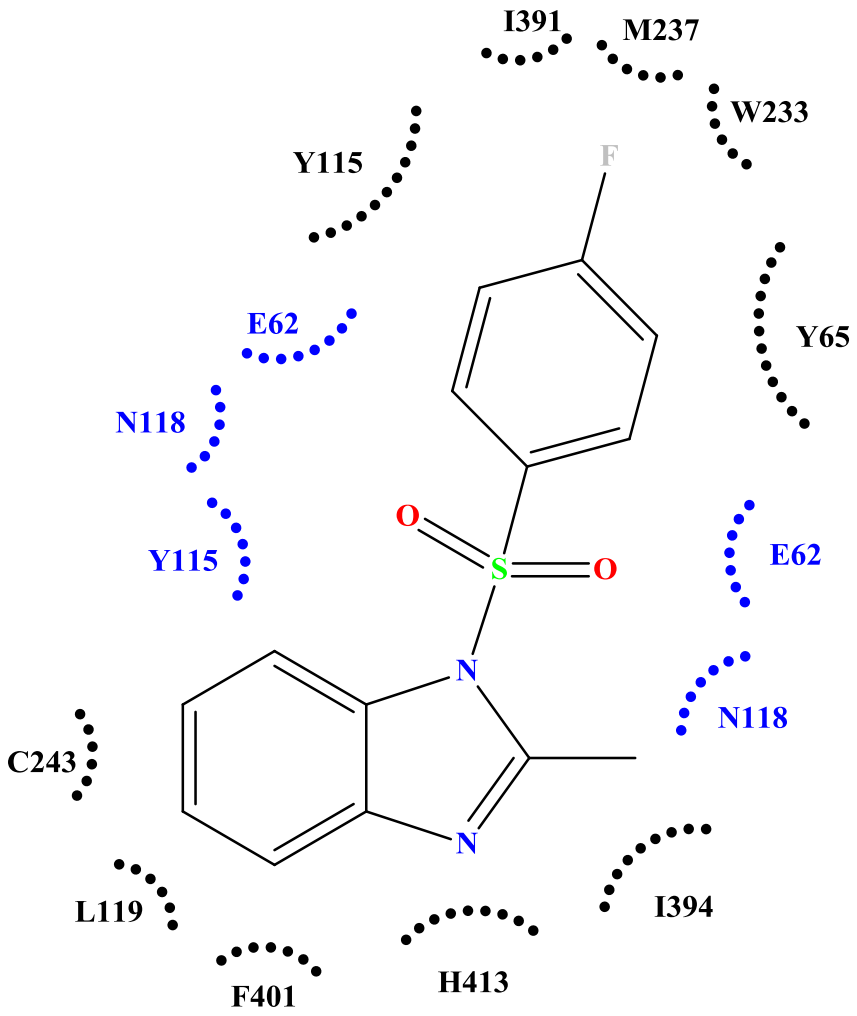

Figure 22. Two dimensional map showing CB7 contact with ALDH3A1. Hydrophobic interactions are shown by black arcs and van der Waals interactions are shown by blue arcs.

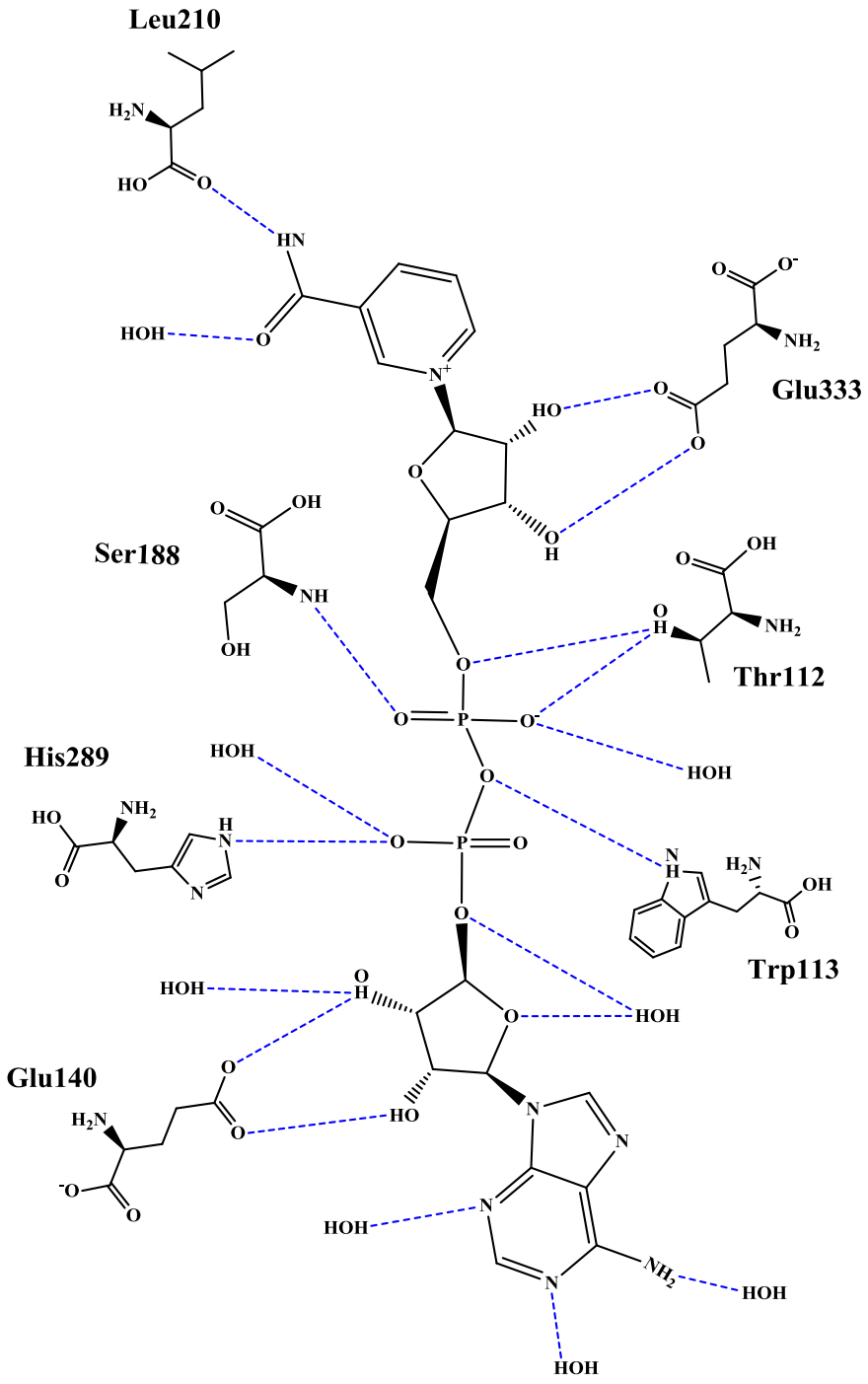

Figure 23. Two dimensional map showing NAD^+ binding with ALDH3A1. Two dimensional map highlighting the hydrogen bonding interactions between NAD^+ and residues of ALDH3A1 present in its Rossmann fold. Blue dotted lines represent the hydrogen bonding interactions with a distance of 2.4–3.2Å.

Table 6. Refinement statistics for CB7 bound to ALDH3A1.

Data collection	**ALDH3A1 (CB7 + NAD^+ co–crystal)**
Space group	$P2_1$
Cell dimensions	a = 95.2 Å, b = 90.9 Å, and c = 117.9 Å α = 90 °, β = 112.4 °, and γ = 90.0 °
Resolution (Å)	50–1.95 (1.98–1.95)
R_{merge}	0.072 (0.34)
I/σ_I	10.9 (4.5)
Completeness	96.3 % (92.6%)
Redundancy	2.8 (2.8)
Refinement	
Resolution (Å)	108.96–1.94
No. of reflections	125, 475
R_{work}/ R_{free}	0.21/ 0.25
No. of atoms	
Protein	14073
Ligand/ Ion	267
Water	979
B–factor (overall)	32.1
RMSD Bond angles (°)	1.07 °
RMSD Bond lengths (Å)	0.05

3. Crystal structure of ALDH3A1 with CB25

The chemical name of CB25 is 1–{[4–(1, 3–benzodioxol–5–ylmethyl) piperazin–1–yl] methyl}–1H–indole–2, 3–dione. Orthorhombic crystals were obtained that belonged to space group $P2_12_12_1$ with unit cell dimensions of a = 61.3, b = 86.4, c = 170.2 and diffracted up to 2.3 Å resolution. Each asymmetric unit contained a dimer. Structure was determined by performing molecular replacement using the apo–form of ALDH3A1 structure as the search model (RCSB code 3SZA). Molecular replacement was performed using MolRep program provided by CCP4 Interface software. In our electron density map, we see the presence of indole–2, 3–dione and piperazine group (Figure 24A). The group involved in forming the most crucial interaction is indole–2, 3–dione. The 3–keto group of the indole–2, 3–dione ring bound within the substrate binding site and forming an adduct with the active site nucleophile (Cys243 in ALDH3A1). The distance between Cys243 and the carbonyl–carbon, as well as the out–of–plane displacement of the carbonyl oxygen, is consistent with the formation of adduct between these two reactive groups. That this covalent bond is reversible is supported by the fact that addition of dithiothreitol to the reaction solution after preincubation restores the enzymatic activity. There is sufficient electron density to model the indole–2, 3–dione and the N–piperazine moiety, but insufficient electron density is present to model the terminal benzyl–dioxol moiety. Modeling of the benzyl–dioxol moiety onto the crystallographically observed partial structure, suggests that the benzyl–dioxol lies at the interface between the exit of the substrate binding site and bulk solvent. Two dimensional map showing interactions of CB25 with the ALDH3A1 active site residues is shown in Figure 24B. Detailed refinement statistics are provided in Table 7. A detailed SAR study needs to be done to proper-

ly analyze and understand how this compound can be made selective for ALDH3A1 since it also inhibits ALDH1A1.

(A)

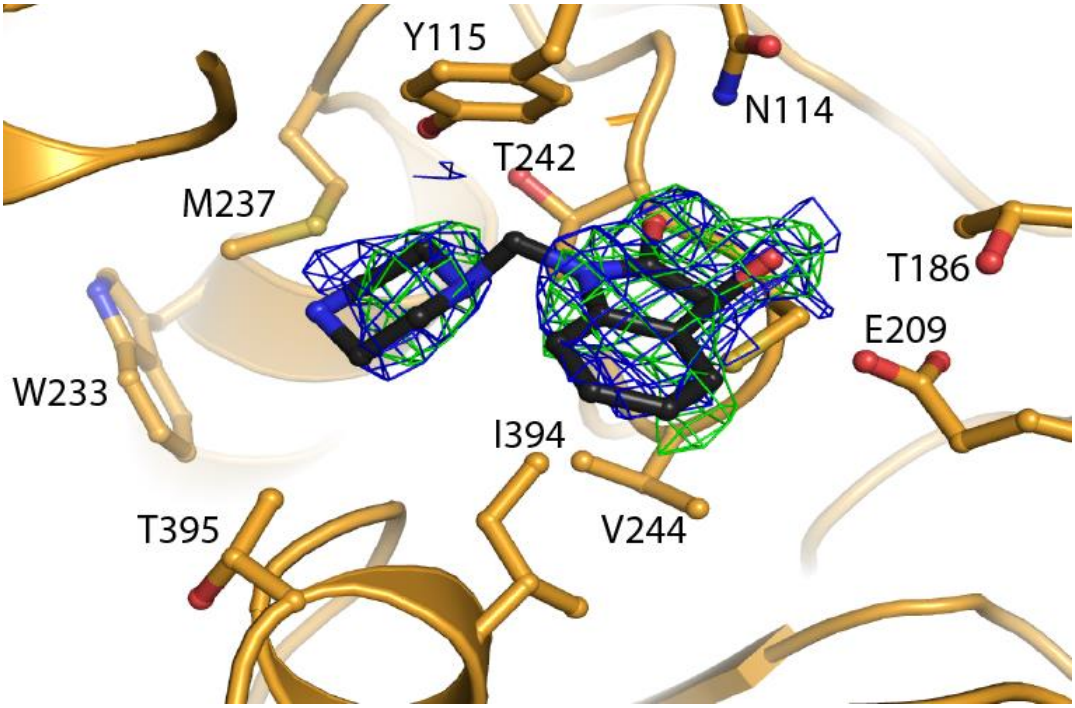

Figure 24. (A) Density map showing the binding of CB25 with ALDH3A1. The electron density maps displayed are the original figure of merit (σ–A weighted) F_o-F_c map contoured at 2.5 standard deviations (green) and the original figure–of–merit weighted $2F_o$-F_c map contoured at 1 standard deviation (blue) superimposed on the final refined model of CB25 bound in the enzyme active site.

(B)

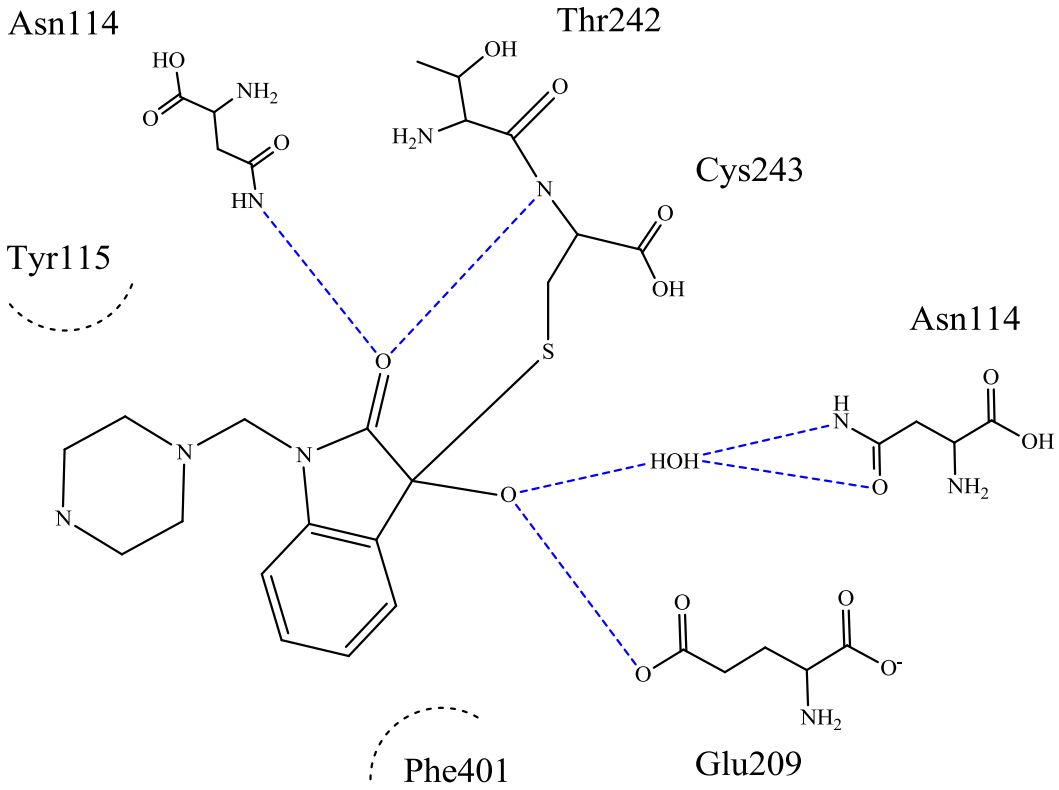

Figure 24. (B) Two dimensional map showing CB25 binding with ALDH3A1. Two dimensional map highlighting interaction of CB25 with active site residues of ALDH3A1. CB25 forms a covalent adduct with Cys243 of ALDH3A1. In addition, we also see some hydrogen bonding interactions. Dotted lines represent the hydrogen bonding interactions within a distance of 2.4–3.2 Å and dotted arcs indicate the residues involved in hydrophobic interaction that lie within a distance of 3.4–4.0 Å from CB25.

Table 7. Refinement statistics for CB25 bound to ALDH3A1.

Data collection	**ALDH3A1 (CB25 co–crystal)**
Space group	$P2_12_12_1$
Cell dimensions	a = 61.3 Å, b = 86.4 Å, and c = 170.61 Å α = 90 °, β = 90 °, and γ = 90.0 °
Resolution (Å)	50.0–2.30 (2.34–2.30)
R_{merge}	6.0 (14.6)
I/ σ_I	16.3 (6.7)
Completeness	96.0 % (88.0 %)
No. of reflections	39, 454
Redundancy	3.4 (2.7)
Refinement	
Resolution (Å)	48.0–2.30
R_{work}/ R_{free}	17.5/ 22.2
No. of atoms	
Protein	6913
Ligand/ Ion	12
Water	649
B–factor (overall)	18.47
B–factor (protein)	18.40
B–factor (ligand/ ion)	27.40/ 36.93
B–factor (water)	21.03
RMSD Bond angles (°)	1.143°
RMSD Bond lengths (Å)	0.006

G. Expression and Activity of ALDH3A1 and ALDH1A1 in Cancer Cell Lines

We examined various cancer cell lines to determine the level of ALDH1A1 and ALDH3A1 expression since these two enzymes are known to metabolically inactivate cyclophosphamide and its derivatives. As previously reported (Moreb et al., 2007), we found A549 cells express both ALDH1A1 and ALDH3A1 (Figure 25A, 25B). In our Western blot experiment, we saw the bands for recombinant ALDH3A1 slightly higher than that of ALDH3A1 from cell lysates. This is because our recombinant protein has a Histidine tag that gives it a slightly higher molecular weight. We quantified the relative expression levels of each isoenzyme through reference to purified recombinantly expressed enzymes. Based on these Western blots, A549 cells expresses ALDH1A1 at about 1% of total lysate protein and ALDH3A1 at about 2% of total lysate (Figure 26A and 26b). SF767 cells also demonstrated robust ALDH3A1 expression, but lacked detectable expression of ALDH1A1 (Figure 25A, 25B). HEK–293 and CCD13Lu cells had no detectable expression of ALDH1A1 or ALDH3A1 (Figure 25A and 25B).

To confirm that protein expression correlates with ALDH activity, we performed activity assays. While benzaldehyde is a substrate for either enzyme, ALDH1A1 will not use $NADP^+$ as a cofactor, therefore the ability to oxidize benzaldehyde in this assay is primarily due to ALDH3A1 (Figure 27). A549 cell lysates had an activity of 282 nmol/ min/ mg. Based on the specific activity of recombinantly ALDH3A1 purified in our lab (32 μmol/ min/ mg), the activity assay confirmed the immunoblot and demonstrated that ALDH3A1 is active and present at ~2% of total lysate protein. Similarly, in SF767 cells, western blot analysis and enzyme assays show that ALDH3A1 is expressed at 1% of total cellular protein (Figure 26C). HEK–293 and CCD13Lu cells had no detectable

ALDH1A1 or ALDH3A1 activity as shown in western blot and enzyme activity assays (Figure 25A and 25B).

The ability of CB29 to inhibit ALDH3A1 activity in cancer cell lysates was also examined using this same activity assay. As shown in Figure 27A, when CB29 is added to the A549 and SF767 cell lysates, the ALDH3A1 activity is diminished significantly: (~95% in A549; ~90% in SF767, right panel). The activity of the recombinant ALDH3A1 also decreased significantly with 50 μM CB29 (~98%, Figure 27A, left panel). Cell lysate activity from SF767 and A549 were also decreased with CB7 and its analogs A10, A20, A21, A64, A70, B27 and B37 (Figure 27B). These data suggest that ALDH3A1 possesses robust activity in tumor cell extracts, and that CB29 and CB7 specifically target the activity of ALDH3A1 in the context of tumor whole cell lysates. These cell lines provide a convenient system to investigate the potentiation of mafosfamide by ALDH3A1 inhibition as A549 cells express both ALDH3A1 and ALDH1A1, SF767 cells express predominantly ALDH3A1, and CCD13Lu or HEK–293 cells do not express detectable levels of several ALDH isoforms.

(A)

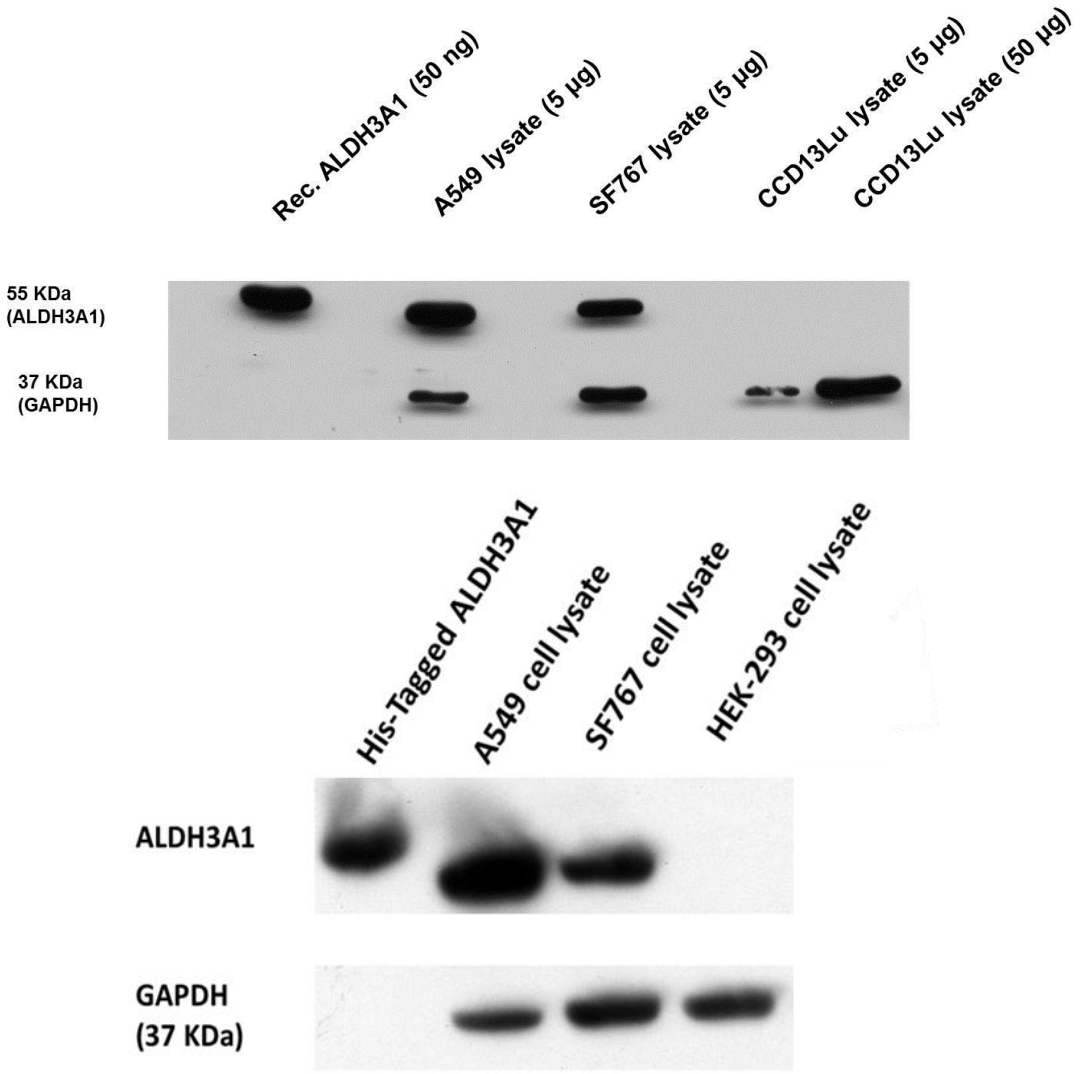

Figure 25. (A) ALDH expression in A549, SF767, HEK293 and CCD13Lu cells. Lysates from various cancer cell lines (A549, SF767, HEK–293 and CCD13Lu) were examined for ALDH3A1 expression. Purified recombinant His–tagged ALDH3A1 protein is taken as positive control and GAPDH serves as a loading control. Purified recombinant ALDH3A1 has a slightly higher band because it is His–tagged and travels slowly on SDS–PAGE gel.

(B)

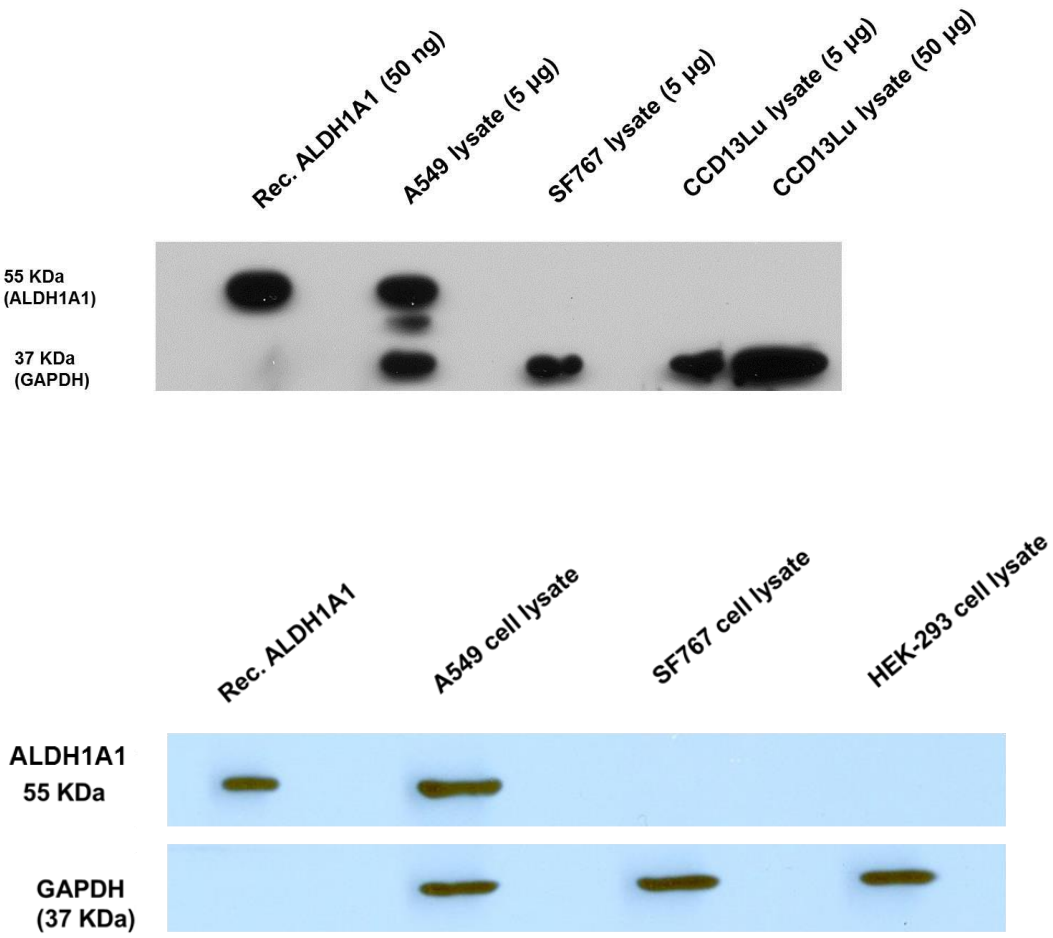

Figure 25. (B) Expression of ALDH1A1 in tumorigenic and non–tumorigenic cells. Lysates from various cancer cell lines (A549, SF767, HEK–293 and CCD13Lu) were examined for ALDH1A1 expression. Purified recombinant ALDH1A1 protein is taken as positive control and GAPDH serves as a loading control.

(C)

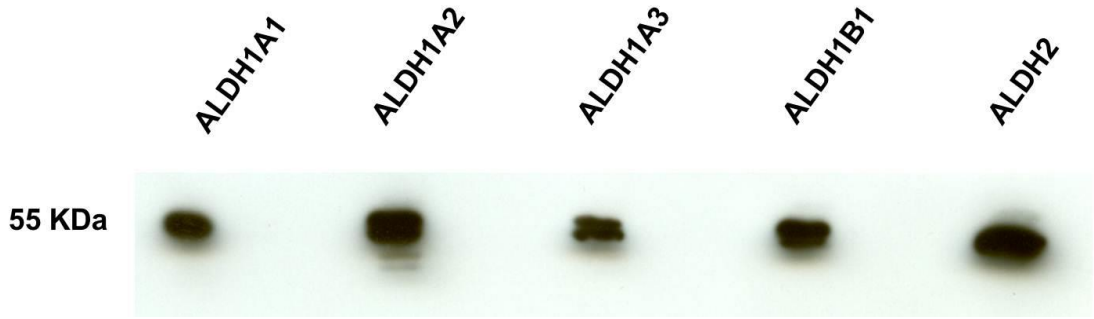

Figure 25. (C) Cross reactivity of ALDH1A1 antibody. Figure shows the cross reactivity of ALDH1A1 antibody, Abcam (ab–23375) with other ALDH subtypes. Human ALDH1 isoforms (ALDH1A1, ALDH1A2, ALDH1A3, and ALDH1B1) and ALDH2 were purified in the lab and were provided by Lanmin Zhai. Each lane was loaded with between 50 and 70 ng of the purified recombinant human ALDH1A1, ALDH1A2, ALDH1A3, ALDH1B1 and ALDH2 isoenzymes respectively and were detected using ALDH1A1 antibody.

(A)

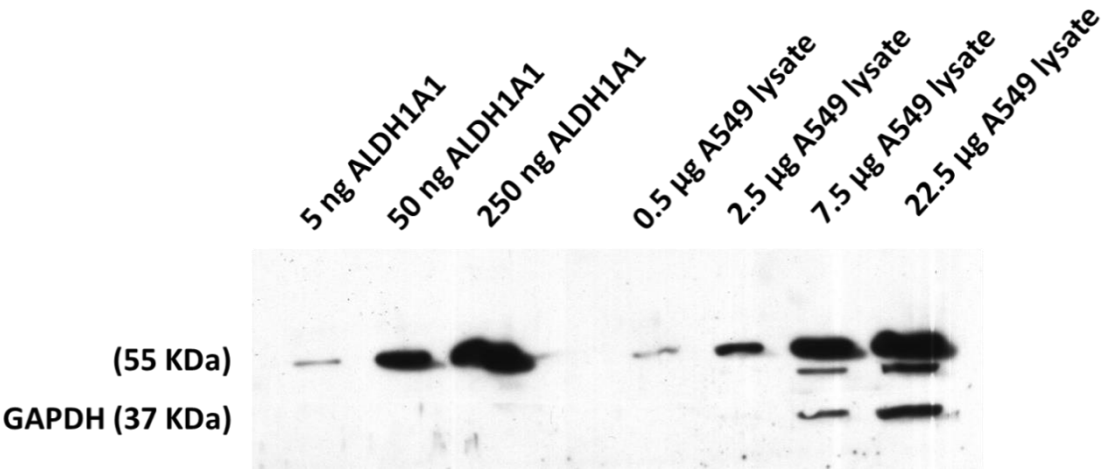

Figure 26. Quantitation of ALDH1A1 and ALDH3A1 in A549 and SF767 cells. (A) Quantitation of ALDH1A1 expression in A549 cell line. Serial dilutions of A549 cell lysates (0.5 µg–22.5 µg) were compared against serial dilutions of recombinantly purified ALDH1A1 (5 ng–250 ng). Purified recombinant ALDH1A1 protein served as positive control and GAPDH served as a loading control.

(B)

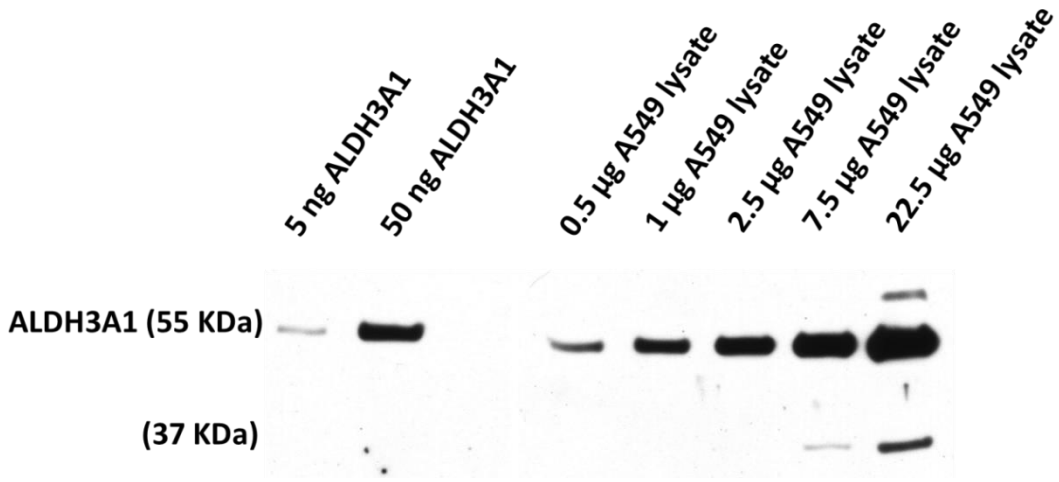

Figure 26. (B) Quantitation of ALDH3A1 expression in A549 cell line. Serial dilutions of A549 cell lysates (0.5 µg–22.5 µg) were compared against serial dilutions of recombinantly purified ALDH1A1 (5 ng–50 ng). Purified recombinant His–tagged ALDH3A1 protein served as positive control and GAPDH served as a loading control.

(C)

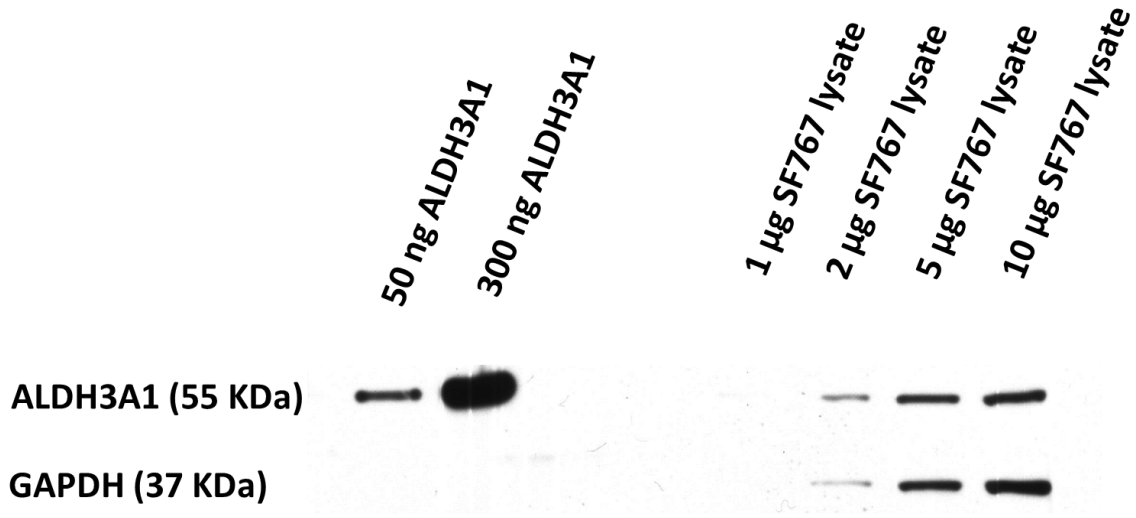

Figure 26. (C) Quantitation of ALDH3A1 expression in SF767 cell line. Serial dilutions of SF767 cell lysates (1 µg–10 µg) were compared against serial dilutions of recombinantly purified ALDH3A1 (50 ng–300 ng). Purified recombinant His–tagged ALDH3A1 protein served as positive control and GAPDH served as a loading control.

(A)

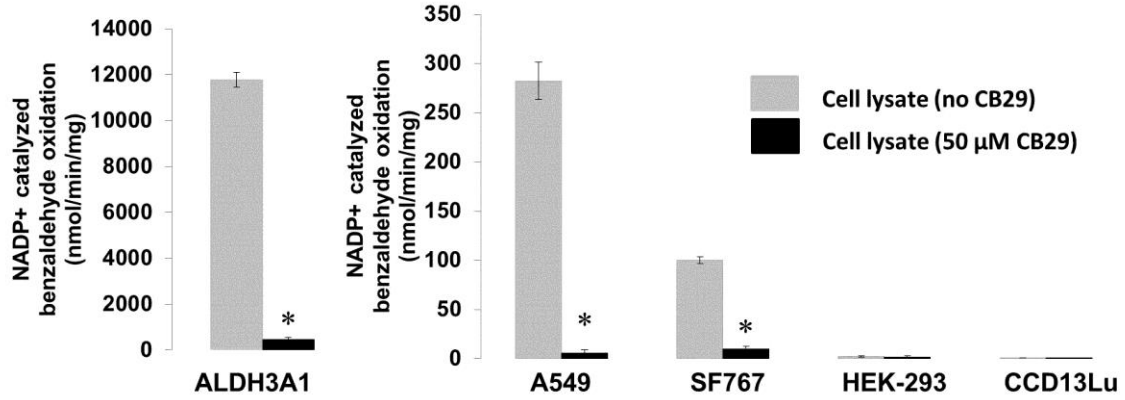

(B)

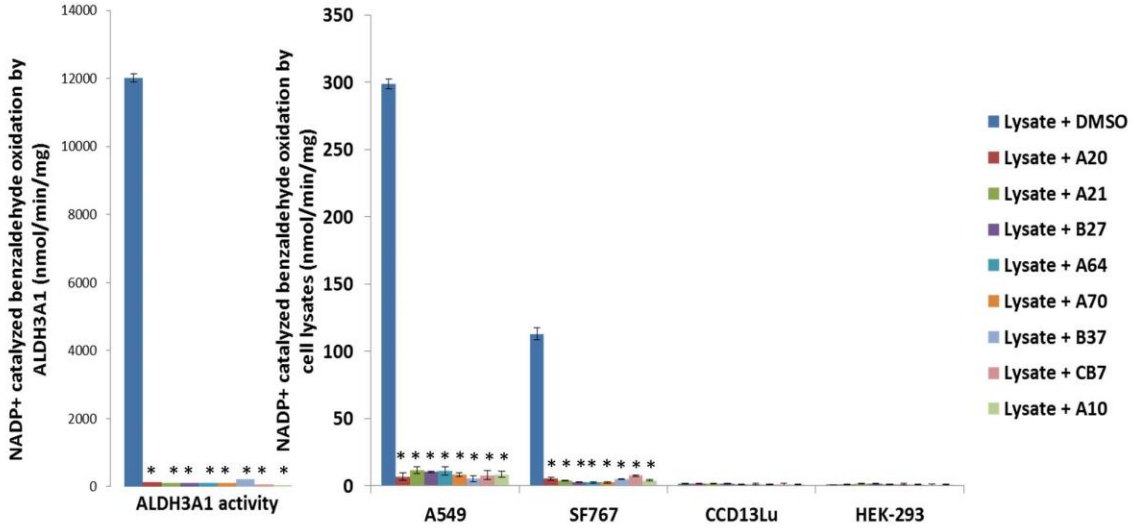

Figure 27. ALDH3A1 inhibition in cancer cell lysates by ALDH3A1 inhibitors.

A549, SF767, HEK–293 and CCD13Lu cell lysate activity were tested in the presence of 1.5 mM $NADP^+$ and 1 mM benzaldehyde and in the presence and absence of **(A)** 50 µM CB29 and **(B)** 10 µM CB7 and its analogs. The p values were calculated using the Student's *t* test comparing activity in the absence and presence of inhibitor (CB29) (*, $p < 0.001$, n=3).

H. Sensitization of tumor cells to mafosfamide through inhibition of ALDH3A1

ALDH3A1 has been shown to directly influence cellular sensitivity to the effects of cyclophosphamide treatment. We want to test the ability of our inhibitors to increase the sensitivity of tumor cells to cyclophosphamide and its derivatives as a means to widen the therapeutic window for this anti–neoplastic agent (Boesch et al., 1996; Sreerama et al., 1995). Toward this end, we evaluated the ability of CB7 and CB29 and selected analogs to increase the sensitivity of lung adenocarcinoma (A549) and glioblastoma (SF767) cells toward mafosfamide. These compounds were chosen because they were selective to ALDH3A1 activity and showed no inhibition to ALDH1A1 activity or ALDH2 *in vitro*. Also these compounds had high solubility and could easily form a homogenous 100 µM solution in the presence of 0.25% DMSO and demonstrated the lowest general cytotoxicity at concentrations as high as 100 µM. The ED_{50} values for mafosfamide on A549 and SF767 cells were 125 µM and 150 µM, respectively, while CCD13Lu and HEK–293 cells were more sensitive to mafosfamide having an ED_{50} values of 40 µM and 80 µM, respectively (Figure 28).

1. Treatment with CB29 analogs

Treatment with mafosfamide decreased cell proliferation in all cell lines (Figure 29A and 29B, DMSO control vs. mafosfamide, 100 % vs. 59 ± 14% (A549), $p < 0.001$, 100% vs. 68 ± 4% (SF767), $p<0.001$). Treatment with ALDH3A1 inhibitors B1, B2, B4, B9, B11, B15, A18 and CB29 had little effect on cell proliferation (Figure 29A and 29B, grey bars) as single agents. At doses that inhibited ALDH3A1 in cell lysates (50 µM), we did not observe cytotoxicity in either A549 or SF767 cells except for analog B21

($p<0.005$). We tested doses as high as 100 μM and did not see significant cytotoxicity in the absence of mafosfamide (data not shown). Co–treatment of cells with compounds B1, B2, B4, B9, B11, B15, as well as CB29 decreased cell proliferation relative to mafosfamide alone (Figure 29A and 29B). Similar experiments were performed with CCD13Lu and HEK293 cells (devoid of ALDH3A1 expression). Treatment with mafosfamide in the presence of ALDH3A1 inhibitors did not significantly enhance mafosfamide sensitivity in HEK–293 and CCD13Lu cells (Figure 29C and 29D). Since SF767 cells do not express ALDH1A1, we performed a dose–dependent study for sensitization toward mafosfamide in these cells. We used the parent compound, CB29 as well as analogs B4 and B9 based on the degree of mafosfamide–induced enhancement we observed in Panel A and B. We observed a dose–dependent decrease in cell proliferation (Figure 29E) as the concentration of compounds B4, B9 and CB29 increased.

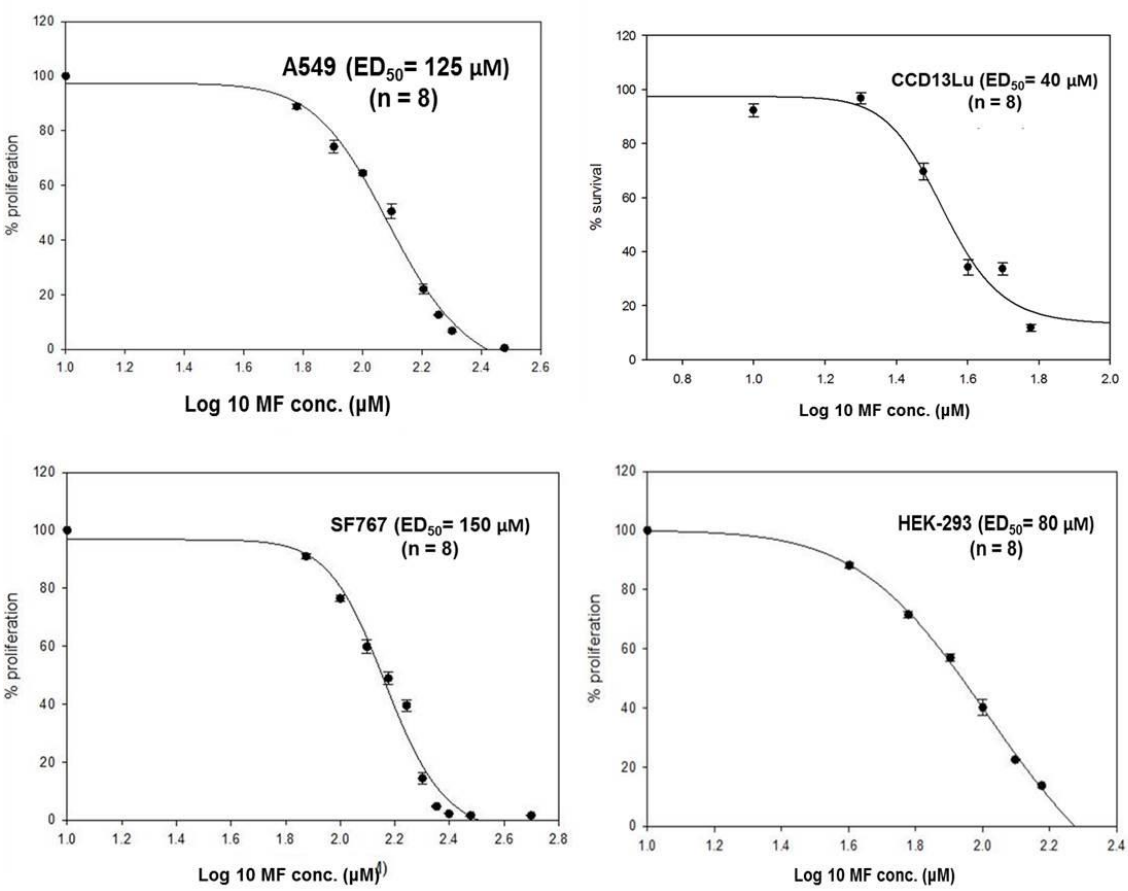

Figure 28. Determination of mafosfamide ED_{50} values in various cell lines. 5000 A549 and CCD13Lu cells and 10, 000 SF767 and HEK–293 cells treated with increasing concentration of mafosfamide. Figure shows logarithmic plot for approximate ED_{50} values of mafosfamide on various cell lines (A549, SF767, HEK293 and CCD13Lu respectively).

Figure 29. Chemosensitivity experiments in cancer cells with CB29 analogs. Cells were simultaneously treated with mafosfamide (MF) in combination with ALDH3A1 inhibitors (50 µM). **(A)** A549 and **(B)** SF767 cells treated with mafosfamide (125 µM) for 19 hours. **(C)** CCD13Lu cells treated with 40 µM mafosfamide for 19 hours. **(D)** HEK–293 cells treated with 80 µM mafosfamide for 19 hours. Cell proliferation was determined using the MTT assay. The DMSO concentration was limited to 0.25% (v/ v). The p values were calculated by comparing the cellular proliferation of mafosfamide treated cells to that of mafosfamide in combination with ALDH3A1 inhibitor treated cells (*, $p \leq 0.001$, n = 10–15) or DMSO treated cells to that of compound treated cells (**, $p \leq 0.005$, n = 10–15). Grey bars represent compound treatment alone and black bars represent compound and mafosfamide treatment. Each bar represents the mean value ± SE. **(E)** SF767 cells treated with increasing concentrations of B4, B9, and CB29 and either the presence or absence of 125 µM mafosfamide (n= 10–15).

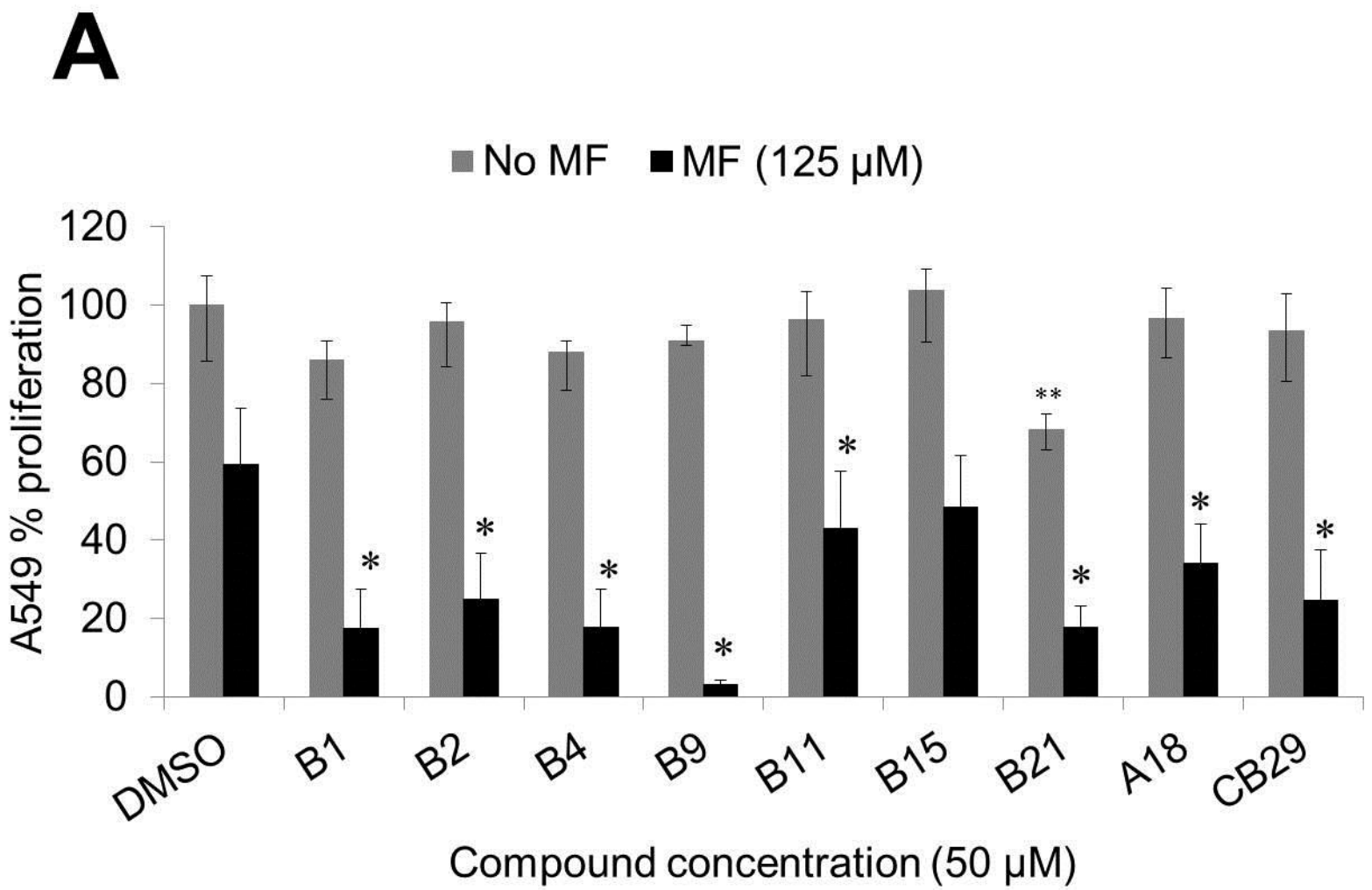
A
No MF
MF (125 µM)
A549 % proliferation
120
100
80
60
40
20
0
DMSO
B1
B2
B4
B9
B11
B15
B21
A18
CB29
Compound concentration (50 µM)

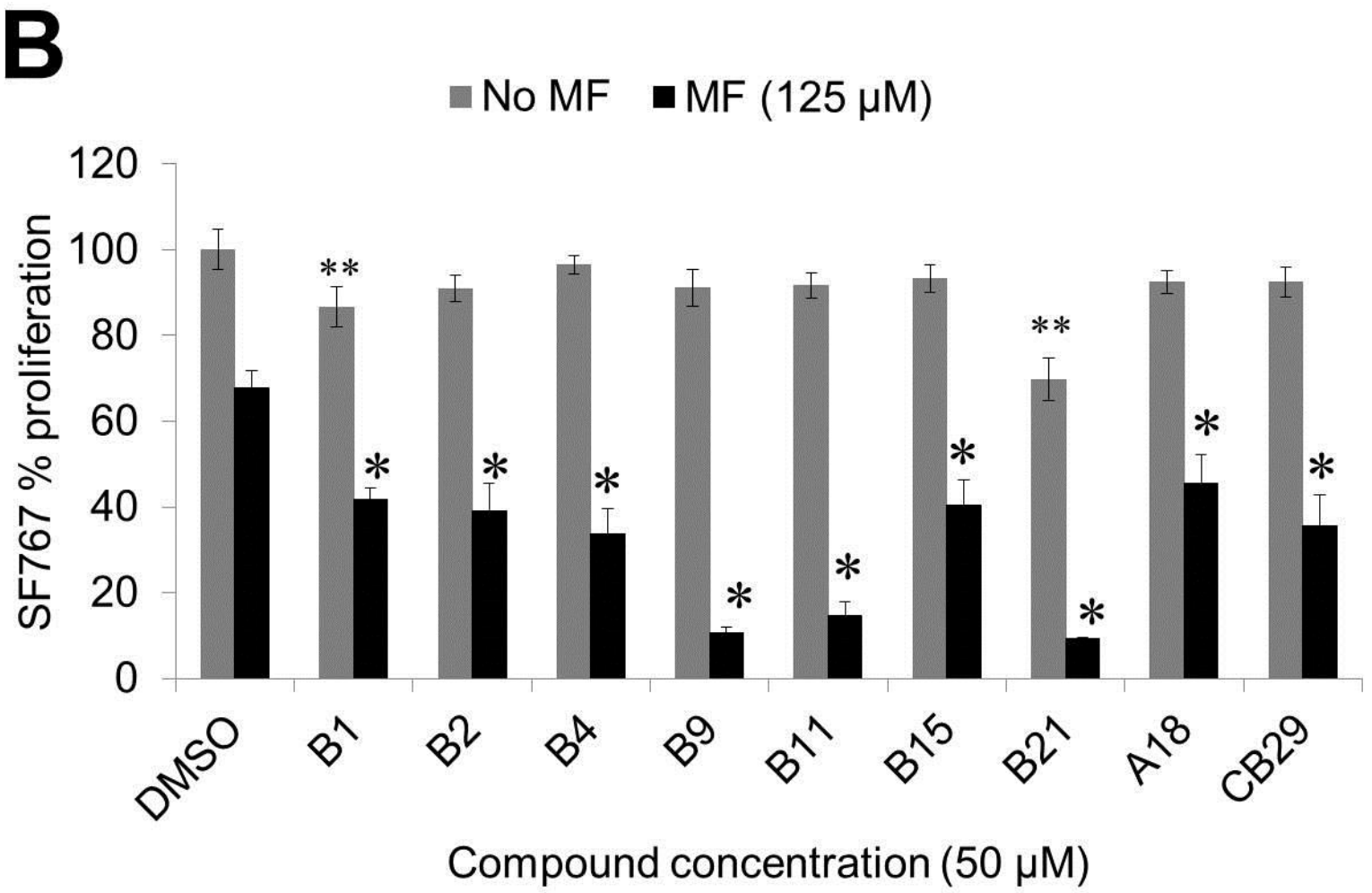
B
No MF
MF (125 μM)
SF767 % proliferation
120
100
80
60
40
20
0
**
*
DMSO
B1
B2
B4
B9
B11
B15
B21
A18
CB29
Compound concentration (50 μM)

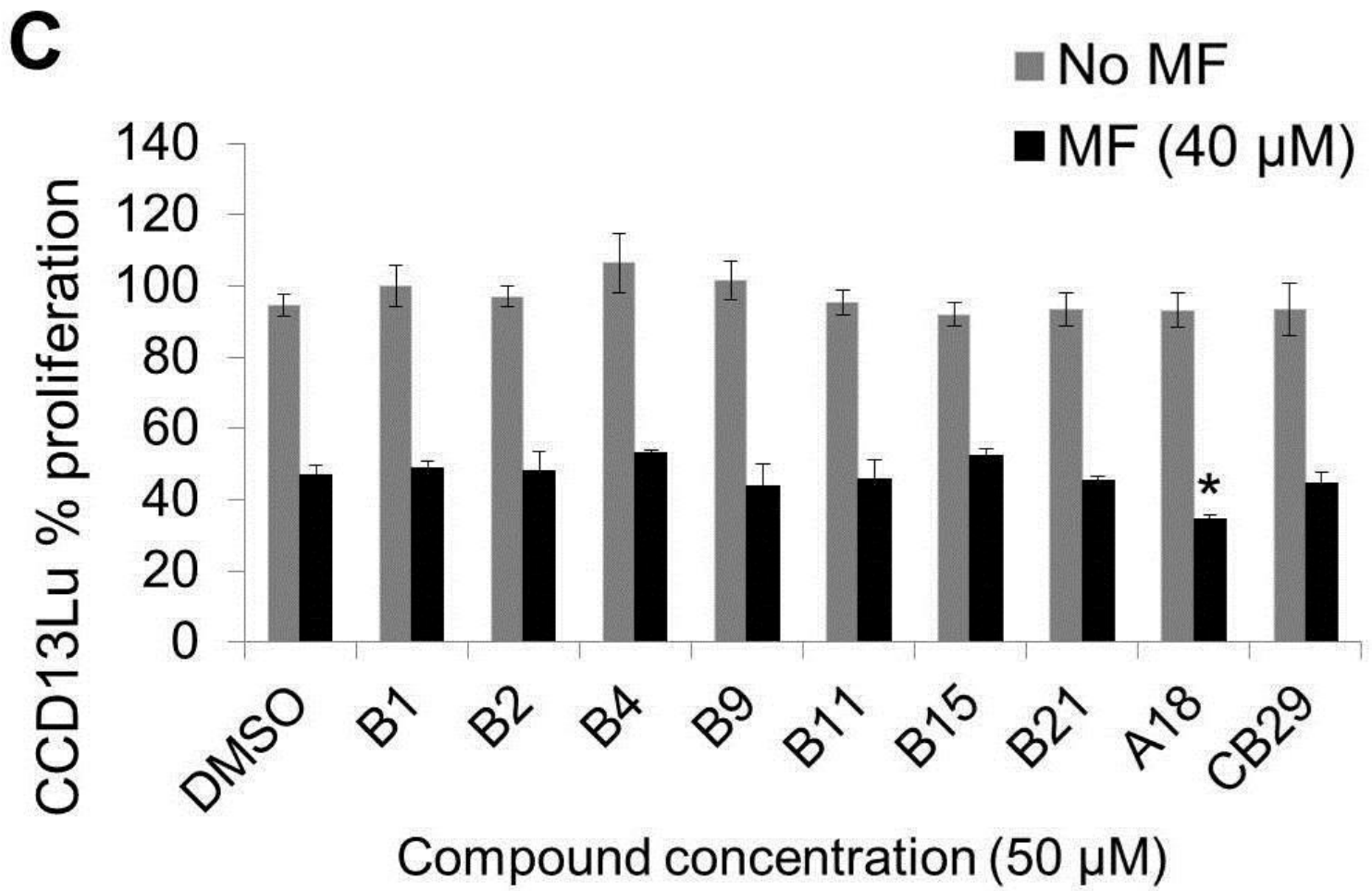
C
No MF
MF (40 µM)
CCD13Lu % proliferation
140
120
100
80
60
40
20
0
*
DMSO
B1
B2
B4
B9
B11
B15
B21
A18
CB29
Compound concentration (50 µM)

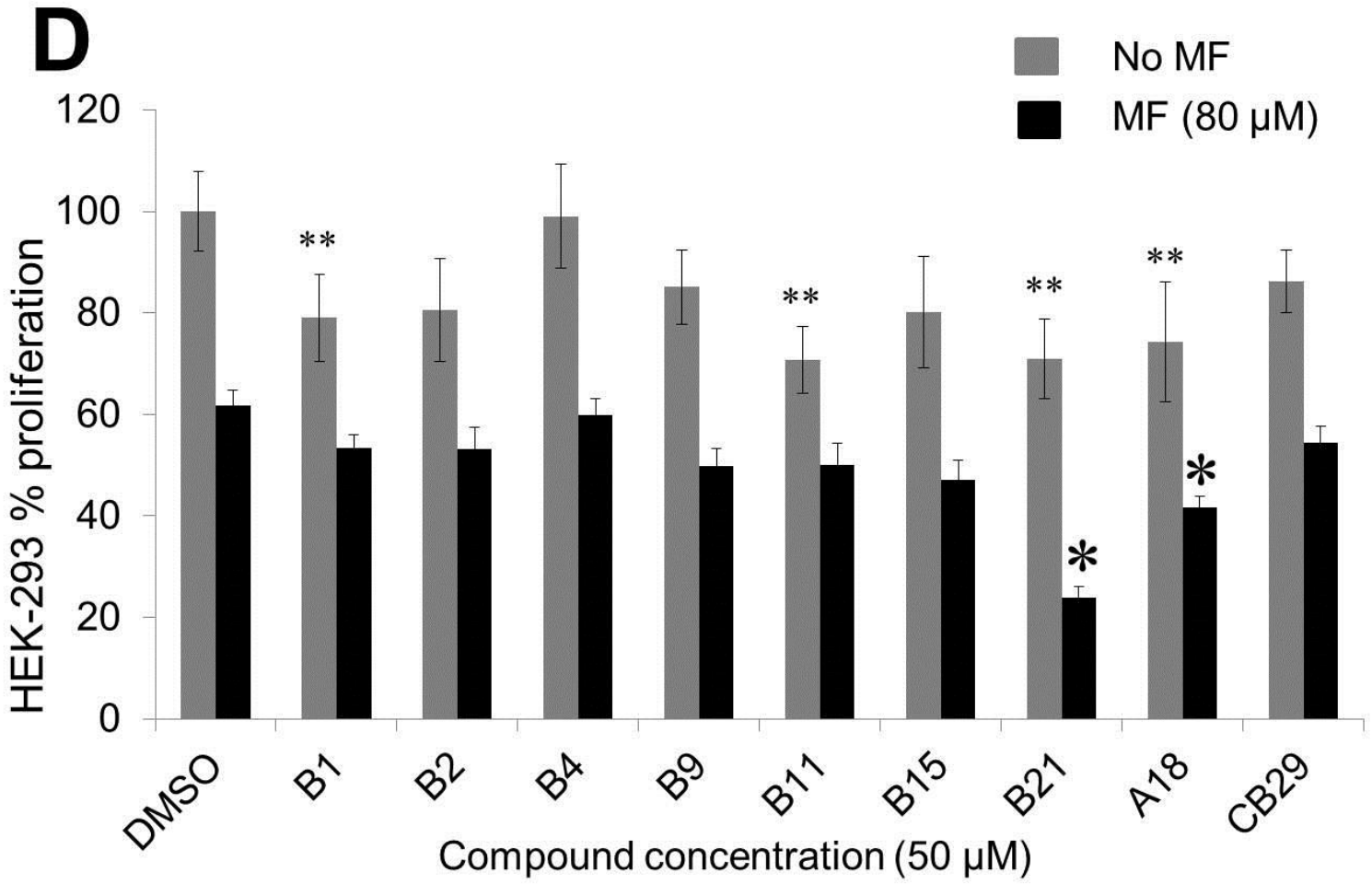
D
No MF
MF (80 μM)
HEK-293 % proliferation
120
100
80
60
40
20
0
**
**
**
**
*
*
DMSO
B1
B2
B4
B9
B11
B15
B21
A18
CB29
Compound concentration (50 μM)

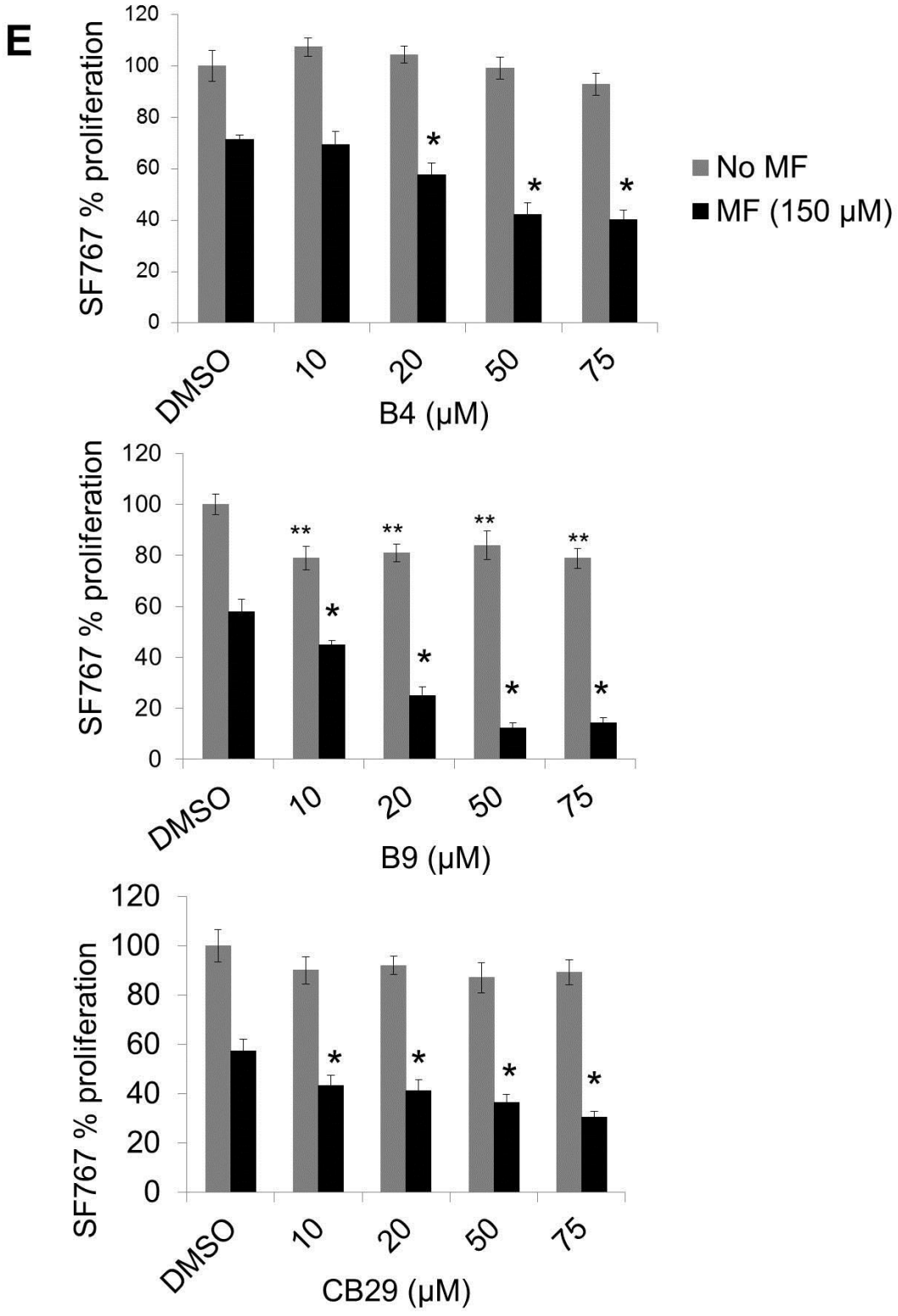
E
SF767 % proliferation
120
100
80
60
40
20
0
DMSO
10
20
50
75
B4 (μM)
No MF
MF (150 μM)
B9 (μM)
CB29 (μM)

2. Treatment with CB7 analogs

Mafosfamide chemosensitivity experiments were also conducted with CB7 and its analogs A10, A20, A21, A64, A70, B37 and B27. All of these compounds were very selective for ALDH3A1 activity and showed no inhibition to ALDH1A1 and ALDH2. These compounds also had high solubility and could easily form a homogenous 100 μM solution in the presence of 0.25% DMSO and demonstrated the lowest general cytotoxicity at concentrations as high as 50 μM. Mafosfamide treatment decreased cell proliferation in all cell lines (Figure 30A and 30B, DMSO control vs. mafosfamide, 100 % vs. 49 ± 3% (A549), $p < 0.001$, 100% vs. 45 ± 2% (SF767), $p<0.005$). Treatment with ALDH3A1 inhibitors A10, A20, A21, CB7, A64, A70, B37 and B27 had little effect on cell proliferation (Figure 30A and 30B, grey bars) as single agents. At doses that inhibited ALDH3A1 in cell lysates (10 μM), we did not observe significant cytotoxicity in either A549 or SF767 cells ($p<0.005$). We tested doses as high as 50 μM and did not see significant cytotoxicity in the absence of mafosfamide ($p<0.005$). Co–treatment of cells with 10 μM compounds A20, A21, A64, A70, B37 and B27 increased sensitivity to mafosfamide in SF767 and A549 cell lines (Figure 30A and 30B). Compound A10 was cell line dependent and exhibited some cytotoxicity in A549 cells and seemed to enhance mafosfamide sensitivity in CCD13Lu cell line (Figure 30C). We further performed a dose–dependent study for the three most potent compounds for sensitization toward mafosfamide in A549 and SF767 cells. We used the parent compound, CB7 as well as analogs A64 and A70 for our study. We observed a dose–dependent decrease in cell proliferation (Figure 31) as the concentration of compounds CB7, A64 and A70 increase.

Figure 30. Chemosensitivity experiments in cancer cells with CB7 analogs. Cells were simultaneously treated with mafosfamide (MF) in combination with ALDH3A1 inhibitors (10 µM). **(A)** A549 and **(B)** SF767 cells treated with mafosfamide (125 µM) for 19 hours. **(C)** CCD13Lu cells treated with 40 µM mafosfamide for 19 hours. Cell proliferation was determined using the MTT assay. The DMSO concentration was limited to 0.25% (v/ v). The p values were calculated by comparing the cellular proliferation of mafosfamide treated cells to that of mafosfamide in combination with ALDH3A1 inhibitor treated cells (*, $p \leq 0.001$, $n = 10–15$) or DMSO treated cells to that of compound treated cells (**, $p \leq 0.005$, $n = 10–15$). Black bars represent compound treatment alone and grey bars represent compound and mafosfamide treatment. Each bar represents the mean value ± SE.

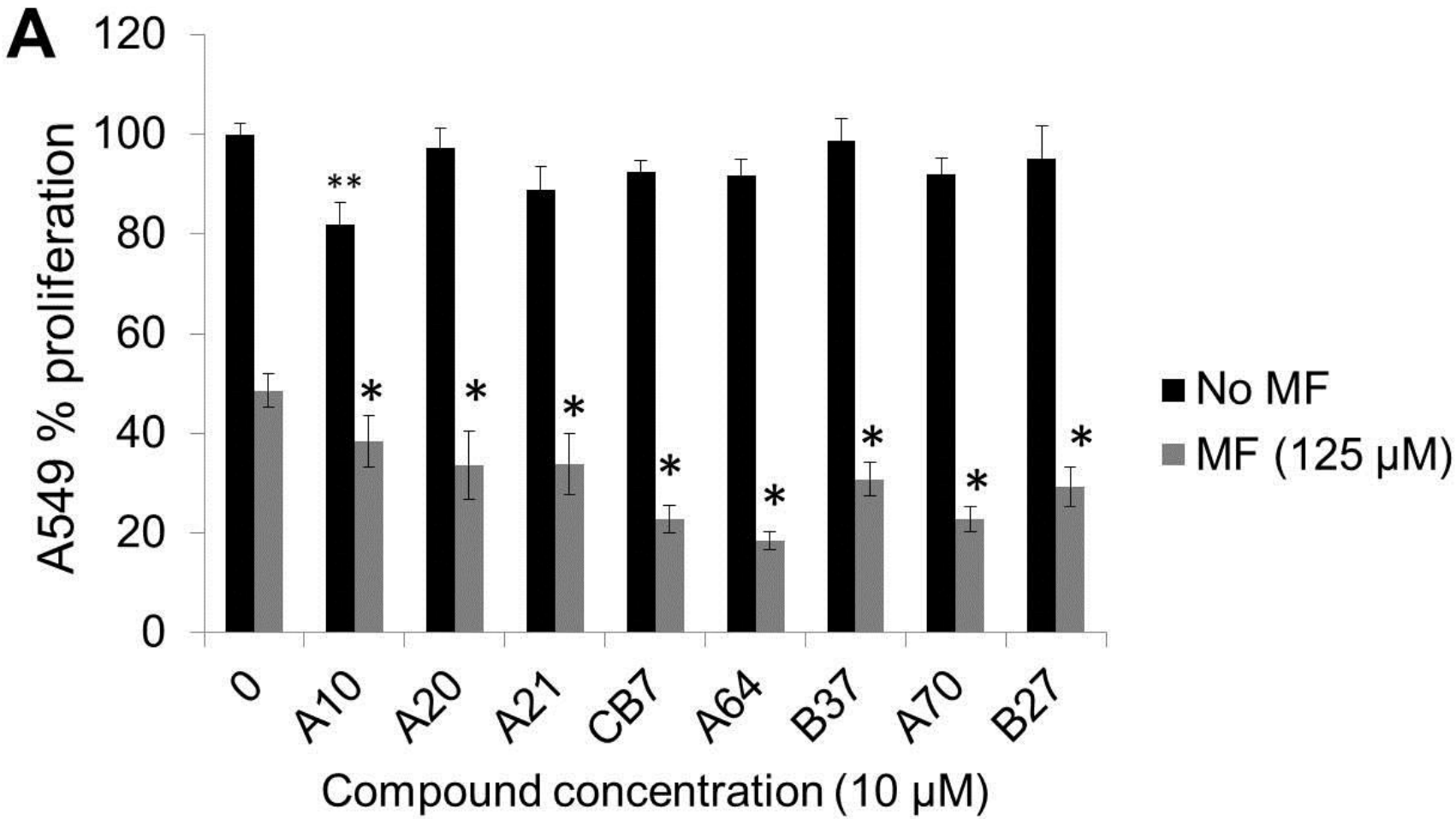
A
120
100
80
60
40
20
0
A549 % proliferation
**
*
*
*
*
*
*
*
*
0
A10
A20
A21
CB7
A64
B37
A70
B27
Compound concentration (10 μM)
No MF
MF (125 μM)

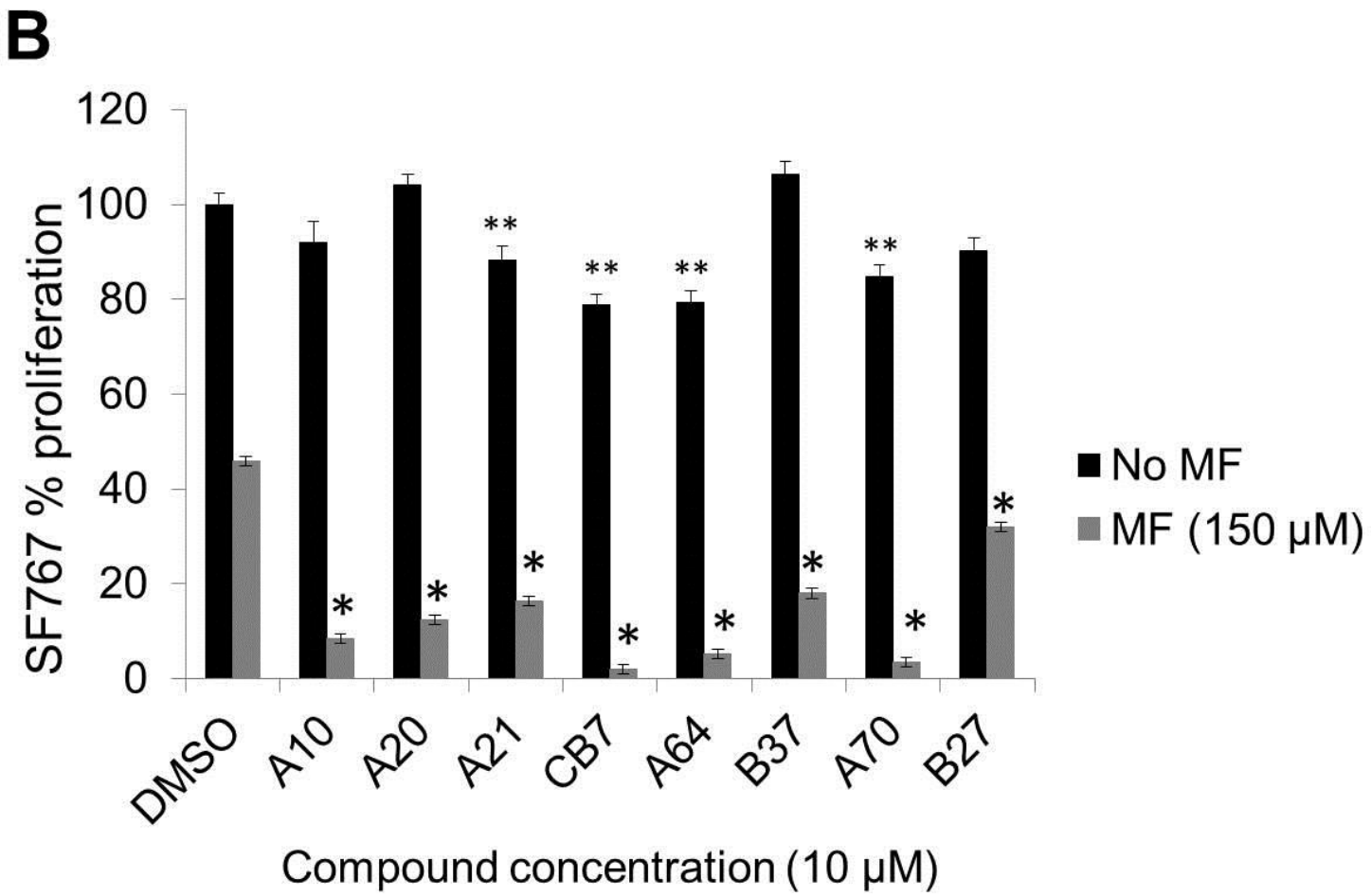
B
SF767 % proliferation
120
100
80
60
40
20
0
DMSO
A10
A20
A21
CB7
A64
B37
A70
B27
Compound concentration (10 μM)
No MF
MF (150 μM)

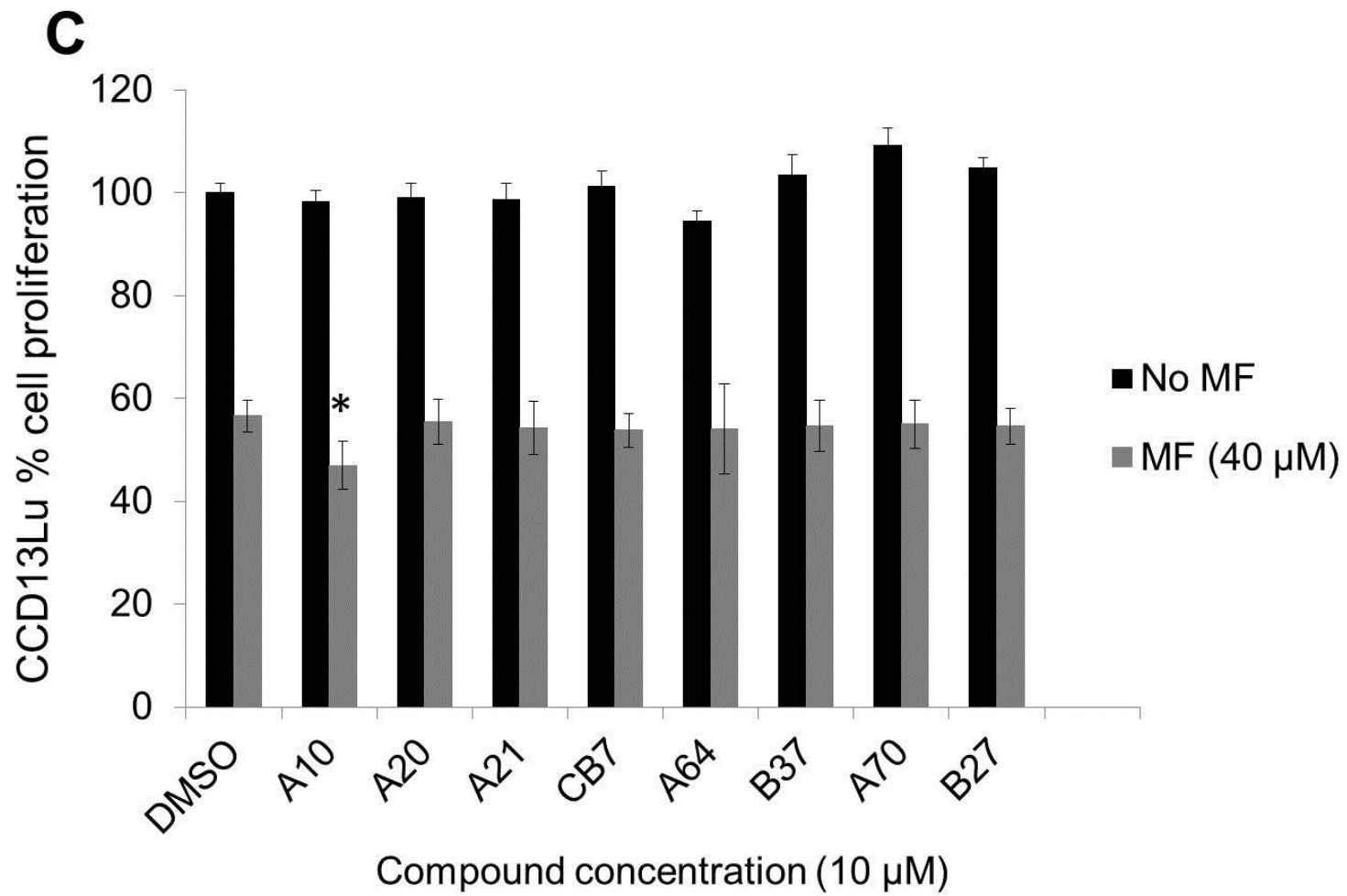
C
CCD13Lu % cell proliferation
120
100
80
60
40
20
0
*
No MF
MF (40 μM)
DMSO
A10
A20
A21
CB7
A64
B37
A70
B27
Compound concentration (10 μM)

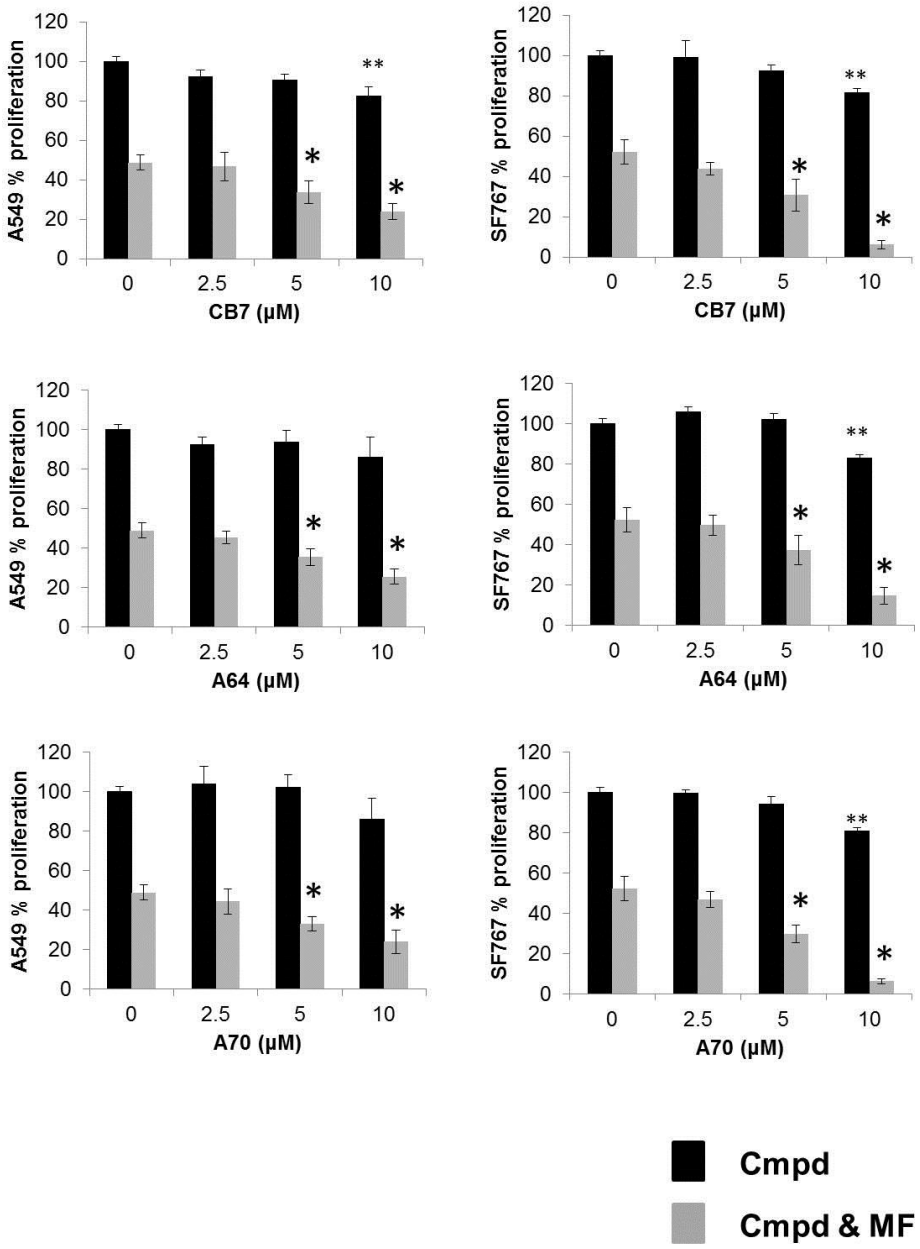

Figure 31. Dose dependent study with CB7 analogs. A549 and SF767 cells treated with increasing concentrations of CB7, A64, and A70 in the presence or absence of 125 and 150 μM mafosfamide respectively. The p values were calculated by comparing the cellular proliferation of mafosfamide treated cells to that of mafosfamide in combination with ALDH3A1 inhibitor treated cells (*, $p \leq 0.001$, $n = 10–15$) or DMSO treated cells to that of compound treated cells (**, $p \leq 0.005$, $n = 10–15$).

IV. Discussion

Drug resistance is one of the major causes of therapeutic failure during cancer treatment. Some of the important mechanisms include altered rate of drug import or export, target mutation, gene amplification, increased DNA repair and increased expression of drug metabolizing enzymes. As one of the major contributors to drug resistance, drug metabolizing enzymes are attractive targets for reversing such resistance (Swanson et al., 2010). Cyclophosphamide is an oxazaphosphorine prodrug used in the treatment of a spectrum of cancers but its clinical utility is often limited by bone marrow toxicity as dosages are increased to overcome resistance in tumors. Cyclophosphamide forms an intermediate known an aldophosphamide when activated by cytochrome P450. By undergoing a non–enzymatic beta–elimination reaction, aldophosphamide forms phosphoramide mustard which is the DNA–alkylating agent that targets rapidly dividing cells. ALDH isoenzymes and ALDH1A1, in particular, are known for their ability to confer resistance to derivatives of cyclophosphamide. The contribution of ALDH3A1 toward cyclophosphamide resistance is more controversial, with some studies supporting a role and others refuting (Moreb et al., 2007; Ganaganur et al., 1994; Sreerama and Sladek 1995; Sladek, 1999; Moreb et al., 2005; Giorgianni et al., 2000). We have previously shown that non–selective covalent inhibitors of ALDH family members can sensitize A549 cells to the cytotoxic effects of aldophosphamide (Khanna et al., 2011), which is consistent with earlier studies in which siRNA knockdown of both ALDH1A1 and ALDH3A1 were required for maximal sensitivity to aldophosphamide (Moreb et al., 2007). What is clear from both *in vitro* and cell–based work is that ALDH1A1 exhibits greater catalytic efficiency toward aldophosphamide than ALDH3A1, although the au-

thors of one study indicated that the purified recombinant enzyme (identical to that used in these studies) exhibited "considerable activity" toward aldophosphamide (Giorgianni et al., 2000). These authors also concluded that only upon high level of expression, does ALDH3A1 play a significant role in conferring resistance to derivatives of cyclophosphamide (Giorgianni et al., 2000), something that both A549 and SF767 cells exhibit. Consequently, identification of cell permeable selective inhibitors for ALDH3A1, and/ or ALDH1A1, may provide a means to understand their individual contributions toward aldophosphamide metabolism and potentially widen the therapeutic window during treatment regimens that could be individually targeted according to the levels of these two ALDH family members.

In addition to aldehyde oxidation, aldehyde dehydrogenases are known to catalyze the hydrolysis of para–nitrophenylacetate (Sidhu et al., 1975). Competition assays have also shown that ester hydrolysis occurs at the aldehyde binding site (Sidhu et al., 1975). In spite of sharing the same catalytic site for catalysis, the mechanism of reaction, however, varies. In the case of ALDH2, aldehyde oxidation involves a nucleophilic reaction of the substrate with active site Cysteine (Cys302) resulting in formation of a thiohemiacetal. This is followed by hydride transfer to NAD^+ yielding a thioester intermediate and NADH. The thioester is eventually hydrolyzed to the carboxylic acid product in a reaction that involves activation of water by an adjacent glutamate (Glu268). The esterase activity is stimulated by cofactor NAD^+, but the co–factor is not essential for the reaction. Reaction is initiated by nucleophilic attack on the carbonyl carbon of the substrate by Cys302, forming an intermediate thioester and subsequently releasing the corresponding alcohol by hydrolysis of the intermediate through activation of water by Glu268 (Mann et

al., 1999). Interestingly, kinetic and mutagenic studies in class 3 human stomach aldehyde dehydrogenase showed that NAD^+ binding had inhibitory effect on the esterase activity of stomach ALDH3 but had an activating effect on ALDH2 based esterase activity (Mann et al., 1999). Despite having differential effects for NAD^+ on esterase activity, the fact that dehydrogenase and esterase reactions share the same catalytic site and same residues of ALDH for their respective reactions provides us evidence enough that these two assays can be used for inhibitor screen and validation. Previous experience in high–throughput screening from our lab has shown that NADH based absorbance at 340 nm wavelength shows absorbance and fluorescence overlap with many compounds in the screening library leading to false results. Therefore, we chose to use an esterase based assay (λ= 405nm) for our screen that has minimum overlap with the absorbance properties of the compounds in the library.

Our initial round of screening provided us with 436 compounds that had >60% inhibition of esterase activity. Out of all these compounds, only 71 compounds reproduced inhibition of esterase activity in our second round. We bought these 71 compounds from commercial vendors and tested them for dehydrogenase (second) assay. Only 55 inhibited dehydrogenase activity of ALDH3A1. Some of these compounds had structural similarity with each other. But an interesting thing to note was that many of our hits showed inhibition to both ALDH3A1 and ALDH1A1 activity having minimal to almost no effect on ALDH2 activity. We see this trend possibly due to structural similarity between ALDH1A1 and ALDH3A1 in their active site. Interestingly, two compounds, namely CB7 and CB29 were the most selective inhibitors for ALDH3A1 activity.

A. Characterization of CB29 binding

Our steady state kinetic experiments showed that CB29 displays a competitive inhibition pattern toward both aldehyde and coenzyme substrates, suggesting that the compound can bind to both the free enzyme and the enzyme–coenzyme species along the reaction pathway. Our kinetic data is further supported by crystallographic data where we see CB29 binding in the aldehyde binding pocket. We can clearly see that the binding of aldehyde substrate requires that the inhibitor is displaced in order for the aldehyde to bind in a position conducive to catalysis. With respect to the mode of interaction with the coenzyme ($NADP^+$) species, earlier studies have shown that the coenzyme molecule in ALDH isoenzymes undergoes an isomerization event during catalysis with a minimum of two conformations for the coenzyme, referred to as the "hydride transfer" and "hydrolysis" conformations (Perez Miller et al., 2003). The mode of binding displayed by CB29 likely requires that it bind to ALDH3A1 when the coenzyme is in the "hydrolysis" conformation, since the methyl sulfonyl moiety lies very close to catalytic cysteine and would overlap with the position of the nicotinamide ring when it adopts the hydride transfer conformation (Figure 32A). This explains why CB29 is competitive to $NADP^+$ binding as well. Based on this binding pattern, we propose a model for CB29 as shown below (Figure 32B).

Our SAR study showed that ALDH3A1 cannot tolerate larger substituents at the R1 position without decreasing inhibitory potency [B5, B18, B22, B6]. We see this trend due to steric clashes that would occur with the side chains of Leu119, Tyr412 and Phe401 in this region. Our SAR study further showed that substitution of the linking amine group in CB29 (IC_{50} 16 μM) with an ether linkage is deleterious to potency (IUSC–12417; IC_{50}

>100 μM) (Table 3B). The deleterious nature of substituting an ether linkage for this amino linkage in CB29 is possibly due to the loss of a hydrogen bonding interaction with the peptide carbonyl group of Glu61 or due to the difference in bond distance and angle geometries of the respective atoms, or a combination of both. Our SAR data further showed that acetamide at the para position of aniline although was not greatly crucial for the potency of CB29 but played an important role in terms of ALDH3A1 selectivity. We saw when acetamide was substituted with larger amides such as isobutyramide (B13) or isopentanamide (B16), these compounds (B13 and B16, respectively) demonstrated greater inhibition towards both ALDH1A1 and ALDH3A1. Analogs that have bigger amides at the para position of aniline and larger substitutions at the R1 position (B22) showed greater selectivity towards ALDH1A1 than ALDH3A1 at 100 μM. We will require crystal structure of ALDH1A1 complexed to these compounds to explain this selectivity pattern. However, this information at least provides us a starting point for the development of selective inhibitors of ALDH1A1. In addition, our crystal structure showed that substituents on the nitrobenzene ring contribute to hydrogen bond, while the latter half of the molecule contributes to hydrophobic interactions (Figure 19). Based on these results, we propose that further enhancements toward new more potent compounds should exploit potential hydrogen bonding interactions with the side chains of Asn118, Gln122, and His413, which would create a more even distribution of hydrogen bonding interactions.

(A)

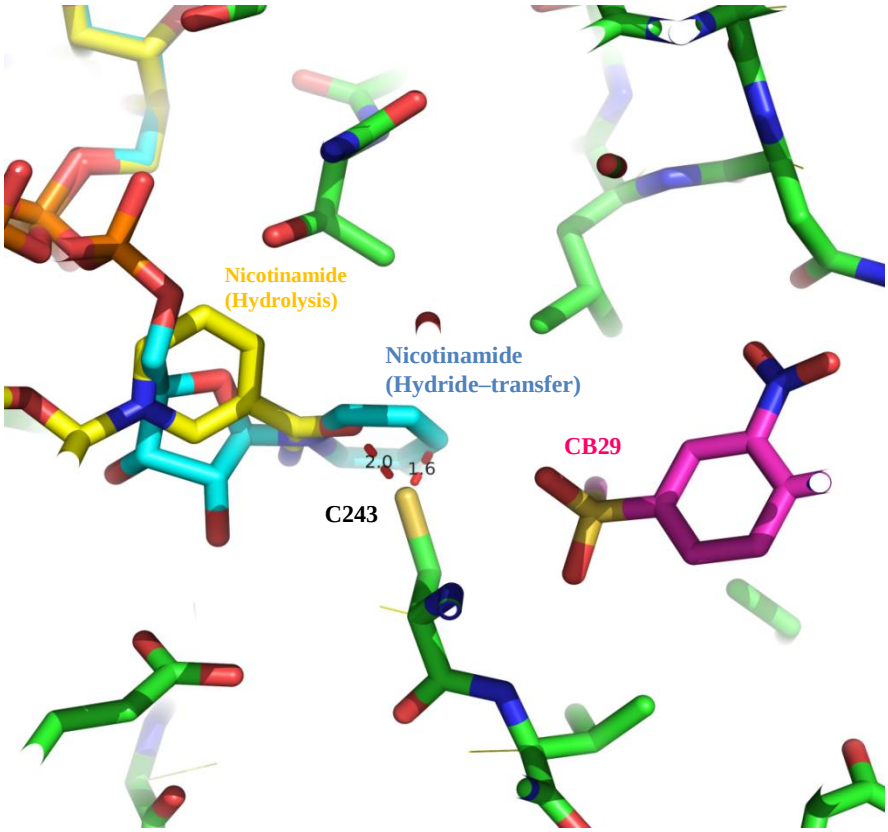

Figure 32. (A) CB29 preventing the formation of hydride transfer conformation. The active site of ALDH3A1 with bound CB29 into which the two commonly observed conformations of coenzyme have been modeled based on a structural alignment of ALDH3A1 with the active site of ALDH2 in which dual conformations of coenzyme are observed (RCSB code 1o00). The conformation of Cys243 induced by the binding of CB29 to ALDH3A1 is incompatible with either the hydride–transfer conformation of coenzyme (1.53 Å between the Sulfur of Cys243 and the C4 position of NAD^+) or the hydrolysis conformation of the coenzyme (2.14 Å between the Sulfur atom of Cys243 and the carboxyamide oxygen of NAD^+).

(B)

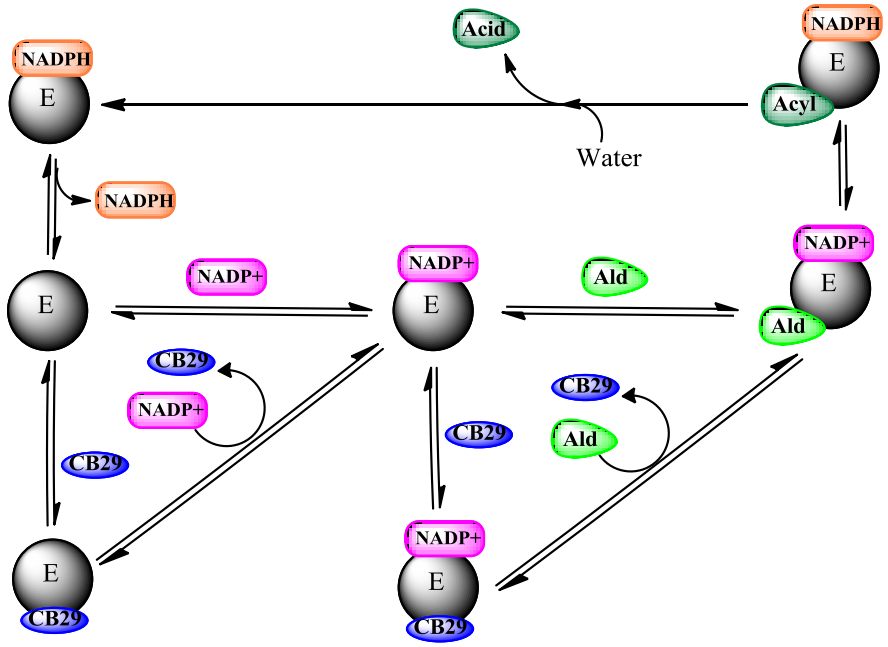

Figure 32. (B) Kinetic mechanism of CB29 binding. The reaction initiates with $NADP^+$ binding into the Rossmann fold subsequently followed by the binding of benzaldehyde. This is followed by thiohemiacetal formation, hydride transfer, hydrolysis and carboxylic acid formation. CB29 competes with binding of both aldehyde and $NADP^+$.

B. Selectivity of CB29 for ALDH3A1 versus ALDH1A1 and ALDH2

We compared the structure of CB29 to the list of all the reported inhibitors of ALDH family for defining isozyme selectivity. A highly selective reversible inhibitor of ALDH2, CVT–10216, which is an analog of daidzin, looked particularly interesting because its methyl–sulfonyl moiety linked to an aniline group resembles that of CB29 (Figure 33A) (Overstreet et al., 2009). As a structure of human ALDH2 with CVT–10216 is not yet available, we examined the human ALDH2 structure with bound to daidzin (PDB accession code 2vle) to compare its mode of binding to that of CB29 (Figure 33B). Daidzin binds to ALDH2 via its planar isoflavone ring (Figure 33A, shown in blue) that forms an extensive van der Waals contact with Phe170, Trp177, Phe296 and Phe459 in the central region of the substrate binding pocket (Figure 33C) (Lowe et al., 2008). The phenolic hydroxyl moiety does not form a direct hydrogen bond with the protein; rather it forms a hydrogen bond with an ordered water molecule which is, in turn, hydrogen–bonded to Glu268, the general base residue important for catalysis. The solvent exposed glucosyl moiety at the opposing end of daidzin is not greatly critical for selectivity since several substitutions at this position were still highly selective and potent for ALDH2 (Lowe et al., 2008). Overall it seems like the planar isoflavone ring accounts for ALDH2 selectivity. CVT–10216 maintains the same central isoflavone ring, but substitutes a methylsulfonylamino group in place of the hydroxyl on the benzene ring (Figure 33). Based on the ALDH2–daidzin structure, it is difficult to imagine how the methylsulfonylamino group can be accommodated within the active site without structural rearrangement. As large scale motions of the active site in ALDH2 have not been observed to date, we propose that CVT–10216 slides back away from Glu268 such that the sulfonyl group in

CVT–10216 can now interact with the active site cysteine loop in a manner similar to the sulfonyl group in CB29. However, the additional amino group between the aromatic ring and the sulfonyl moiety is necessary in CVT–10216 to bring the sulfonyl oxygens within hydrogen bonding distance of the peptide nitrogen in this loop. If these sulfonyl groups interact similarly, as we propose, what accounts for the highly selective nature of their respective interactions in ALDH3A1 and ALDH2? We believe it is the differences in the topologies of their respective substrate binding sites. The site in ALDH3A1 is narrow and curved through its middle region while that of ALDH2 is largely a straight cylinder with similar proportions throughout. Thus, the single bond linkage between the aromatic rings in daidzin and CVT–10216 are optimal for the cylindrical site in ALDH2, while the amino linker and the rotations made possible by these two single bonds between the aromatic rings in CB29 are optimal for the narrower and curved nature of the ALDH3A1 site but not for cylindrical pocket of ALDH2 (Figure 33D).

In order to understand the specificity of CB29 for ALDH3A1 over ALDH1A1, we examined the substrate–binding site of sheep liver ALDH1A1 (PDB accession code 1bxs). The substrate binding cleft in human ALDH1A1, based on sheep ALDH1A1 structure, is much larger than either that of ALDH3A1 or ALDH2 (Figure 33E). The enlarged substrate site in ALDH1A1 is primarily due to the substitution of Phe459 by Val and Met124 by Gly. We believe that this large substrate binding site would form fewer favorable contacts with CB29 than those observed in ALDH3A1, which has a relatively narrow pocket (Figure 33E). However, analogs of CB29 such as B13, B16, B19, B22 and IUSC–12416 with larger substituents at the R1 and R2 positions were inhibitory towards ALDH1A1 activity. We believe we see this trend because analogs with larger substitu-

tions at R1 and R2 positions fill this larger substrate–binding site of ALDH1A1 and possibly form new productive interactions with ALDH1A1 which stabilize these compounds.

(A)

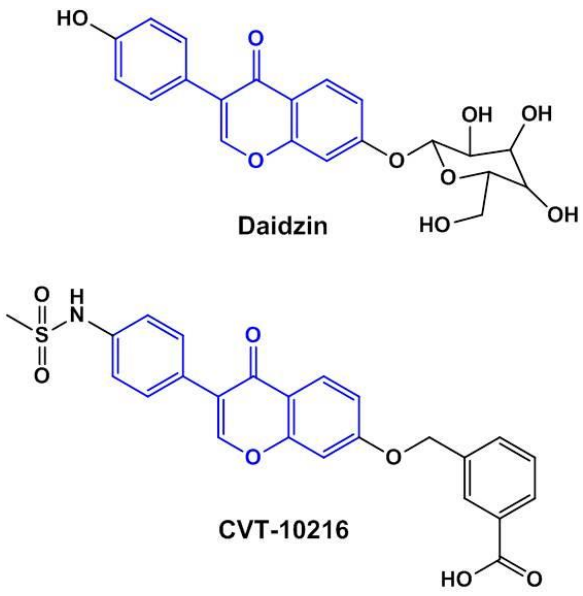

(B)

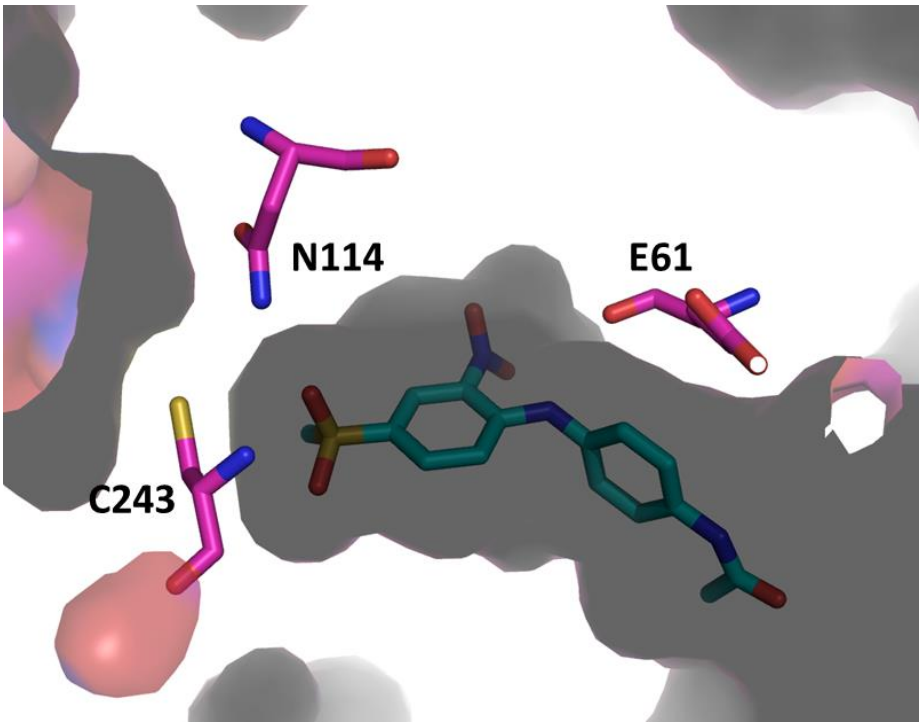

Figure 33. Selectivity of CB29 for ALDH3A1 against ALDH1A1, ALDH2. (A) Structure of daidzin and its analog CVT–10216. Blue region shows the common planar isoflavone ring. **(B)** CB29 (sky–blue) bound with in the catalytic pocket of ALDH3A1.

(C)

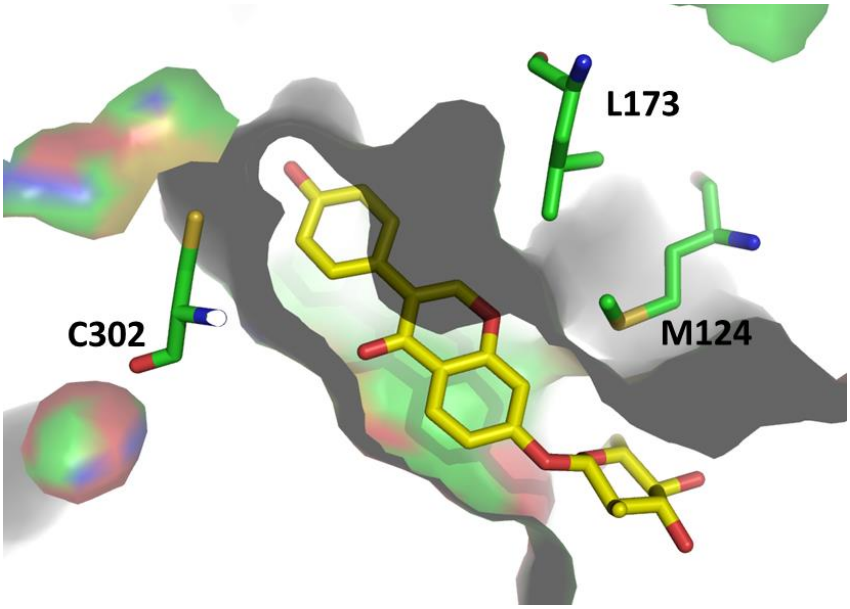

(D)

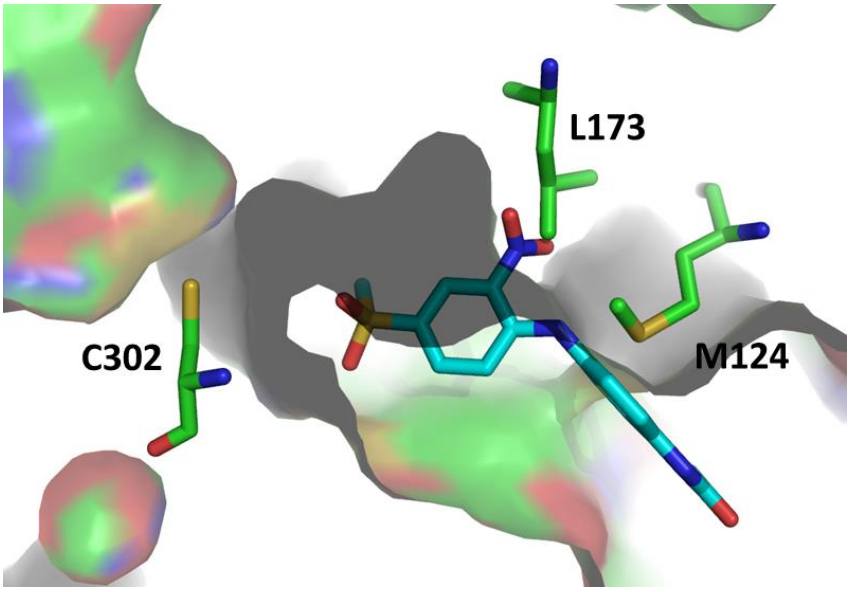

Figure 33. Selectivity of CB29 for ALDH3A1 against ALDH1A1, ALDH2. (C) Daidzin (yellow) bound within the cylindrical pocket of ALDH2. **(D)** Position of CB29 within the ALDH2 substrate site based on superimposition of the ALDH3A1 and ALDH2 structure (RCSB code 1O00). This figure shows the potential steric clashes that could occur between CB29 (sky–blue) and the ALDH2 substrate site.

(E)

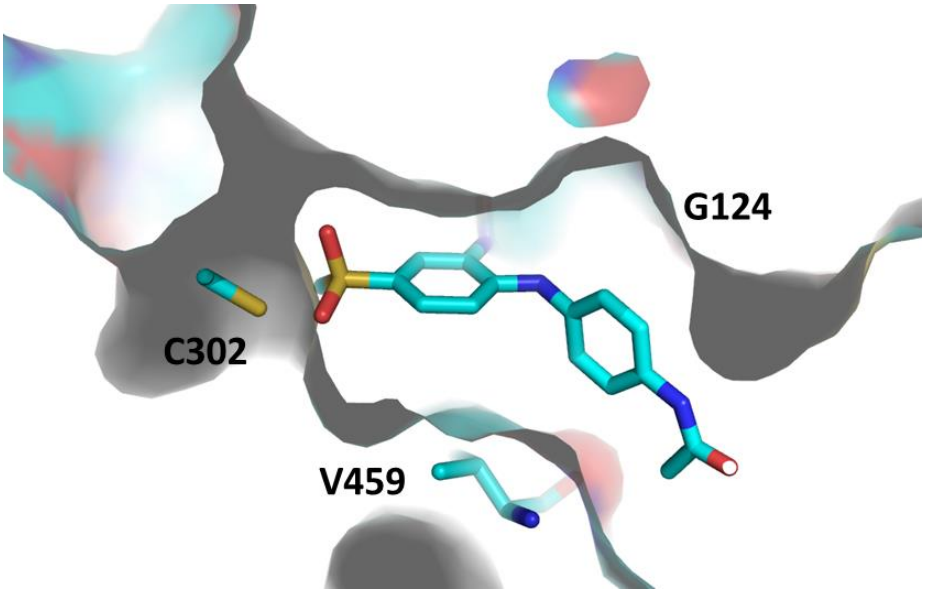

Figure 33. Selectivity of CB29 for ALDH3A1 against ALDH1A1, ALDH2. (E) Position of CB29 within the sheep ALDH1A1 substrate site based on superimposition of the ALDH3A1 and sheep ALDH1A1 (RCSB code 1BXS) structures. This view shows the larger available space for CB29 (sky–blue) within the ALDH1 active site.

C. Characterization of CB7 binding

Steady state competition experiments have shown that CB7 exhibits a competitive mode of inhibition with respect to benzaldehyde with a Ki of 0.1 μM and non–competitive mode of inhibition with respect to $NADP^+$ with a Ki of 0.1 μM. This is consistent with our crystallographic evidence since we saw binding of CB7 in the presence of NAD^+, which is an analog of $NADP^+$ (Figure 21B).

Based on this binding pattern, we propose a model for CB7 as shown below (Figure 34). The general catalytic mechanism of ALDH involves initial binding of $NAD(P)^+$ followed by the binding of aldehyde. Based on our steady state kinetics, we propose that ALDH3A1 initially binds to $NADP^+$ to form E–$NADP^+$ complex. Since, CB7 is non–competitive to $NADP^+$, this complex formation is not interrupted by CB7. The next step is the formation of E–$NADP^+$–Aldehyde complex. This complex formation is interrupted by CB7 since it is competitive to aldehyde binding. The binding can be reversed by using higher concentration of aldehyde that displaces CB7 away from the active site. This is subsequently followed by a product release step (carboxylic acid followed by NADPH).

Our SAR studies on the available analogs of CB7 showed that our original hit compound, CB7, was the most potent. To put this SAR into context, we used the structural information available from CB7–ALDH3A1–NAD^+ crystal structure. The proximity of the benzyl substituent of the benzimidazole moiety to Cys243, Phe401, Leu119 and Tyr115 explains the detrimental effects of adding substituents to the R2 and R3 positions (Table 4, figure 20 and figure 22). Moreover, the nicotinamide carbonyl oxygen is 3.9 Å from the benzimidazole ring such that a methyl group at the R2 position would create steric overlap with this portion of the NAD^+ molecule. In addition, the side chain of Tyr65

influences substitutions at the R1 and R4/R8 positions, where larger substituents create a steric clash with Tyr65. In addition, Tyr115 also impacts the available space surrounding the ortho R4/R8 positions. On the other hand, substitutions at the R5 and R6 positions were tolerated because of the small cavity between Trp233 and Tyr65. Our SAR study also suggests that smaller substitutions, preferably electron withdrawing halogens, were optimal at the R6 position. This is likely due to the presence of Trp233 at a distance of 4 Å and Met237 at a distance of 3.5 Å from the R6 position. Overall, our SAR data was fully supported by our structural data and explained why CB7 was the most potent of the series and why substitutions at various positions were detrimental to binding.

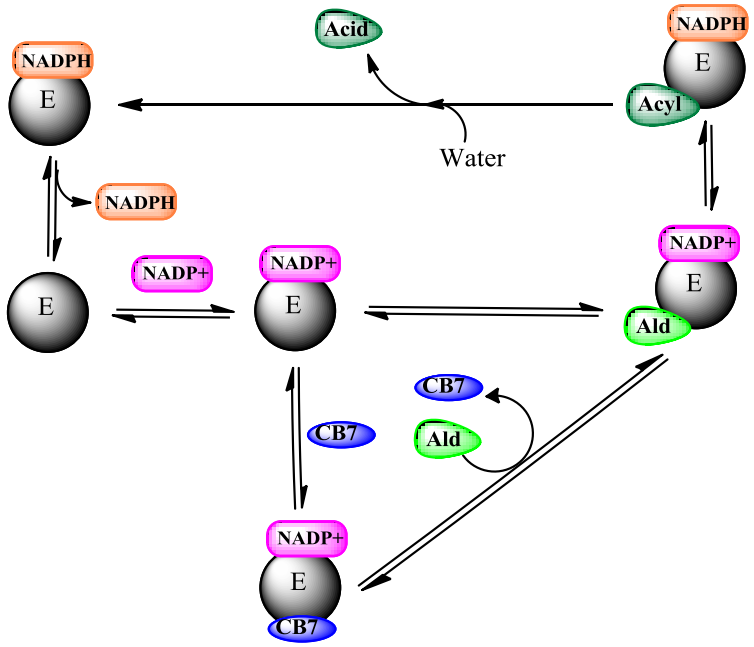

Figure 34. Mechanism of CB7 inhibition. The reaction initiates with $NADP^+$ binding into the Rossmann fold subsequently followed by the binding of benzaldehyde. This is followed by thiohemiacetal formation, hydride transfer, hydrolysis and carboxylic acid formation. CB7 competes with aldehyde binding showing no effect on $NADP^+$ binding.

D. Probing CB7 binding of ALDH3A1 site using Q122A and Q122W mutants

We compared the crystal structure of human ALDH3A1 against two other closely related isozymes human ALDH2 and ALDH1A1 from sheep (Figure 35) to compare their active site. Upon structural alignment, we identified one important residue, tryptophan that is present in both ALDH1A1 and ALDH2 active site but not in ALDH3A1. In the ALDH3A1 active site, a glutamine residue is present in the position corresponding to tryptophan. In order to investigate how much contribution glutamine makes in CB7 binding, we decided to mutate glutamine to either alanine or tryptophan. Kinetic parameters (K_{cat}, K_m, K_{cat}/ K_m) were determined for benzaldehyde and propionaldehyde oxidation for mutants and wild type ALDH3A1 (Table 8). K_i was further determined for CB7 against Q122A, Q122W and wild type ALDH3A1 as well (Table 8). Results showed that the alanine mutation did not show a drastic effect on enzyme's turnover rate of benzaldehyde (4.91 $\mu M^{-1}\,min^{-1}$ for wild type ALDH3A1 and 3.2 $\mu M^{-1}\,min^{-1}$ for Q122A mutant) and propionaldehyde (0.05 $\mu M^{-1}\,min^{-1}$ for wild type ALDH3A1 and 0.049 $\mu M^{-1} min^{-1}$ for Q122A mutant). The Ki value for CB7 binding was also unchanged (Ki = 0.2 µM for WT enzyme and Q122A). However, when glutamine was mutated to tryptophan, CB7 was not inhibitory at all to Q122W activity up to 250 µM concentration. The turnover rate of benzaldehyde decreased 3 fold (1.7 $\mu M^{-1}\,min^{-1}$) as compared to the rate of wild type enzyme whereas that for propionaldehyde was 80% (0.039 $\mu M^{-1}\,min^{-1}$) of the rate of wild type enzyme. This data clearly supported the idea that glutamine was the major amino acid that was responsible for imparting selectivity to CB7.

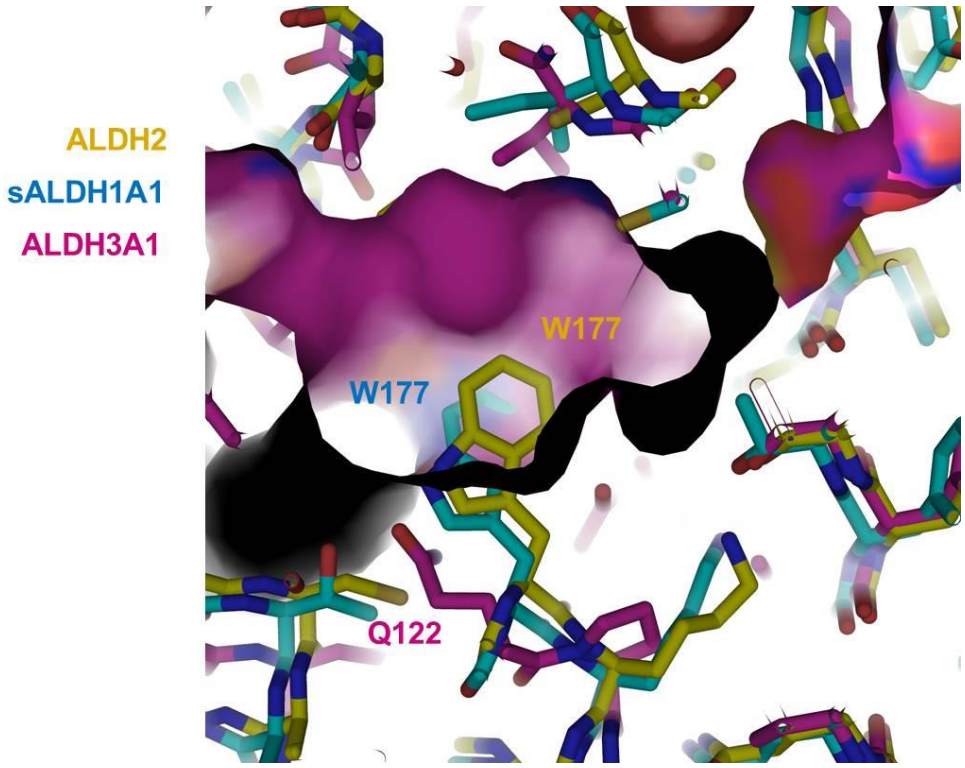

Figure 35. Structural alignment of sheep ALDH1A1, ALDH2 and ALDH3A1. Catalytic surface of ALDH3A1 is shown in pink color. ALDH1A1, ALDH2 and ALDH3A1 are represented is sky blue, yellow and pink color respectively. The figure shows that ALDH3A1 has a glutamine at 122 position instead of tryptophan, which is present in ALDH2 and sALDH1A1.

Table 8. Catalytic activity of WT ALDH3A1, Q122A and Q122W. Structural comparison showed that ALDH3A1 has a glutamine at 122 position instead of tryptophan, which is present in ALDH2 and sALDH1A1. Two mutations (Q122A and Q122W) were introduced at this position to study their kinetic properties.

	Benzaldehyde	Benzaldehyde	CB7	Propionaldehyde
	K_m	K_{cat}/ K_m	K_i	K_{cat}/ K_m
	(µM)	Min^{-1} $µM^{-1}$	(µM)	Min^{-1} $µM^{-1}$
wt	279 ± 23	4.91 ± 0.25	0.2	0.05 ± 0.003
Q122A	425 ± 38	3.2 ± 0.13	0.2	0.049 ± 0.003
Q122W	257 ± 35	1.73 ± 0.27	NI 250 µM)	0.039 ± 0.005

E. Sensitization toward mafosfamide

Several of the selective inhibitors of ALDH3A1 reported here enhance the anti–proliferative effects of mafosfamide in SF767 cells, which express only ALDH3A1, as well as in A549 cells which express both ALDH1A1 and ALDH3A1. The enhancements increase in a dose–dependent manner in SF767 cells with CB29 analogs, where ALDH3A1 is the sole target (Figure 29E). In the case of CB7 analogs as well, we see a dose dependent increment in mafosfamide sensitivity both in A549 and SF767 cells (Figure 31). In our hands, the antibodies utilized for detection of ALDH1A1 also detect ALDH1A2, ALDH1A3, ALDH1B1, and ALDH2 (Figure 25C), therefore SF767 appears devoid of all ALDH1 subtypes, as well as ALDH2, giving us a good model system to study the contribution of ALDH3A1 to mafosfamide resistance.

In the case of CB29 analogs, the dose–response in SF767 cells matches reasonably the *in vitro* IC_{50} data in which both assays produced values between 15 and 50 μM (Table 3A, 3B and Figure 29E). The data presented here suggest that ALDH3A1 can make a substantial contribution to detoxication of derivatives of cyclophosphamide, even in the face of competing enzymes, such as ALDH1A1. These data are consistent with the siRNA studies where knockdown of both ALDH1A1 and ALDH3A1 was required for maximal sensitivity toward mafosfamide (Moreb et al., 2007).

Cell based chemosensitivity experiments conducted with CB7 analogs show a similar phenotypic effect in A549 and SF767 cells. Even though the dose–responses were in the lower micromolar range (5–7.5 μM), nearly 20 fold higher than its IC_{50} values, the fact that we see the effect in a much lower concentration than the analogs CB29 (15–50 μM range) makes us believe that we are targeting ALDH3A1. It is also supported by the

fact that the CB7 class is highly potent and thus would be expected to require lower concentrations than the CB29 class for cellular efficacy. The variability in concentration between *in vitro* kinetics versus cell based assays could be affected by other factors such as membrane permeability, cellular metabolism and high concentration of competing aldehydes inside the cells.

One interesting result that we observed in our study was that SF767 cells were sensitized more to CB7 analogs as compared to A549 cell lines. This is likely due to the co–expression of ALDH1A1 and ALDH3A1, both of which contribute to chemoresistance for mafosfamide, whereas SF767 only expresses ALDH3A1. Hence, inhibition of ALDH3A1 still leaves the alternative pathway for mafosfamide metabolism active in A549 cells. In order to see even a higher chemosensitivity in A549 cells, a proper strategy would be to use both ALDH1A1 and ALDH3A1 selective inhibitors. Since SF767 cells have no ALDH1A1 expression, using ALDH3A1 inhibitors achieves maximum mafosfamide sensitivity. Our experiments also showed that normal lung cells (CCD13Lu) did not show any detectable expression of ALDH1, ALDH2 and ALDH3A1 isozymes. These cells also had a lower ED_{50} value for mafosfamide (40 μM). However, when normal lung cells become tumorigenic, they show much higher expression of ALDH1A1 and ALDH3A1, and their ED_{50} value for mafosfamide increases by almost 3.25 fold (125 μM). Variable ED_{50} values and protein expression patterns of ALDH isozymes in normal versus tumorigenic cells makes an important point that ALDH isozymes could be involved in such a high degree of chemoresistance. Also, since normal lung cells (CCD13Lu) were not affected by 10 μM concentrations of CB7 and most analogs, we infer that these inhibitors target ALDH3A1 activity to inhibit cell proliferation in A549

and SF767 cells. These inhibitors were also not able to increase the chemosensitivity to mafosfamide in CCD13Lu cells, which again supports our hypothesis that ALDH3A1 inhibitors can be used to increase chemosensitivity in ALDH3A1 positive cells.

F. Comparison of catalytic site of ALDH1A1, ALDH2 and ALDH3A1

Even though earlier studies have identified inhibitors that target ALDHs in general, having isozyme selective inhibitors would be helpful in studying functions of individual enzymes. Structural comparisons of catalytic sites have shown distinct structural features of three important enzymes ALDH1A1, ALDH2 and ALDH3A1 as shown in Figure 36. ALDH1A1 has a funnel shaped catalytic site. ALDH2 has a cylindrical shaped catalytic site whereas ALDH3A1 unlike ALDH2 has a curved shaped opening in its catalytic site. The pocket is narrow at its outer opening and broader inside (Figure 36). This structural diversity would provide us an advantage for the development of selective inhibitors for each of these isozymes. Provided that we know the structural properties of these three enzymes, having regulators that govern their functions would provide us with an additional advantage to study them individually.

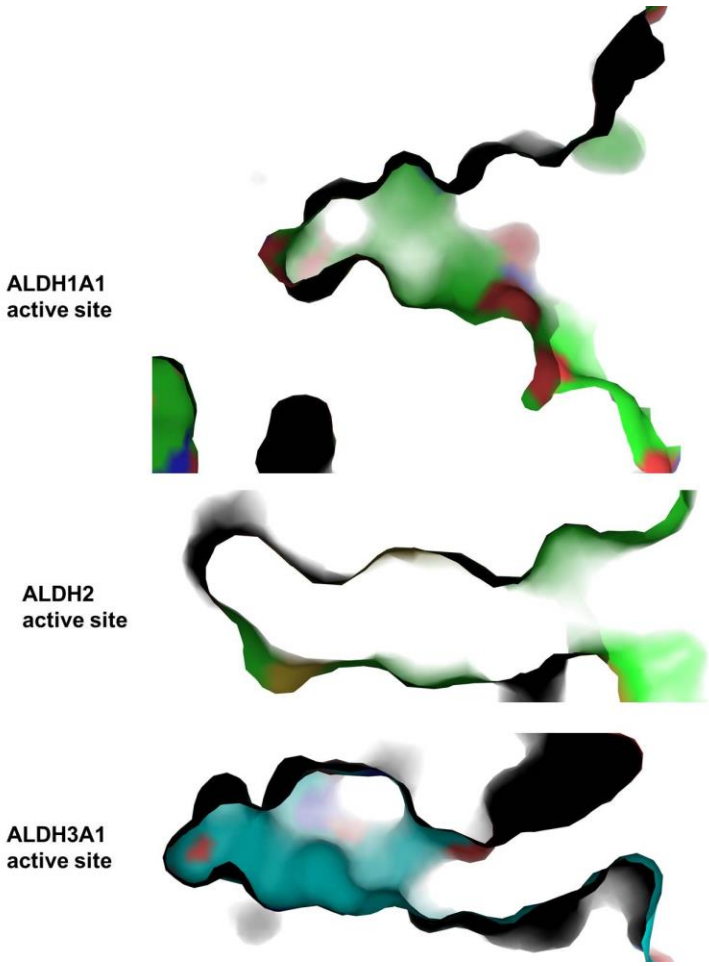

Figure 36. Active site comparison of ALDH1A1, ALDH2 and ALDH3A1. Comparison of the active site of ALDH1A1, ALDH2 and ALDH3A1

Since many exogenously administered drugs are active in their aldehyde form, identification of isozyme selective inhibitors for various ALDH isozymes will help us investigate their individual contributions toward drug metabolism. It will also help us understand the individual contribution of different forms of ALDH towards metabolism of numerous cytotoxic aldehydes, including those linked to cellular differentiation, detoxication of peroxidic aldehydes, as well as metabolism of neurotransmitters. In this study,

we characterized two selective inhibitors of ALDH3A1, an enzyme implicated in aldophosphamide metabolism. Even though, the catalytic efficiency of ALDH3A1 is 1/ 7^{th} than that of ALDH1A1 for aldophosphamide (Giorgianni et al., 2000), the expression levels in some cancer cell lines are such that an impact on aldophosphamide metabolism cannot be ignored. Indeed, some cells such as the (SF767) glioblastoma cell line only express ALDH3A1 and have ED_{50} values similar to those cells in which both enzymes are expressed in similar levels (A549). Therefore, selective ALDH3A1 inhibitors are useful tools that can be used to manipulate the contributions of ALDH3A1 toward aldophosphamide metabolism, as well as other biologically relevant aldehydes.

V. Future Directions

Our study has helped us identify two classes of compounds that selectively inhibit ALDH3A1 activity. Some of the analogs did not exhibit great phenotypic properties possibility due to poor permeability or stability. At this point, we do not know what makes these inhibitors permeable or stable. Fortunately, we have altogether six important analogs (B4, B9, CB29, CB7, A64, A70) that exhibit promising phenotypic property in cells based studies. An interesting follow up study would be to conduct a pharmacokinetic and pharmacodynamic study with these compounds by testing them in mice. We would be interested in knowing how much of these compound can be administered to mice, which are the ones with least toxicity and what would be the optimal route for administration. We would also like to know the half–life and the rate at which these compounds are eliminated from the body. If successful, compounds with optimal pharmacokinetic and pharmacodynamic properties would further be tested in tumorigenic mouse models to see their effect along with cyclophosphamide in treating resistant forms of lung adenocarcinomas and glioblastoma.

These two scaffolds can also be used as tools to study the contribution of ALDH3A1 in cellular function. One important approach would be to develop a covalent inhibitor of ALDH3A1 by using the CB29 scaffold. The methyl carbon attached to sulfonyl group lies at an approximate distance of 4.2 Å away from the active site sulfur (Cys302) (Figure 37). Since Cysteine is a nucleophile, this property can be exploited to create covalent inhibitors of ALDH3A1. The analogs that could possibly bind to ALDH3A1 covalently with their possible reaction mechanism are shown below (Figure 38).

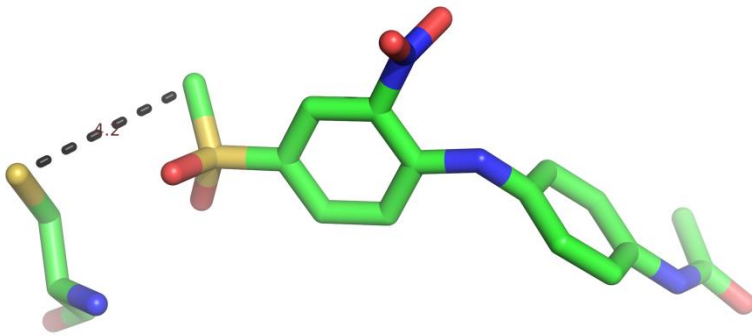

Figure 37. Structure based design of covalent inhibitors. Figure showing the immediate distance (4.2Å) between methyl carbon (attached to sulfonyl sulfur) and sulfur from Cys302 that can be exploited for making covalent inhibitors.

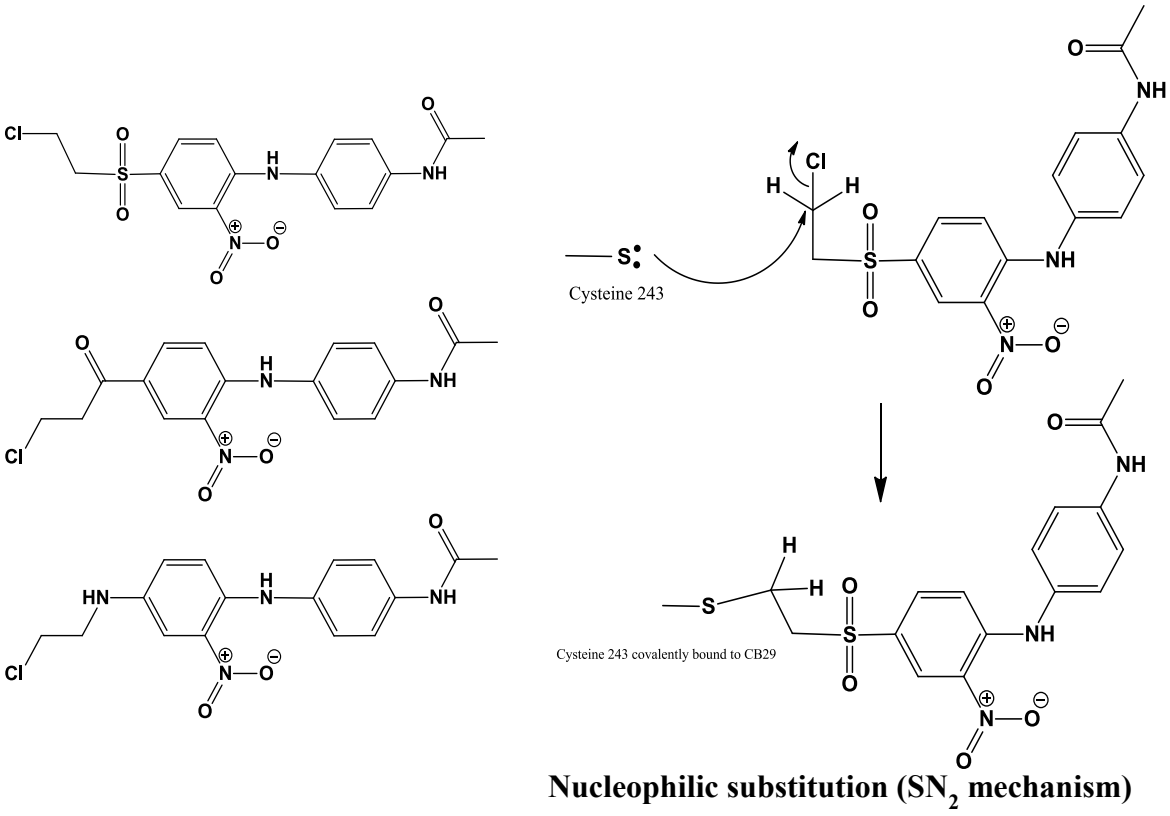

Figure 38. Possible mechanism of action. List of possible analogs that can exhibit a SN2 mechanism based covalent modification of ALDH3A1.

For example, if we specifically want to completely knockdown ALDH3A1 activity (just like by using siRNA), these covalent inhibitors can be important tools since they do not inhibit ALDH1A1 or ALDH2 activity. In addition, CB7 can also be used as a chemical tool to study the contribution of ALDH3A1 in metabolism of various exogenous and endogenous aldehydes.

Besides ALDH3A1, there are several other ALDH3 isoforms such as ALDH3A2, ALDH3B1, ALDH3B2, which are not characterized for their functions. Mutation in ALDH3A2 is implicated in Sjogren–Larson syndrome whereas ALDH3B1 is implicated in schizophrenia. Compounds identified in this study can be used as starting scaffolds for designing inhibitors for these other enzymes that are closely related to ALDH3A1.

References

Abriola, D. P., Fields, R., Stein, S., Mackerell, A. D. Jr., & Pietruszko, R. (1987). Active site of human liver aldehyde dehydrogenase. *Biochemistry, 26,* 5679–84.

Akaboshi, S., Hogema, B. M., Novelletto A., Malaspina, P., Salomons, G. S., Maropoulos, G. D., Jakobs, C., Grompe, M., & Gibson K. M. (2003). Mutational spectrum of the succinate semialdehyde dehydrogenase (ALDH5A1) gene and functional analysis of 27 novel disease–causing mutations in patients with SSADH deficiency. *Human Mutation, 22,* 442–50.

Banfi, P., Lanzi, C., Falvella, F. S., Gariboldi, M., Gambetta, R. A., & Dragani, T. A. (1994). The daunorubicin–binding protein of Mr 54, 000 is an aldehyde dehydrogenase and is down–regulated in mouse liver tumors and in tumor cell lines. *Molecular Pharmacology, 46,* 896–900.

Baumgartner, M. R., Hu, C. A., Almashanu, S., Steel, G., Obie, C., Aral, B., Rabier, D., Kamoun, P., Saudubray, J. M., & Valle, D. (2000). Hyperammonemia with reduced ornithine, citrulline, arginine and proline: a new inborn error caused by a mutation in the gene encoding delta(1)–pyrroline–5–carboxylate synthase. *Human Molecular Genetics, 9,* 2853–8.

Beedham, C., Peet, C. F., Panoutsopoulos, G. I., Carter, H., & Smith, J. A. (1995). Role of aldehyde oxidase in biogenic amine metabolism. *Progress in Brain Research, 106,* 345–353.

Blaney, S. M., Balis, F. M., Berg, S., Arndt, C. A. S., Heideman, R., Geyer, J. R., Packer, R., Adamson, P. C., Jaeckle, K., Klenke, R., Aikin, A., Murphy, R., McCully, C., & Poplack, D. G. (2005). Intrathecal Mafosfamide: A Clinical Pharmacology and Phase I trial. *Journal of Clinical Oncology, 23(7),* 1555–1563.

Boesch, J. S., Lee, C., & Lindahl, R. G. (1996). Constitutive expression of class 3 aldehyde dehydrogenase in cultured rat corneal epithelium. *Journal of Biological Chemistry, 271,* 5150–5157.

Braun, T., Bober, E., Singh, S., Agarwal, D. P., & Goedde, H. W. (1987). Evidence for a single peptide at the amino–terminal end of human mitochondrial aldehyde dehydrogenase. *FEBS Letters, 215,* 233–236.

Canuto, R. A., Ferro, M., Muzio, G., Bassi, A. M., Leonarduzzi, G., Maggiora, M., Adamo, D., Poli, G. & Lindahl, R. (1994). Role of aldehyde metabolizing enzymes in mediating effects of aldehyde products of lipid peroxidation in liver cells. *Carcinogenesis, 15,* 1359–1364.

Canuto, R. A., Muzio, G., Ferro, M., Maggiora, M., Federa, R., Bassi, A. M., Lindahl, R., & Dianzani, M. U. (1999). Inhibition of class–3 aldehyde dehydrogenase and cell growth by restored lipid peroxidation in hepatoma cell lines. *Free Radical Biology Medicine, 26,* 333–3340.

Chen, Z., Zhang, J., & Stamler, J. (2002). Identification of the enzymatic mechanism of nitroglycerin bioactivation. *Proceedings of National Academy of Sciences, 99,* 8306–8311.

Chung, S., Hedlund, E., Hwang, M., Kim, D. W., Shin, B. S., Hwang, D. Y., Kang, U. J., Isacson, O., & Kim, K. S. (2005). The homeodomain transcription factor Pitx3 facilitates differentiation of mouse embryonic stem cells into AHD2–expressing dopaminergic neurons. *Molecular and Cellular Neuroscience, 28,* 241–252.

Crabb, D. W., Edenberg, H. J., Bosron, W. F., & Li, T. K. (1989). Genotypes for aldehyde dehydrogenase deficiency and alcohol sensitivity. The inactive ALDH2(2) allele is dominant. *Journal of Clinical Investigation, 83(1),* 314–316.

D'Ambrosio, K., Pailot, A., Talfournier, F., Didierjean, C., Benedetti, E., Aubry, A., Branlant, G., & Corbier, C. (2006). The first crystal structure of a thioacylenzyme intermediate in the ALDH family: new coenzyme conformation and relevance to catalysis. *Biochemistry, 45,* 2978–2986.

Dickman, E. D., Thaller, C., & Smith, S. M. (1997). Temporally–regulated retinoic acid depletion produces specific neural crest, ocular and nervous system defects. *Development, 124,* 3111–3121.

Downes, J. E., Swann, P. G., & Holmes, R. S. (1993). Ultraviolet light–induced pathology in the eye: associated changes in ocular aldehyde dehydrogenase and alcohol dehydrogenase activities. *Cornea, 12,* 241–248.

Duester, G. (2000). Families of retinoid dehydrogenases regulating vitamin A function: production of visual pigment and retinoic acid. *European Journal of Biochemistry, 267,* 4315–4324.

Dupe, V., Matt, N., Garnier, J. M., Chambon, P., Mark, M., & Ghyselinck, N. B. (2003). A newborn lethal defect due to inactivation of retinaldehyde dehydrogenase type 3 is prevented by maternal retinoic acid treatment. *Proceedings of National Academy of Sciences, 100,* 14036–14041.

Emsley, P., & Cowtan, K. (2004). Coot–model building tools for molecular graphics. *Acta Crystallographica: Section D, Biological Crystallography, 60,* 2126–2132.

Enomoto, N., Takase, S., Takada, N., & Takada, A. (1991). Alcoholic liver disease in heterozygotes of mutant and normal aldehyde dehydrogenase–2 genes. *Hepatology, 13,* 1071–1075.

Esterbauer, H., Schaur, R.J., & Zollner, H. (1991). Chemistry and biochemistry of 4–hydroxynonenal, malonaldehyde and related aldehydes. *Free Radical Biology and Medicine, 11,* 81–128.

Estey, T., Piatigorsky, J., Lassen, N., & Vasiliou, V. (2007). ALDH3A1: a corneal crystallin with diverse functions. *Experimental Eye Research, 84,* 3–12.

Estey, T., Cantore, M., Weston, P. A., Carpenter, J. F., Petrash, J. M., & Vasiliou, V. (2007). Mechanisms involved in the protection of UV–induced protein inactivation by the corneal crystallin ALDH3A1. *Journal of Biological Chemistry, 282,* 4382–4392.

Fan, X., Molotkov, A., Manabe, S., Donmoyer, C. M., Deltour, L., Foglio, M. H., Cuenca, A. E., Blaner, W. S., Lipton, S. A., & Duester, G. (2003). Targeted disruption of Aldh1a1 (Raldh1) provides evidence for a complex mechanism of retinoic acid synthesis in the developing retina. *Molecular and Cellular Biology, 23,* 4637–4648.

Farres, J., Wang, X., Takahashi, K., Cunningham, S. J., Wang, T. T., & Weiner, H. (1997). Effects of changing glutamate 487 to lysine in rat and human liver mitochondrial aldehyde dehydrogenase. A model to study human (Oriental type) class 2 aldehyde dehydrogenase. *Journal of Biological Chemistry, 269*, 13854–13860.

Fukumoto, S., Yamauchi, N., Moriguchi, H., Hippo, Y., Watanabe, A., Shibahara, J., Taniguchi, H., Ishikawa, S., Ito, H., Yamamoto, S., Iwanari, H., Hironaka, M., Ishikawa, Y., Niki, T., Sohara, Y., Kodama, T., Nishimura, M., Fukayama, M., Dosaka–Akita, H., & Aburatani, H. (2005). Overexpression of the aldo–keto reductase family protein AKR1B10 is highly correlated with smokers' non–small cell lung carcinomas. *Clinical Cancer Research, 11*, 1776–1785.

Giorgianni, F., Bridson, P. K., Sorrentino, B. P., Pohl, J., & Blakley, R. L. (2000). Inactivation of aldophosphamide by human aldehyde dehydrogenase isozyme 3. *Biochemical Pharmacology, 60(3)*, 325–338.

Gyamfi, M. A., Kocsis, M. G., He, L., Dai, G., Mendy, A. J., & Wan, Y. J. (2006). The role of retinoid X receptor alpha in regulating alcohol metabolism. *Journal of Pharmacology and Experimental Therapeutics, 319*, 360–368.

Galter, D., Buervenich, S., Carmine, A., Anvret, M., & Olson, L. (2003). ALDH1 mRNA: presence in human dopamine neurons and decreases in substantia nigra in Parkinson's disease and in the ventral tegmental area in schizophrenia. *Neurobiology of Disease, 14*, 637–647.

Ganaganur, R. K., Sreerama, L., & Sladek, N. E. (1994). Intrinsic cellular resistance to oxazaphosphorines exhibited by a human colon carcinoma cell line expressing relatively large amounts of a class–3 aldehyde dehydrogenase. *Biochemical Pharmacology, 48(10),* 1943–1952.

Ganaganur, R. K., Varadahalli, D. R., Sreerama, L., Lee, M. J. C., Nagasawa, H. T., & Sladek, N. E. (1998). Inhibition of human class 3 Aldehyde Dehydrogenase, and sensitization of tumor cells that express significant amounts of this enzyme to oxazaphosphorines, by chlorpropamide analogues. *Biochemical Pharmacology, 55,* 465–474.

Goedde, H. W., Agarwal, D. P., Fritze, G., Meier–Tackmann, D., Singh, S., Beckmann, G., Bhatia, K., Chen, L. Z., Fang, B., Lisker, R., Paik, Y. K., Rothhammer, F., Saha, N., Segal, B., Srivastava, L. M., & Czeizel, A. (1992). Distribution of ADH2 and ALDH2 genotypes in different populations. *Hum. Gen., 88,* 344–6.

Goedde, H. W., & Agarwal, D. P. (1990). Pharmacogenetics of aldehyde dehydrogenase (ALDH). *Pharmacology and Therapeutics, 45,* 345–371.

Hammen, P. K., Lali–Hassani, A., Hallenga, K., Hurley, T. D., & Weiner, H. (2002). Multiple conformations of NAD and NADH when bound to human cytosolic and mitochondrial aldehyde dehydrogenase. *Biochemistry, 41,* 7156–7168.

Haselbeck, R. J., Hoffmann, I., & Duester, G. (1999). Distinct functions for Aldh1 and Raldh2 in the control of ligand production for embryonic retinoid signaling pathways. *Developmental Genetics, 25,* 353–364.

Hempel, J., Liu, Z. J., Perozich, J., Rose, J., Lindahl, R., & Wang, B.C. (1997). Conserved residues in the aldehyde dehydrogenase family. Locations in the class 3 tertiary structure. *Advances in Experimental Medicine and Biology, 414*, 9–13.

Hsu, L. C., & Chang, W. C. (1991). Cloning and characterization of a new functional human aldehyde dehydrogenase gene. *Journal of Biological Chemistry, 266(19),* 12257–65.

Hsu, L. C., Chang, W. C., Hiraoka, L., & Hsieh, C. L. (1994). Molecular cloning, genomic organization, and chromosomal location of an additional human aldehyde dehydrogenase gene, ALDH6. *Genomics, 24(2),* 333–3341.

Hu, G., Chong, R. A., Yang, Q., Wei, Y., Blanco, M. A., Li, F., Reiss, M., Au, J. L., Haffty, B. G., & Kang, Y. (2009). MTDH activation by 8q22 genomic gain promotes chemoresistance and metastasis of poor–prognosis breast cancer. *Cancer Cell, 15,* 9–20.

Huang, J., Hu, N., Goldstein, A. M., Emmert–Buck, M. R., Tang, Z. Z., Roth, M. J., Wang, Q. H., Dawsey, S. M., Han, X. Y., Ding, T., Li, G., Griffen, C., & Taylor, P. R. (2000). High frequency allelic loss on chromosome 17p13.3–p11.1 in esophageal squamous cell carcinomas from a high incidence area in northern China. *Carcinogenesis, 21,* 2019–2026.

Hui, P., Nakayama, T., Morita, A., Sato, N., Hishiki, M., Saito, K., Yoshikawa, Y., Tamura, M., Sato, I., Takahashi, T., Soma, M., Izumi, Y., Ozawa, Y., & Cheng, Z. (2007). Common single nucleotide polymorphisms in Japanese patients with essential hypertension: aldehyde dehydrogenase 2 gene as a risk factor independent of alcohol consumption. *Hypertension Research, 30,* 585–592.

Hurley, T. D., Steinmetz, C. G., & Weiner, H. (1999). Three–dimensional structure of mitochondrial aldehyde dehydrogenase. Mechanistic implications. *Advances in Experimental Medicine and Biology, 463,* 15–25.

Isse, T., Oyama, T., Matsuno, K., Ogawa, M., Narai–Suzuki, R., Yamaguchi, T., Murakami, T., Kinaga, T., Uchiyama, I., & Kawamoto, T. (2005). Paired acute inhalation test reveals that acetaldehyde toxicity is higher in aldehyde dehydrogenase 2 knockout mice than in wild–type mice. *The Journal of Toxicological Sciences, 30,* 329–337.

Isse, T., Oyama, T., Matsuno, K., Uchiyama, I., & Kawamoto, T. (2005). Aldehyde dehydrogenase 2 activity affects symptoms produced by an intraperitoneal acetaldehyde injection, but not acetaldehyde lethality. *The Journal of Toxicological Sciences, 30,* 315–28.

Jacobs, F. M., Smits, S. M., Noorlander, C. W., von Oerthel, L., van der Linden, A. J., Burbach, J. P., & Smidt, M. P. (2007). Retinoic acid counteracts developmental defects in the substantia nigra caused by Pitx3 deficiency. *Development, 134,* 2673–84.

Jez, J. M., Flynn, T. G., & Penning, T. M. (1997). A new nomenclature for the aldo–keto reductase superfamily. *Biochemical Pharmacology, 54,* 639–647.

Jo, S. A., Kim, E. K., Park, M. H., Han, C., Park, H. Y., Jang, Y., Song, B. J., & Jo, I. (2007). A Glu487Lys polymorphism in the gene for mitochondrial aldehyde dehydrogenase 2 is associated with myocardial infarction in elderly Korean men. *Clinica Chemica Acta, 382,* 43–7.

Kaiser, J. (2005). Chemist want NIH to curtail database. *Science, 308 (5723),* 774.

Kamino, K., Nagasaka, K., Imagawa, M., Yamamoto, H., Yoneda, H., Ueki, A., Kitamura, S., Namekata, K., Miki, T., & Ohta, S. (2000). Deficiency in mitochondrial aldehyde dehydrogenase increases the risk for late–onset Alzheimer's disease in the Japanese population. *Biochemical and Biophysical Research Communications, 273,* 192–6.

Khanna, M., Chen, C. H., Kimble–Hill, A., Parajuli, B., Perez–Miller, S., Baskaran, S., Kim, J., Dria, K., Vasiliou, V., Mochly–Rosen, D. and Hurley, T. D. (2011). Discovery of a novel class of covalent inhibitor for aldehyde dehydrogenase. *Journal of Biological Chemistry, 286(50),* 43486–43494.

Kim, B., Lee, H. J., Choi, H. Y., Shin, Y., Nam, S., Seo, G., Son, D. S., Jo, J., Kim, J., Lee, J., Kim, J., Kim, K., & Lee, S. (2007). Clinical validity of the lung cancer biomarkers identified by bioinformatics analysis of public expression data. *Cancer Research, 67,* 7431–7438.

Kim, H., Lapointe, J., Kaygusuz, G., Ong, D. E., Li, C., van de Rijn, M., Brooks, J. D., & Pollack, J. R. (2005). The retinoic acid synthesis gene ALDH1A2 is a candidate tumor suppressor in prostate cancer. *Cancer Research, 65(18),* 8118–8124.

King, G., & Holmes, R. (1997). Human corneal and lens aldehyde dehydrogenases. Purification and properties of human lens ALDH1 and differential expression as major soluble proteins in human lens (ALDH1) and cornea (ALDH3). *Advances in Experimental Medicine and Biology, 414,* 19–27.

Kirsch, M., & De, G. H. (2001). NAD(P)H, a directly operating antioxidant? *FASEB Journal, 15,* 1569–1574.

Klyosov, A. A., Rashkovetsky, L. G., Tahir, M. K., & Keung, W. M. (1996). Possible role of liver cytosolic and mitochondrial aldehyde dehydrogenases in acetaldehyde metabolism. *Biochemistry, 35*, 4445–4456.

Larson, H. N., Weiner, H., Hurley, T. D. (2005). Disruption of the co–enzyme binding site and the dimer interface revealed in the crystal structure of mitochondrial aldehyde dehydrogenase "Asian variant". *Journal of Biological Chemistry, 280(34),* 30550–30556.

Larson, H. N., Zhou, J., Chen, Z., Stamler, J. S., Weiner, H., & Hurley, T. D. (2007). Structural and functional consequences of coenzyme binding to the inactive asian variant of mitochondrial aldehyde dehydrogenase: roles of residues 475 and 487. *Journal of Biological Chemistry, 282,* 12940–12950.

Lassen, N., Pappa, A., Black, W. J., Jester, J. V., Day, B. J., Min, E., & Vasiliou, V. (2006). Antioxidant function of corneal ALDH3A1 in cultured stromal fibroblasts. *Free Radical Biology and Medicine, 41,* 1459–1469.

Lassen, N., Bateman, J. B., Estey, T., Kuszak, J. R., Nees, D. W., Piatigorsky, J., Duester, G., Day, B. J., Huang, J., Hines, L. M., & Vasiliou, V. (2007). Multiple and additive functions of ALDH3A1 and ALDH1A1: cataract phenotype and ocular oxidative damage in Aldh3a1(-/-)/ Aldh1a1(-/-) knock–out mice. *Journal of Biological Chemistry, 282,* 25668–25676.

Lee, A. Y., Chung, S. K, & Chung, S. S. (1995). Demonstration that polyol accumulation is responsible for diabetic cataract by the use of transgenic mice expressing the aldose reductase gene in the lens. *Proceedings of National Academy of Sciences, 92,* 2780–2784.

Levi, B. P., Yilmaz, O. H., Duester, G., & Morrison, S. J. (2008). Aldehyde dehydrogenase 1a1 is dispensable for stem cell function in the mouse hematopoietic and nervous systems. *Blood, 113,* 1670–1680.

Lemonde, H. A., Custard, E. J., Bouquet, J., Duran, M., Overmars, H., Scambler, P. J., & Clayton P. T. (2003). Mutations in SRD5B1 (AKR1D1), the gene encoding delta(4)–3–oxosteroid 5–β–reductase, in hepatitis and liver failure in infancy. *Gut, 52,* 1494–1499.

Li, Z., Srivastava, S., Yang, X., Mittal, S., Norton, P., Resau, J., Haab, B., & Chan, C. (2007). A hierarchical approach employing metabolic and gene expression profiles to identify the pathways that confer cytotoxicity in HepG2 cells. *BMC Systems Biology, 1,* 21.

Li, Y., Zhang, D., Jin, W., Shao, C., Yan, P., Xu, C., Sheng, H., Liu, Y., Yu, J., Xie, Y., Zhao, Y., Lu, D., Nebert, D. W., Harrison, D. C., Huang, W., & Jin, L. (2006). Mitochondrial aldehyde dehydrogenase–2 (ALDH2) Glu504Lys polymorphism contributes to the variation in efficacy of sublingual nitroglycerin. *Journal of Clinical Investigation, 116,* 506–511.

Lindahl, R. (1992). Aldehyde dehydrogenases and their role in carcinogenesis. *Critical Reviews in Biochemistry and Molecular Biology, 27(4–5),* 283–335.

Lipinski, C., Hopkins, A. (2004). Navigating chemical space for biology and medicine. *Nature, 432(7019),* 855–861.

Liu, Z. J., Sun, Y. J., Rose, J., Chung, Y. J., Hsiao, C. D., Chang, W. R., Kuo, I., Perozich, J., Lindahl, R., Hempel, J., & Wang, B. C. (1997). The first structure of an aldehyde dehydrogenase reveals novel interactions between NAD and the Rossmann fold. *Nature Structural Biology, 4,* 317–326.

Lowe, E. D., Gao, G. Y., Johnson, L. N., & Keung, W. M. (2008). Structure of daidzin, a naturally occurring anti–alcohol addiction agent, in complex with human mitochondrial aldehyde dehydrogenase. *Journal of Medicinal Chemistry, 51(15),* 4482–4487.

Luckey, S. W., & Petersen, D. R. (2001). Metabolism of 4–hydroxynonenal by rat Kupffer cells. *Archives in Biochemistry and Biophysics, 389,* 77–83.

Luczak, S. E., Elvine–Kreis, B., Shea, S. H., Carr, L. G., Wall, T. L. (2002). Genetic risk for alcoholism relates to level of response to alcohol in Asian–American men and women. *Journal of Studies on Alcoholism, 63,* 74–82.

Mandel, S., Grunblatt, E., Riederer, P., Amariglio, N., Jacob–Hirsch, J., Rechavi, G., & Youdim, M. B. (2005). Gene expression profiling of sporadic Parkinson's disease substantia nigra pars compacta reveals impairment of ubiquitin–proteasome subunits, SKP1A, aldehyde dehydrogenase, and chaperone HSC–70. *Annals of New York Academy of Sciences, 1053,* 356–75.

Mann, C. J., & Weiner, H. (1999). Differences in the roles of conserved glutamic acid residues in the active site of human class 3 and class 2 aldehyde dehydrogenases. *Protein Science, 8(10),* 1922–1929.

Manthey, C. L., Landkamer, G. J., & Sladek, N. E. (1990). Identification of the mouse aldehyde dehydrogenases important in aldophosphamide detoxification. *Cancer Research, 50,* 4991–5002.

Manzer, R., Qamar, L., Estey, T., Pappa, A., Petersen, D. R., & Vasiliou, V. (2003). Molecular cloning and baculovirus expression of the rabbit corneal aldehyde dehydrogenase (ALDH1A1) cDNA. *DNA Cell Biology, 22,* 329–338.

Marcato, P., Dean, C. A., Pan, D., Araslanova, R., Gillis, M., Joshi, M., Helyer, L., Pan, L., Leidal, A., Gujar, S., Giacomantonio, C. A., & Lee, P. W. (2011). Aldehyde dehydrogenase activity of breast cancer stem cells is primarily due to isoform ALDH1A3 and is predictive of metastasis. *Stem Cells, 29(1),* 32–45.

Marchitti, S. A., Brocker, C., Stagos, D., & Vasiliou, V. (2008). Non–P450 aldehyde oxidizing enzymes: the aldehyde dehydrogenase superfamily. *Expert Opinion on Drug Metabolism and Toxicology, 4(6),* 697–720.

Marchitti, S. A., Deitrich, R. A., & Vasiliou, V. (2007). Neurotoxicity and metabolism of the catecholamine–derived 3,4–dihydroxyphenylacetaldehyde and 3, 4–dihydroxyphenylglycoaldehyde: the role of aldehyde dehydrogenase. *Pharmacological Reviews, 59(2),* 59125–50.

Maring, J. A., Deitrich, R. A., & Little, R. (1985). Partial purification and properties of human brain aldehyde dehydrogenases. *Journal of Neurochemistry, 45,* 1903–10.

Marlier, A., & Gilbert, T. (2004). Expression of retinoic acid–synthesizing and–metabolizing enzymes during nephrogenesis in the rat. *Gene Expression Patterns, 5,* 179–85.

Matsuda, T., Yabushita, H., Kanaly, R. A., Shibutani, S., & Yokoyama, A. (2006). Increased DNA damage in ALDH2–deficient alcoholics. *Chemical Research in Toxicology, 19,* 1374–1378.

McMahon, R. E. (1982). Chapter 5: Alcohols, aldehydes, and ketones. *Metabolic basis of detoxication: metabolism of functional groups.* Eds. Jakoby, W.B., Bend, J.R. and Coldwell, J. NY, Academic Press.

Mills, P. B., Struys, E., Jakobs, C., Plecko, B., Baxter, P., Baumgartner, M., Willemsen, M. A., Omran, H., Tacke, U., Uhlenberg, B., Weschke, B., & Clayton, P. T. (2006). Mutations in antiquitin in individuals with pyridoxine–dependent seizures. *Nature Medicine, 12,* 307–9.

Minor, W., Cymborowski, M., Otwinowski, Z., & Chruszcz, M. (2006). HKL–3000: the integration of data reduction and structure solution from diffraction images to an initial model in minutes. *Acta Crystallogr. D. Biol. Crystallogr., 62,* 859–866.

Molotkov, A., & Duester, G. (2003). Genetic evidence that retinaldehyde dehydrogenase Raldh1 (Aldh1a1) functions downstream of alcohol dehydrogenase Adh1 in metabolism of retinol to retinoic acid. *Jour. of Biological Chemistry, 278,* 36085–90.

Moreb, J. S., Gabr, A., Vartikar, G. R., Gowda, S., Zucali, J. R., & Mohuczy, D. (2005). Retinoic acid down–regulates aldehyde dehydrogenase and increases cytotoxicity of 4–hydroperoxycyclophosphamide and acetaldehyde. *Journal of Pharmacology and Experimental therapeutics, 312,* 339–345.

Moreb, J. S., Mohuczy, D., Ostmark, B., & Zucali, J. R. (2007). RNAi–mediated knock-down of aldehyde dehydrogenase class–1A1 and class–3A1 is specific and reveals that each contributes equally to the resistance against 4–hydroperoxycyclophosphamide. *Cancer Chemotherapy, Pharmacology, 59,* 127–136.

Moreb, J. S., Baker, H. V., Chang, L. J., Amaya, M., Lopez, M. C., Ostmark, B., & Chou, W. (2008). ALDH isozymes down–regulation affects cell growth, cell motility and gene expression in lung cancer cells. *Molecular Cancer, 7(87).*

Muto, M., Hitomi, Y., Ohtsu, A., Ebihara, S., Yoshida, S., & Esumi, H. (2000). Association of aldehyde dehydrogenase 2 gene polymorphism with multiple esophageal dysplasia in head and neck cancer patients. *Gut, 47,* 256–261.

Muzio, G., Trombetta, A., Martinasso, G., Canuto, R. A., & Maggiora, M. (2003). Antisense oligonucleotides against aldehyde dehydrogenase 3 inhibit hepatoma cell proliferation by affecting MAP kinases. *Chemico–Biological Interactions, 143–*1*44*, 37–43.

Nees, D. W., Wawrousek, E. F., Robison, W. G. Jr., & Piatigorsky, J. (2002). Structurally normal corneas in aldehyde dehydrogenase 3a1–deficient mice. *Molecular and Cellular Biology, 22,* 849–55.

Niederreither, K., Fraulob, V., Garnier, J. M., Chambon, P., & Dollé, P. (2002). Differential expression of retinoic acid–synthesizing (RALDH) enzymes during fetal development and organ differentiation in the mouse. *Mechanisms of Development, 110,* 165–71.

Niederreither, K., Subbarayan, V., Dolle, P., & Chambon, P. (1999). Embryonic retinoic acid synthesis is essential for early mouse post–implantation development. *Nature Genetics, 21,* 444–448.

Ogawa, M., Isse, T., Oyama, T., Kunugita, N., Yamaguchi, T., Kinaga, T., Narai, R., Matsumoto, A., Kim, Y. D., Kim, H., Uchiyama, I., & Kawamoto, T. (2006). Urinary 8–hydoxydeoxyguanosine (8–OHdG) and plasma malondialdehyde (MDA) levels in Aldh2 knock–out mice under acetaldehyde exposure. *Industrial Health, 44,* 179–83.

Ogawa, M., Oyama, T., Isse, T., Saito, K., Tomigahara, Y., Endo, Y., & Kawamoto, T. (2007). A comparison of covalent binding of ethanol metabolites to DNA according to Aldh2 genotype. *Toxicological Letters, 168,* 148–54.

Ohsawa, I., Nishimaki, K., Yasuda, C., Kamino, K, & Ohta, S. (2003). Deficiency in a mitochondrial aldehyde dehydrogenase increases vulnerability to oxidative stress in PC12 cells. *Journal of Neurochemistry, 84,* 1110–7.

Onenli–Mungan, N., Yüksel, B., Elkay, M., Topaloğlu, A. K., Baykal, T., & Ozer, G. (2004). Type II hyperprolinemia: a case report. *Turk. J. Pediatrics, 46,* 167–9.

Overstreet, D. H., Knapp, D. J., Breese, G. R., & Diamond, I. (2009). A selective ALDH2 inhibitor reduces anxiety in mice. *Pharmacology, Biochemistry and Behavior, 94(2),* 255–261.

Pappa, A., Estey, T., Manzer, R., Brown, D., & Vasiliou, V. (2003). Human aldehyde dehydrogenase 3A1 (ALDH3A1): biochemical characterization and immunohistochemical localization in the cornea. *Biochemical Journal, 376,* 615–23.

Pappa, A., Sophos, N. A., & Vasiliou, V. (2001). Corneal and stomach expression of aldehyde dehydrogenases: from fish to mammals. *Chemico–Biological Interaction, 130–2,* 181–91.

Pappa, A., Brown, D., Koutalos, Y., DeGregori, J., White, C., & Vasiliou, V. (2005) Human aldehyde dehydrogenase 3A1 inhibits proliferation and promotes survival of human corneal epithelial cells. *J. of Biological Chemistry, 280,* 27998–8006.

Pappa, A., Chen, C., Koutalos, Y., Townsend, A. J., & Vasiliou, V. (2003). Aldh3a1 protects human corneal epithelial cells from ultraviolet and 4–hydroxy–2–nonenal–induced oxidative damage. *Free Radical Biology and Medicine, 34,* 1178–89.

Parajuli, B., Kimble–Hill, A. C., Khanna, M., Ivanova, Y., Meroueh, S., & Hurley, T. D. (2011). Discovery of novel regulators of aldehyde dehydrogenase isozymes. *Chemico–Biological Interactions, 191(1–3),* 153–158.

Pei, Y., Reins, R. Y., & McDermott, A. M. (2006). Aldehyde dehydrogenase (ALDH) 3A1 expression by the human keratocyte and its repair phenotypes. *Experimental Eye Research, 83,* 1063–73.

Peng, G. S., Chen, Y. C., Tsao, T. P., Wang, M. F., & Yin, S. J. (2007). Pharmacokinetic and pharmacodynamics basis for partial protection against alcoholism in Asians, heterozygous for the variant ALDH2*2 gene allele. *Pharmacogenetics Genomics, 17,* 845–55.

Penning, T. M., & Byrns, M. C. (2009). Steroid hormone transforming aldo–keto reductases and cancer. *Annals of New York Academy of Sciences, 1155,* 33–42.

Pereira, F., Rosenmann, E., Nylen, E., Kaufman, M., Pinsky, L., & Wrogemann, K. (1991). The 56 kDa androgen binding protein is an aldehyde dehydrogenase. *Biochemical and Biophysical Research Communications, 175,* 831–8.

Perez–Miller, S., & Hurley, T. D. (2003). Coenzyme isomerization is integral to catalysis in aldehyde dehydrogenase. *Biochemistry, 42(23),* 7100–7109.

Perozich, J., Kuo, I., Lindahl, R., & Hempel, J. (2001). Coenzyme specificity in aldehyde dehydrogenase. *Chemico–Biological Interaction, 130–132,* 115–24.

Picklo, M. J., Olson, S. J., Markesbery, W. R., & Montine, T. J. (2001). Expression and activities of aldo–keto oxidoreductases in Alzheimer disease. *J Neuropathology and Experimental Neurology, 60,* 686–95.

Reichard, J. F., Vasiliou, V., & Petersen, D. R. (2000). Characterization of 4–hydroxy–2–nonenal metabolism in stellate cell lines derived from normal and cirrhotic rat liver. *Biochimica et Biophysica Acta,1487,* 222–32.

Reisdorph, R., & Lindahl, R. (2007). Constitutive and 3–methylcholanthrene–induced rat ALDH3A1 expression is mediated by multiple xenobiotic response elements. *Drug Metabolism and Disposition, 35,* 386–93.

Ribes, V., Wang, Z., Dolle, P., & Niederreither, K. (2006). Retinaldehyde dehydrogenase 2 (RALDH2)–mediated retinoic acid synthesis regulates early mouse embryonic forebrain development by controlling FGF and sonic hedgehog signaling. *Development, 133(2),* 351–361.

Rizzo, W. B., & Carney, G. (2005). Sjogren–Larsson syndrome: diversity of mutations and polymorphisms in the fatty aldehyde dehydrogenase gene (ALDH3A2). *Human Mutation, 26,* 1–10.

Ross, S. A., McCaffery, P. J., Drager, U. C., & De Luca, L. M. (2000). Retinoids in embryonal development. *Physiological Review, 80,* 1021–1054.

Schnier, J. B., Kaur, G., Kaiser, A., Stinson, S. F., Sausville, E. A., Gardner, J., Nishi, K., Bradbury, E. M., & Senderowicz, A. M. (1999). Identification of cytosolic aldehyde dehydrogenase 1 from non–small cell lung carcinomas as a flavopiridol–binding protein. *FEBS Letters, 454,* 100–4.

Segel, I. H. (1993). Simple inhibition systems. *Enzyme Kinetics: Behavior and Analysis of Rapid Equilibrium and Steady–State Enzyme Systems, John Wiley and Sons, Inc.,* 100–159.

Sidhu, R. S., & Blair, A. H. (1975). Human liver aldehyde dehydrogenase. Esterase activity. *Journal of Biological Chemistry, 250(19),* 7894–98.

Sladek, N. E. (1999). Aldehyde dehydrogenase–mediated cellular relative insensitivity to the oxazaphosphorines. *Current Pharmaceutical Design, 5,* 607–25.

Sladek, N. E., Kollander, R., Sreerama, L., & Kiang, D. T. (2002). Cellular levels of aldehyde dehydrogenases (ALDH1A1 and ALDH3A1) as predictors of therapeutic responses to cyclophosphamide–based chemotherapy of breast cancer: a retrospective study. Rational individualization of oxazaphosphorine–based cancer chemotherapeutic regimens. *Cancer Chemo. and Pharmacology, 49,* 309–21.

Sladek, N. E. (1994). Metabolism and pharmacokinetic behavior of cyclophosphamide and related oxazaphosphorines. *Oxford England,* 79–156.

Sohling, B., & Gottschalk, G. (1993). Purification and characterization of a coenzyme–A dependent succinate semialdehyde dehydrogenase from Clostridium kluyveri. *European Journal of Biochemistry, 212,* 121–127.

Spengler, S. J., & Singer, B. (1988). Formation of interstrand cross–links in chloroactaldehyde–treated DNA demonstrated by ethidium bromide fluorescence. *Cancer Research, 48,* 4804–4806.

Sreerama, L., Rekha, G. K., & Sladek, N. E. (1995). Phenolic antioxidant–induced overexpression of class–3 aldehyde dehydrogenase and oxazaphosphorine–specific resistance. *Biochemical Pharmacology, 49(5),* 669–675.

Sreerama, L. & Sladek, N. E. (1993). Identification and characterization of a novel class 3 aldehyde dehydrogenase overexpressed in a human breast adenocarcinoma cell line exhibiting oxazaphosphorine–specific acquired resistance. *Biochemical Pharmacology, 45,* 2487–505.

Sreerama, L., & Sladek, N.E. (1995). Human breast adenocarcinoma MCF–7/ 0 cells electroporated with cytosolic class 3 aldehyde dehydrogenases obtained from tumor cells and a normal tissue exhibit differential sensitivity to mafosfamide. *Drug Metabolism and Disposition, 23(10),* 1080–1084.

Sreerama, L., & Sladek, N. E. (1997). Cellular levels of class 1 and class 3 aldehyde dehydrogenases and certain other drug–metabolizing enzymes in human breast malignancies. *Clinical Cancer Research, 3,* 1901–14.

Sreerama, L., & Sladek, N. E. (1997). Class 1 and class 3 aldehyde dehydrogenase levels in the human tumor cell lines currently used by the National Cancer Institute to screen for potentially useful antitumor agents. *Advances in Experimental Medicine and Biology, 414,* 81–94.

Srivastava, S., Chandra, A., Wang, L. F., Seifert, Jr. W. E., DaGue, B. B., Ansari, N. H., Srivastava, S. K., & Bhatnakar, A. (1998). Metabolism of the lipid peroxidation product 4–hydroxy–*trans*–2–nonenol, in isolated perfused rat heart. *Journal of Biological Chemistry, 273,* 10893–900.

Steinmetz, C. G., Xie, P., Weiner, H., & Hurley, T. D. (1997). Structure of mitochondrial aldehyde dehydrogenase: the genetic component of ethanol aversion. *Structure, 5,* 701–11.

Stephanou, P., Pappas, P., Vasiliou, V., & Marselos, M. (1999). Prepubertal regulation of the rat dioxin–inducible aldehyde dehydrogenase (ALDH3). *Advances in Experimental Medicine and Biology, 463,* 143–50.

Storms, R. W., Trujillo, A. P., Springer, J. B., Shah, L., Colvin, O. M., Luderman, S. M., & Smith, C. (1999). Isolation of primitive human hematopoietic progenitors on the basis of aldehyde dehydrogenase activity. *Proceedings of National Academy of Sciences, 96,* 9118–23.

Suzen, S., & Buyukbingol, E. (2003). Recent studies of aldose reductase enzyme inhibition for diabetic complications. *Current Medicinal Chemistry, 10,* 1329–1352.

Swanson, H. I., Njar, V. C., Castro, D. J., Gonzalez, F. J., William, D. E., Huang, Y., Kong, A. N., Doloff, J. C., Ma, J., Waxman, D. J., & Scott, E. E. (2010). Targeting drug metabolizing enzymes for effective chemoprevention and chemotherapy. *Drug Metabolism and Disposition, 38(4),* 539–544.

Sydow, K., Daiber, A., Oelze, M., Chen, Z., August, M., Wendt, M., Ullrich, V., Mülsch, A., Schulz, E., Keaney, J. F. Jr., Stamler, J. S., & Münzel, T. (2004). Central role of mitochondrial aldehyde dehydrogenase and reactive oxygen species in nitroglycerin tolerance and cross–tolerance. *Journal of Clinical Investigation, 113,* 482–489.

Uma, L., Hariharan, J., Sharma, Y., & Balasubramanian, D. (1996). Corneal aldehyde dehydrogenase displays antioxidant properties. *Experimental Eye Research, 63,* 117–20.

Ueshima, Y., Matsuda, Y., Tsutsumi, M., & Takada, A. (1993). Role of the aldehyde dehydrogenase–1 isozyme in the metabolism of acetaldehyde. *Alcohol Alcohol, 1B(Suppl),* 15–9.

Van den Hoogen, C., van der, H. G., Cheung, H., Buijs, J. T., Lippitt, J. M., Guzman–Ramirez, N., Hamdy, F. C., Eaton, C. L., Thalmann, G. N., Cecchini, M. G., Pelger, R. C., & van der Pluijm, G. (2010). High aldehyde dehydrogenase activity identifies tumor–initiating and metastasis–initiating cells in human prostate cancer. *Cancer Research, 70,* 5163–73.

Vasiliou, V., Bairoch, A., Tipton, K. F., & Nebert, D. W. (1999). Eukaryotic aldehyde dehydrogenase (ALDH) genes: human polymorphisms, and recommended nomenclature based on divergent evolution and chromosomal mapping. *Pharmacogenetics, 9,* 421–34.

Vasiliou, V., Pappa, A., & Petersen, D. R. (2000). Role of aldehyde dehydrogenases in endogenous and xenobiotic metabolism. *Chemico–Biological Interactions, 129,* 1–19.

Vasiliou, V., Pappa, A., & Estey, T. (2004). Role of human aldehyde dehydrogenases in endobiotic and xenobiotic metabolism. *Drug Metabolism Review, 36,* 279–99.

Vasiliou, V., & Nebert, D. W. (2005). Analysis and update of the human aldehyde dehydrogenase (ALDH) gene family. *Human Genomics, 2,* 138–143.

Velázquez–Fernández, D., Laurell, C., Geli, J., Höög, A., Odeberg, J., Kjellman, M., Lundeberg, J., Hamberger, B., Nilsson, P., & Bäckdahl, M. (2005). Expression profiling of adrenocortical neoplasms suggests a molecular signature of malignancy. *Surgery, 138,* 1087–94.

Wall, T. L., Johnson, M. L., Horn, S. M., Carr, L. G., Smith, T. L., & Schuckit, M. A. (1999). Evaluation of the self–rating of the effects of alcohol form in Asian Americans with aldehyde dehydrogenase polymorphisms. *Journal of Studies on Alcohol, 60,* 784–789.

Wang, X., Penzes, P., & Napoli, J. L. (1996). Cloning of a cDNA encoding an aldehyde dehydrogenase and its expression in Escherichia coli. Recognition of retinal as substrate. *Journal of Biological Chemistry, 271,* 16288–16293.

Wang, B., Wang, J., Zhou, S., Tan, S., He, X., Yang, Z., Xie, Y. C., Li, S., Zheng, C., & Ma, X. (2008). The association of mitochondrial aldehyde dehydrogenase gene (ALDH2) polymorphism with susceptibility to late–onset alzheimer's disease in Chinese. *Journal of Neurological Science, 268(1–2),* 172–5.

Wang, J.S., Fang, Q., Sun, D.J., Chen, J., Zhou, X.L., Lin, G.W., Lu, H.Z., & Fei, J. (2001). Genetic modification of hematopoietic progenitor cells for combined resistance to 4–hydroperoxycyclophosphamide, vincristine, and daunorubicin. *Acta Pharmacologica Sinica, 22,* 949–55.

Ward, R. J., McPherson, A. J., Chow, C., Ealing, J., Sherman, D. I., Yoshida, A., & Peters, T. J. (1994). Identification and characterization of alcohol–induced flushing in Caucasian subjects. *Alcohol Alcohol, 29,* 433–8.

Weiner, H., Hu, J. H., & Sanny, C. G. (1976). Rate limiting steps for the esterase and dehydrogenase reaction catalyzed by horse liver aldehyde dehydrogenase. *Journal of Biological Chemistry, 251(13),* 3853–5.

Wong, R. H., Wang, J. D., Hsieh, L. L., Du, C. L., & Cheng, T. J. (1998). Effects on sister chromatid exchange frequency of aldehyde dehydrogenase 2 genotype and smoking in vinyl chloride workers. *Mutation Research, 420,* 99–107.

Yokoyama, A., Muramatsu, T., Omori, T., Yokoyama, T., Matsushita, S., Higuchi, S., Maruyama, K., & Ishii, H. (2001). Alcohol and aldehyde dehydrogenase gene polymorphisms and oropharyngolaryngeal, esophageal and stomach cancer in Japanese alcoholics. *Carcinogenesis, 22,* 433–39.

Yoshida, A., Rzhetsky, A., Hsu, L. C., & Chang, C. (1998). Human aldehyde dehydrogenase gene family. *European Journal of Biochemistry, 251,* 549–57.

Yoshida, A., Hsu, L. C., & Yanagawa, Y. (1993). Biological role of human cytosolic aldehyde dehydrogenase 1: hormonal response, retinal oxidation and implication in testicular feminization. *Adv. in Experimental Medicine and Biology, 328,* 37–44.

Yoshida, A., Hsu, L. C., & Dave, V. (1992). Retinal oxidation activity and biological role of human cytosolic aldehyde dehydrogenase. *Enzyme, 46,* 239–44.

Yoshida, A., Dave, V., Ward, R. J., & Peters, T. J. (1989). Cytosolic aldehyde dehydrogenase (ALDH1) variants found in alcohol flushers. *Annals of Human Genetics, 53,* 1–7.

Yoshida, A., Huang, I. Y., & Ikawa, M. (1984). Molecular abnormality of an inactive aldehyde dehydrogenase variant commonly found in Orientals. *Proceedings of National Academy of Sciences, 81,* 258–61.

Zhai, Y., Sperkova, Z., & Napoli, J. L. (2001). Cellular expression of retinal dehydrogenase types 1 and 2: effects of vitamin A status on testis mRNA. *Journal of Cellular Physiology, 186,* 220–32.

Zhang, J. H., Chung, T. D., & Oldenburg, K. R. (1999). A simple statistical parameter for use in evaluation and validation of high throughput screening assays. *Journal of Biomolecular Screen, 4(2),* 67–73.

Zhao, D., McCaffery, P., Ivins, K. J., Neve, R. L., Hogan, P., Chin, W. W., & Dräger, U. C. (1996). Molecular identification of a major retinoic–acid–synthesizing enzyme, a retinaldehyde–specific dehydrogenase. *European Journal of Biochemistry*, *240,* 15–22.

Ziouzenkova, O., Orasanu, G., Sharlach, M., Akiyama, T. E., Berger, J. P., Viereck, J., Hamilton, J. A., Tang, G., Dolnikowski, G. G., Vogel, S., Duester, G., & Plutzky, J. (2007). Retinaldehyde represses adipogenesis and diet–induced obesity. *Nature Medicine, 13*, 695–702.

CURRICULUM VITAE

Bibek Parajuli

Education

Hanover College, Hanover, IN	B.S.	Chemistry	2004-2008
Indiana University, Indianapolis, IN	Ph.D.	Biochemistry	2008-2013

Honors, Awards and Fellowships

Indiana University Graduate fellowship
Honorable Mention (Indiana University Cancer Research Day)
Best Poster Award (Indiana University Biochemistry Research Day, 2012)
Indiana University Travel Grant
Hanover College Merit Based Fellowship
Keith and Gwen White senior year Award in Chemistry (Hanover College)
Selected as student speaker (one among 4 out of 50+ graduate students) to give a 20 minute talk at Annual Biochemistry research day, 2012

Research and Training Experience

Indiana University School of Medicine, Indianapolis, IN
Department of Biochemistry and Molecular Biology 2008- 2013
Doctoral Project
Thesis Advisor: Dr. Thomas D. Hurley
Thesis Title: *Identification, structural and kinetic characterization of small molecule inhibitors of Aldehyde dehydrogenase 3A1 (ALDH3A1).*
Performed high throughput screen to identify isozyme selective inhibitors of ALDH3A1, determined their mode of inhibition by performing steady state kinetics, their molecular basis of selectivity and potency by determining the crystal structure and performing a SAR experiment and tested some of these lead compounds in cancer cells that express ALDH3A1.

Hanover College, Hanover, IN 2007-2008
Department of Chemistry
Thesis advisor: Dr. Steve Boone
Senior year thesis title: *Determination of distribution constant of iodine in two immiscible solutions- carbon tetrachloride (CCl_4) and water by using their absorbance characteristics.*

University of Louisville, Louisville, KY 2007
Department of Chemistry
Research Mentor: Francisco Ibanez
Summer research: *Catalytic reactivity of amino coated nanoparticles.*

Conferences Attended

1. **Parajuli B,** Hurley TD**.** "Identification of small molecule inhibitors of aldehyde dehydrogenase 3A1 (ALDH3A1) by high throughput screening." Department of Biochemistry and Molecular biology, Indiana University School of Medicine, February, 2010.

2. **Parajuli B,** Hurley TD**.** "Identification and kinetic characterization of small molecule inhibitors of ALDH3A1." 15th International Meeting on Enzymology and Molecular Biology of Carbonyl Metabolism, Lexington, KY, July 2010.

3. **Parajuli B,** Hurley TD. "Kinetic and structural characterization of small molecule inhibitors of ALDH3A1: a target for increased sensitivity toward cyclophosphamide." IU Simon Cancer Research Day, (2010/ 2011).

4. **Parajuli B,** Hurley TD. "Kinetic, Structural and Cellular Characterization of isozyme selective small molecule inhibitor of ALDH3A1." Nature Chemical Biology Symposium, Boston, MA, October 2011.

5. **Parajuli B. "**Targeting ALDH isozymes for reversing cancer chemoresistance using small molecule inhibitors." Bluegrass Molecular Biophysics Networking Symposium, University of Kentucky, May 2012.

Publications

1. **Parajuli B**, Kimble-Hill AC, Khanna M, Ivanova Y, Meroueh S, Hurley TD. Discovery of novel regulators of aldehyde dehydrogenase. *Chemico-Biological Interactions*. 2011 May 30; 191(1-3): 153-8. Epub 2011 Feb 22.

2. Khanna M, Chen CH, Kimble-Hill AC, **Parajuli B**, Perez-Miller S, Baskaran S, Kim J, Dria K, Vasiliou V, Mochly-Rosen D, Hurley TD. Discovery of a novel class of covalent inhibitor for aldehyde dehydrogenases. *Journal of Biological Chemistry.* 2011 Dec 16; 286(50): 43486-94.

3. **Parajuli B**, Georgiadis T, Fishel ML, Hurley TD. Development of Selective Inhibitors for Human Aldehyde Dehydrogenase 3A1 (ALDH3A1) for the enhancement of cyclophosphamide based therapy. Manuscript submitted to ChemBioChem.

4. **Parajuli B**, Hurley TD. Structural and kinetic characterization of 2-methylbenzimidazole as a selective and potent inhibitor of ALDH3A1. Manuscript submitted to Journal of Medicinal Chemistry.